

**STUDIES ON THE MECHANICAL AND DIELECTRIC PROPERTIES OF  
UNSATURATED POLYESTER RESIN MODIFIED BY MWCNT,  
GRAPHENE OXIDE AND RUBBER SEED OIL**

*Thesis submitted to  
Cochin University of Science and Technology  
in partial fulfilment of the requirements  
for the award of the degree of  
Doctor of Philosophy*

**Remya Suresh**



**Department of Polymer Science and Rubber Technology  
Cochin University of Science and Technology  
Kochi- 682 022, Kerala, India**

**July 2018**

**Studies on the Mechanical and Dielectric Properties of  
Unsaturated Polyester Resin Modified by MWCNT,  
Graphene Oxide and Rubber Seed Oil**

*Ph. D Thesis*

*Author*

**Remya Suresh**

Research Scholar

Department of Polymer Science and Rubber Technology

Cochin University of Science and Technology

Cochin- 682 022, Kerala, India

E-mail: remyasuresh007@gmail.com

*Supervising guide*

**Dr. Rani Joseph**

Professor (Emeritus)

Department of Polymer Science and Rubber Technology

Cochin University of Science and Technology

Cochin- 682 022, Kerala, India

E-mail: rani@cusat.ac.in

Department of Polymer Science and Rubber Technology

Cochin University of Science and Technology

Cochin- 682 022, Kerala, India

July 2018



**Department of Polymer Science and Rubber Technology**  
**Cochin University of Science and Technology**  
Cochin- 682 022, Kerala, India

---

**Dr. Rani Joseph**  
Professor

Email: rani@cusat.ac.in

18/07/2018

## **Certificate**

This is to certify that the thesis entitled “**Studies on the Mechanical and Dielectric Properties of Unsaturated Polyester Resin Modified by MWCNT, Graphene Oxide and Rubber Seed Oil**” is an authentic record of research work carried out by **Mrs. Remya Suresh** under my supervision and guidance in the Department of Polymer Science and Rubber Technology, Cochin University of Science and Technology, Cochin-22. No part of the work reported in this thesis has been presented for any other degree from any other institution. All the relevant corrections and modifications suggested by the audience during the pre-synopsis seminar and recommended by the Doctoral committee have been incorporated in the thesis.

*Dr. Rani Joseph*  
(Supervising Guide)



## *Declaration*

I hereby declare that the thesis entitled “**Studies on the Mechanical and Dielectric Properties of Unsaturated Polyester Resin Modified by MWCNT, Graphene Oxide and Rubber Seed Oil**” is the bonafide work carried out by me under the supervision of **Dr. Rani Joseph** Professor (Emeritus), Department of Polymer Science and Rubber Technology, Cochin University of Science and Technology, Cochin-22 and has never been included in any other thesis submitted previously for the award of any degree.

Cochin – 22  
18/07/2018

*Remya Suresh*



*Dedicated to...*

*Amma, Achan and Tinju ettan*





---

## Acknowledgements

*I would like to take this opportunity to acknowledge those who have made this mission a success.*

*First and foremost I express my heartfelt gratitude to my God Almighty for the countless blessings on me, for giving me such a wonderful family members, teachers and friends and for giving me good health, strength, patience and wisdom to complete this assignment.*

*I take this opportunity to express my heartfelt gratitude to my supervising guide, Dr. Rani Joseph (Professor, Department of Polymer Science and Rubber Technology, Cochin University of Science and Technology (CUSAT)) for her constant support, guidance, motivation and imperative suggestions. She trained me to think freely without putting any boundaries. Whenever I am approaching my teacher for clearing my doubts, she will explain the answers in a simple manner without any complication so that an ordinary person can also understand the same. Her professional and personal attitude attracted and influenced me a lot. I am really felt very proud to say that I am a student of Rani Teacher.*

*I express my sincere thanks to Dr. Honey John (Head, Department of Polymer Science and Rubber Technology, CUSAT) for her timely advice and constant encouragement. I express my sincere gratitude to Prof. Thomas Kurian (for his concern and prayers for me), Prof. Eby Thomas Thachil and Prof. (Dr.) Sunil K. Narayanankutty, former Heads of Department of PSRT for providing all facilities in the department during my research work.*

*I extend my sincere thanks to Prof. (Dr.) Sunil K. Narayanankutty (my doctoral committee member), for his inspirational talks, care and support throughout my research work. My sincere and heartfelt gratitude to Dr. Philip Kurian (my supervising guide at the time of joining) for his valuable suggestions and support. I am grateful to Dr. K. E. George sir for his motivation, suggestions and support at the time of my thesis correction. Their vast knowledge in the polymer field helped me a lot during the course of my research work.*

*A special word of thanks to Dr. C .P. Reghunathan Nair (for the valuable discussions related to my research), Dr. Prasanth R. Krishna, and Dr. Sailaja G. S. for their timely help and constructive criticisms which really helped me a lot to present my work in a systematic way. Thanks to all the faculty members of Dept. of PSRT, Dr. Abitha, Dr. Jayalatha Gopalakrishnan, Dr. Jinu Jacob George, Dr. Jyotishkumar and Adhoc faculty for their wholehearted support.*

*I thank the office staff of PSRT for their immense help with the administrative part of my research work. I owe immensely to all my teachers right from my school days to the post graduate level for their blessings and concerns.*

*There is no word to express my deep sense of gratitude to all my beloved colleagues including FIP teachers, project fellows etc.*

*I express my sincere thanks to Dr. Ajalesh who connected me to my teacher Dr. Rani Joseph and helped me a lot in fulfilling my dream. My heartfelt thanks to my seniors Dr. Renju, Dr. Jolly (for the combined work we have done), Dr. Abhilash, Dr. Bindu sharmila, Sreedevi teacher, Dr. Maulice, Dr. Sona, Dr. Sreejesh, Dr. Prameela, Dr. Dennymol, Dr. Preetha, Dr. Nisha, Dr. Asha, Dr. Aishwarya, Dr. Saisy, Dr. Zeena, Dr. Vidya, Dr. Reshmi, Dr. Sunitha and Dr. Teena for their concern and suggestions. Special thanks to Dr. Bibinbal who is very special and an asset to our department.*

*No words to express my thanks to Neethu, Dhanya chechi, Divya, Bhagyesh, Jisha, Soumya, Neena chechi, Neena chechi (FIP), Julie chechi, Shadia chechi, Dr. Anju and Nishad for their sincere friendship, support and motivation. Special thanks to my international colleague Kingsly for his support and prayers.*

*Special thanks to Bhavya for helping me in the correction of my thesis. Thank you Venu sir, Gean Sir, Murali chettan, Midhun chettan, Manoj sir, Vishnu R. Nair, Sreekanth and Rohit chettan for your whole hearted support and motivation. I would like to express my sincere thanks to Shinu, Rahana, Asha chichi, Archana, Dileep chettan, Jayesh chettan, Meera and Sona chechi for your love and affection.*

*Thanks to my juniors Sumitha, Sirajunnisa, Praseetha, Ananjana, Liz, Sneha, Sumi, Ashwin chettan, Nisha, Neethu, Jesna, Leya, Bashida, Teena miss, Rijooy sir, Poornima, Shincy, Athul, Basil and Irthaza and wish you all success for the completion of research work.*

*I wish to express my gratitude to Dr. P. Mohanan, Department of Electronics, Cochin University of Science and Technology for permitting me to carry out the EMI shielding measurements. I am thankful to Lakshmi chechi, Dept. of Optoelectronics, Kerala University for Raman Spectral analysis. I express my gratitude to STIC (CUSAT) and Govt. Engineering College (Thrissur) for the characterization facilities provided. I extend my thanks to Mr. Binoop, Indu Photos, Kalamassery, for the sincerity and effort he has taken for formatting of my thesis. I am extremely grateful to my teachers at Union Christian College, Aluva for their constant support and prayers. In this occasion I am remembering Mr. Vishnu, Alpha Chemicals who supported me by providing chemicals at the early stages of my research and who is no longer with us. Thanks and prayers for your family.*

*I am extremely thankful for the financial assistance provided by Council for Scientific and Industrial Research (CSIR), New Delhi. I express my sincere thanks to my senior officers and colleagues at Central Dockyard Laboratory, Naval Dockyard, Visakhapatnam for their support.*

*I am grateful to my family members for their wholehearted love and prayers. I would never have been able to fulfill my long cherished desire without the unselfish care, patience and the sacrifices of my Father S. Suresh and mother, L. Usha. They supported throughout my entire life and gave courage to overcome the hurdles came to my path. My husband, Mr. Tinju was my motivating companion who is very special to me with his understanding, loving and sacrificing nature. I am thankful to my younger sister Reshma, who is always there for me with full support. I express my love and gratitude to my in-laws for their constant unconditional love and support. Very special thanks to my ammamma (Leelamma) who supported me at the final stages of my thesis writing without considering her health issues. Without her support I would never have completed my thesis.*

*Words are not sufficient to express my gratitude to all those who have contributed their time and talents directly or indirectly for the completion of my research work, but surely all of you will be remembered in my prayers.*

*Thanks to one and all*

***Remya Suresh***



## ||| Preface |||

Unsaturated polyester resins (UPRs) are currently the most widely used thermosetting polymer in the areas of aerospace, automotive, marine, infrastructure, military, sports, industrial fields, etc. These are the linear polycondensation products based on unsaturated and saturated acids/anhydrides and diols or oxides. The unsaturation in the backbone provides sites for reaction with vinyl monomers using free-radical initiators, thereby leading to the formation of three dimensional network. However, the brittle nature of them at ambient temperature limits their application in high-value-added areas. Modification of polyesters has been done to improve fracture toughness, impact resistance, and solubility in water and to reduce  $T_g$  and viscosity of polymers. Toughness of the polymers increases due to the presence of flexible units in the backbone, such as long-chain diols (e.g., DEG, dipropylene glycol, triethylene glycol) or long-chain saturated acids (e.g., adipic acid).

Nano materials are considered as advanced class of materials with unique properties related to their dimensions. The most important properties for industrial applications are: very good mechanical properties, electrical conductivity, thermal conductivity, fire resistance or antimicrobial features. It is important to get a very good dispersion of the nano materials in the polymer matrix, since only in this way the properties of the nano materials are transferred to final composite.

Carbon nanotubes (CNTs) and graphene, due to their unique mechanical, electrical and thermal properties attracted great deal of interest among researchers since their discovery. But due to large surface energy and strong interaction, these nano fillers are difficult to be uniformly dispersed in polymer matrix by simple mechanical mixing. Good dispersion of fillers plays an important role in ensuring enhanced mechanical and electrical properties at very low filler concentrations. Different types of surface modifications of nano fillers are reported in order to improve their dispersion in a particular matrix.

There is a growing trend in the use of natural oils (renewable resources), especially their derivatives, into UPRs as impact strength modifiers. These long chain fatty acid derivatives provide flexibility and low T<sub>g</sub> value to UP resins.

In the present work UPRs were modified by nano fillers like multiwalled carbon nanotubes (MWCNTs) and reduced graphene oxide (rGO). Both functionalised and non functionalised MWCNTs were used to compare the effect of functionalization on different properties. In the case of graphene oxide, both rGO and Silver decorated rGO (Ag-rGO) were used in order to study the effect of silver decoration on the surface of graphene oxide. Sonication assisted melt mixing of the aqueous dispersions of the fillers to the polyester has been done to get uniform and homogenous distribution of fillers in the polymer. The mechanical, thermal, dielectric and morphological properties of the nano composites were studied.

This study also includes the incorporation of a bio additive for the enhancement of impact strength and toughness properties of UPR. Fatty acid methyl esters of rubber seed oil (FAMEs of RSO) were incorporated as a bio modifier and the mechanical properties were studied.

The thesis entitled “**Studies on the Mechanical and Dielectric Properties of Unsaturated Polyester Resin Modified by MWCNT, Graphene Oxide and Rubber Seed Oil**” is divided into 6 chapters.

**Chapter 1** gives the significance of modification of commercially used unsaturated polyester resin (UPR) with macro, micro and nano fillers. An introduction of thermosetting polymers with special reference to unsaturated polyester resins and nano fillers viz. MWCNTs and Graphene oxide, used in the study is included. Significance of modification of polyester resin with fatty acid derivatives from bio resources is also discussed with special focus on rubber seed oil. The chapter also presents the scope and objective of the research work.

**Chapter 2** of the thesis gives a detailed description of the materials used and the methods employed for the present study.

**Chapter 3** presents unsaturated polyester/ multiwalled carbon nanotube composites. This chapter is divided in to two parts.

**Part A** focuses on covalent modification of MWCNTs using maleic anhydride by two step reaction process. The functionalised MWCNT is characterized by FTIR, TGA, Raman and TEM analysis.

**Part B** describes the fabrication of MWCNT-UPR composites by sonication followed by molding and curing. The morphology, static and dynamic mechanical properties, dielectric properties and EMI shielding properties of the composites are also reported.

**Chapter 4** presents reduced graphene oxide (rGO) -UPR composites with improved mechanical and dielectric properties. This chapter is divided into part A and B.

**Part A** explains the preparation of rGO/Ag-rGO (silver decorated rGO) nano fillers in which Vitamin-C is used as a reducing agent. Characterization of the nano fillers using FTIR, TGA, ICP-AES, SEM and TEM is also discussed.

**Part B** describes the preparation of rGO/Ag-rGO UPR composites with low filler loading. Thermal, mechanical, dielectric and morphological properties of the composites are discussed.

**Chapter 5** discusses the use of functionalised Rubber seed oil (RSO) as a plasticizing/toughening agent in UP resin. This chapter discusses the role of a non edible oil derivative in the impact properties of UP resin. It is also divided in to two parts.

**Part A** explains the preparation of fatty acid methyl esters of RSO (FAMEs of RSO) by two step trans-esterification process. In this process, partially sulphonated polystyrene (PSS) prepared from expanded polystyrene waste is used as a heterogeneous catalyst. The prepared oil derivative is characterized by GC-MS, FTIR and  $^1\text{H}$ NMR analysis.

**Part B** describes the effect of FAMEs of RSO in polyester resin. The mechanical and morphological properties of the modified resin are studied with special focus on impact and toughness properties.

**Chapter 6** The summary and conclusions of the study and future outlook is mentioned in this chapter.





# Contents

## Chapter 1

<b>INTRODUCTION .....</b>	<b>01 - 42</b>
1.1 Unsaturated polyester resin chemistry .....	03
1.1.1 Classification of polyester resins.....	06
1.1.2 Modifications of polyester resins .....	07
1.2 Nanofillers.....	08
1.2.1 Carbon nanotubes (CNTs) .....	09
1.2.1.1 Modification of carbon nanotubes .....	11
1.2.1.1.a Covalent functionalization .....	12
1.2.1.1.b Non-covalent functionalization.....	14
1.2.2 Graphene nanoplates .....	14
1.3 Toughening agents.....	17
1.3.1 Vegetable oil derivatives as toughening agents .....	18
1.3.2 Toughening mechanism.....	18
1.3.3 Rubber seed oil (RSO) .....	19
1.4 Unsaturated polyester resin/carbon nanotube composites .....	20
1.5 Unsaturated polyester resin/reduced graphene oxide (rGO) composites .....	23
1.6 Vegetable oil modified unsaturated polyester resins.....	26
1.7 Scope and objective of the work.....	29
References.....	31

## Chapter 2

<b>MATERIALS AND METHODS.....</b>	<b>43 - 64</b>
2.1 Materials.....	43
2.1.1 Unsaturated polyester resin (UPR) .....	43
2.1.2 Fillers and modifying agents.....	44
2.1.2.1 Multi-walled carbon nanotubes (MWCNTs) .....	44
2.1.2.2 Graphite fine powder.....	44
2.1.2.3 Rubber seed oil (RSO) .....	45
2.1.3 Chemicals .....	45
2.1.3.1 Chemicals for the processing of UP resins .....	45
2.1.3.2 Chemicals for functionalisation of MWCNTs.....	46
2.1.3.3 Chemicals used for the modification of natural graphite ..	47
2.1.3.4 Chemicals used for the preparation of FAMEs of RSO ..	48
2.2 Experimental methods.....	48
2.2.1 Mechanical stirring.....	49
2.2.2 Ultrasonication .....	49
2.2.3 Direct mixing dispersion technique and molding.....	50

2.3	Characterization techniques .....	50
2.3.1	UV-Vis spectroscopy.....	50
2.3.2	Fourier-Transform Infrared Spectroscopy (FTIR) .....	50
2.3.3	Boehm titrations .....	51
2.3.4	Nuclear Magnetic Resonance Spectroscopy (NMR) .....	51
2.3.5	GC-MS Analysis .....	51
2.3.6	X-Ray Diffraction Technique (XRD) .....	52
2.3.7	Raman spectroscopy .....	53
2.3.8	Inductively Coupled Plasma Atomic Emission Spectrometer (ICP-AES) .....	54
2.3.9	Mechanical properties.....	54
2.3.9.1	Tensile properties.....	54
2.3.9.2	Flexural properties .....	55
2.3.9.3	Impact strength .....	56
2.3.9.4	Dynamic mechanical analysis .....	57
2.3.10	Morphological properties .....	59
2.3.10.1	Scanning Electron Microscopy (SEM) .....	59
2.3.10.2	Transmission Electron Microscopy (TEM) .....	60
2.3.11	Thermo gravimetric analysis (TGA) .....	61
2.3.12	Dielectric properties.....	61
2.3.13	EMI shielding measurements .....	63
	References.....	64

### **Chapter 3**

## **UNSATURATED POLYESTER RESIN MULTI-WALLED CARBON NANOTUBE COMPOSITES .....65 - 103**

### **Part A**

#### **Preparation of maleic anhydride functionalized multi-walled carbon nanotubes**

3.A.1	Introduction.....	66
3.A.2	Experimental .....	68
3.A.2.1	Preparation of MA functionalized MWCNTs.....	68
3.A.2.2	Characterization .....	68
3.A.3	Results and discussion.....	69
3.A.4	Conclusions.....	77
	References.....	77

### **Part B**

#### **Modification of unsaturated polyester resin with MA functionalized MWCNTs**

3.B.1	Introduction.....	81
3.B.2	Experimental.....	83

3.B.2.1	Preparation of MA-MWCNT/ UPR composites .....	83
3.B.2.2	Characterization .....	84
3.B.3	Results and discussion.....	84
3.B.3.1	Dynamic mechanical properties .....	85
3.B.3.2	Static mechanical properties .....	88
3.B.3.3	Thermo gravimetric analysis.....	91
3.B.3.4	Morphological properties.....	92
3.B.3.5	Dielectric properties .....	94
3.B.3.6	EMI shielding effectiveness.....	97
3.B.4	Conclusions.....	99
	Reference .....	100

## **Chapter 4**

### **UNSATURATED POLYESTER RESIN- REDUCED GRAPHENE OXIDE COMPOSITES..... 105 - 146**

#### **Part A**

##### **Preparation of silver decorated reduced graphene oxide nanohybrids**

4.A.1	Introduction.....	106
4.A.2	Experimental .....	107
4.A.2.1	Preparation of silver nano particle decorated reduced graphene oxide nanohybrids .....	107
4.A.2.1.a	Water assisted oxidation of graphite (G) to graphene oxide (GO) .....	108
4.A.2.1.b	Preparation of rGO and rGO-Ag from GO .....	108
4.A.2.2	Characterization .....	109
4.A.3	Results and discussion.....	109
4.A.4	Conclusions.....	119
	References.....	120

#### **Part B**

##### **Modification of unsaturated polyester resin with rGO-Ag nanohybrids**

4.B.1	Introduction.....	124
4.B.2	Experimental.....	126
4.B.2.1	Preparation of rGO and rGO-Ag unsaturated polyester composites.....	126
4.B.2.2	Characterization .....	126
4.B.3	Results and discussion.....	127
4.B.3.1	Dynamic mechanical properties .....	127
4.B.3.2	Static mechanical properties .....	131
4.B.3.3	Thermogravimetric analysis.....	134

4.B.3.4 Morphological properties.....	135
4.B.3.5 Dielectric properties .....	137
4.B.3.6 EMI shielding effectiveness.....	140
4.B.4 Conclusions.....	141
References.....	142

## **Chapter 5**

### **FATTY ACID METHYL ESTERS (FAMES) OF RUBBER SEED OIL (RSO) MODIFIED UNSATURATED**

<b>POLYESTER RESIN .....</b>	<b>147 - 181</b>
------------------------------	------------------

#### **Part A**

##### **Preparation of Fatty Acid Methyl Esters from Rubber Seed Oil**

5.A.1 Introduction.....	148
5.A.2 Experimental.....	150
5.A.2.1 Preparation of fatty acid methyl esters of rubber seed oil (FAMES of RSO). .....	150
5.A.2.2 Characterization .....	151
5.A.3 Results and discussion.....	151
5.A.3.1 Physico-chemical analysis .....	151
5.A.3.2 GC-MS analysis .....	153
5.A.3.3 <sup>1</sup> H NMR analysis.....	157
5.A.3.4 FTIR spectral analysis .....	161
5.A.4 Conclusions.....	162
References.....	163

#### **Part B**

##### **Fatty Acid Methyl Esters of RSO modified Unsaturated Polyester Resin**

5.B.1 Introduction.....	165
5.B.2 Experimental.....	166
5.B.2.1 Fabrication of FAMES of RSO modified unsaturated polyester resin .....	166
5.B.2.2 Characterization .....	167
5.B.3 Results and discussion.....	168
5.B.3.1 Dynamic mechanical properties .....	169
5.B.3.2 Mechanical properties.....	171
5.B.3.3 Thermo gravimetric analysis (TGA) .....	176
5.B.3.4 Morphology and micro structure.....	177
5.B.4 Conclusions.....	179
References.....	180

*Chapter 6*

**SUMMARY AND CONCLUSIONS..... 183 - 191**

**List of Publications..... 193 - 195**

**Curriculum Vitae ..... 197**



## ||| List of Abbreviations and Symbols |||

UPR	- Unsaturated polyester resin
CNT	- Carbon naotubes
MWCNT	- Multi-walled carbon nanotubes
SWCNT	- Single-walled carbon nanotubes
GNS	- Graphene nanosheets
rGO	- reduced graphene oxide
GO	- Graphene oxide
FTIR	- Fourier-transform infrared spectroscopy
UV-Vis	- Ultra-violet visible spectroscopy
XRD	- X-ray diffraction
TEM	- Transmission electron microscopy
SEM	- Scanning electron microscopy
TGA	- Thermo gravimetric analysis
DMA	- Dynamic mechanical analysis
EMI	- Electromagnetic interference
SE	- Shielding effectiveness
SAED	- Selected area electron diffraction pattern
ICP-AES	- Inductively coupled plasma atomic emission spectroscopy
RSO	- Rubber seed oil
FAMEs of RSO-	Fatty acid methyl esters of rubber seed oil
NMR	- Nuclear magnetic resonance
GC/MS	- Gas chromatography mass spectrometry
PSS	- partially sulphonated polystyrene
FRP	- fiber reinforced plastics
MEKP	- Methyl ethyl ketone peroxide
Co.Oct.	- Cobalt octoate
THF	- Tetrahydrofuran
MA	- Maleic anhydride

.....✪✪.....





# Chapter 1

## INTRODUCTION

<b>Contents</b>	1.1 <i>Unsaturated polyester resin chemistry</i>
	1.2 <i>Nanofillers</i>
	1.3 <i>Toughening agents</i>
	1.4 <i>Unsaturated polyester resin/carbon nanotube composites</i>
	1.5 <i>Unsaturated polyester resin/reduced graphene oxide (rGO) composites</i>
	1.6 <i>Vegetable oil modified unsaturated polyester resins</i>
	1.7 <i>Scope and objective of the work</i>

Modification of unsaturated polyester resins to improve their mechanical, dielectric and EMI shielding properties is the topic of the present study. Unsaturated polyester resins (UPRs) are one of the most commonly used thermosetting polymers for the production of composite materials, mainly fiber reinforced composites (FRP). They can also be used for non-reinforced casting resin products. FRP composites are consumed primarily in the areas like aerospace, automotive, marine, infrastructure, military and corrosion resistant tanks and pipes, although they find use in a variety of other applications. On the other hand, the non-reinforced cross-linked unsaturated polyester resin is used to make artificial marbles, gel coats, solid surface counter tops, buttons and automotive putty etc. The world consumption of unsaturated polyester resin is represented in the pie chart given below. About 60% of the total UPR production was from Asia [1].

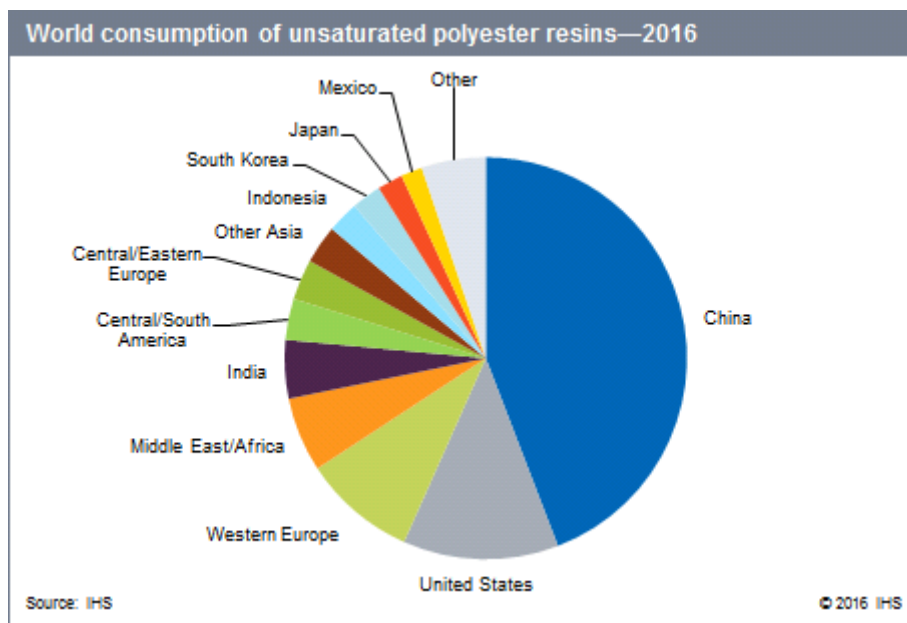


**Fig. 1.1** World consumption of UPR (2016)

The consumption of UPR in India keeps on increasing due to wide variety of industrial and consumer applications (Fig. 1.1). The Indian unsaturated polyester resin market witnessed strong growth in the last couple of years due to robust GDP growth, increased manufacturing activity and core sector growth. According to market forecasts Indian UPR market is expected to reach 445 million pounds by the end of 2018 [2].

The major attractions of UP resins are its low cost, ease of handling, low viscosity, quick curing, light weight and good balance of mechanical and chemical properties [3-5]. But one of the major drawbacks of UPRs is their brittle nature and poor resistance to crack propagation which reduces its use in high load carrying applications [6]. Several modification procedures have been adopted in order to improve the

properties of UPRs which includes natural and synthetic fibers, micro, macro and nanofillers as reinforcing agents, liquid rubbers, thermoplastic elastomers and vegetable oil derivatives as toughening agents.

## **1.1 Unsaturated polyester resin chemistry**

Polyester chains are formed by the poly condensation reaction between unsaturated and saturated acids/anhydrides and diols. These oligomers are generally pale yellow in colour with low degree of polymerization. Depending on the chemical composition and molecular weight these oligomers may be viscous liquids or brittle solids. These oligomers possess high viscosity which can be reduced by dissolving the oligomers in a reactive diluent like styrene. After dissolving the oligomers in styrene it is termed as unsaturated polyester resin. It possesses a viscosity in the range 200-2000 cps. Upon curing the unsaturated portion in the polyester chain reacts with styrene through free radical polymerization reaction thereby leading to the formation of a rigid three dimensional network.

Commonly used unsaturated anhydride is maleic anhydride (MA) and propylene glycol is the commonly used diol. But the usage of MA alone will yield a polyester back bone with high density of double bond which results a brittle product. So phthalic anhydride is used along with MA in order to control the unsaturation because the aromatic double bonds in PA will not take part in the crosslinking reaction with styrene.

Free radical chain growth cross-linking polymerization reaction between polyester resin and styrene takes place in presence of initiators.

A wide range of peroxides and azo and azine compounds can be used as initiators, depending on the reaction temperature. Methyl ethyl ketone peroxide (MEKP) is preferred for room temperature curing process as in the case of large hand lay-up structures. Benzoyl peroxide is used for moderate temperature curing (60°C–90°C) and for hot press or oven curing (130°C–150°C) di-*t*-butyl peroxide or *t*-butyl perbenzoate is used. Accelerators are used to speed up the decomposition of peroxides. Some metal compounds, tertiary amines and mercaptans are used as accelerators. Cobalt naphthenate and cobalt octoate are the most widely used accelerators [7].



Unsaturated polyester resin curing process can be divided into four stages: induction, microgel formation, transition and macrogelation [8]. In the first stage free radicals are consumed by the inhibitors and very little polymerization takes place. Microgel particles are formed in the second stage with high cyclization and cross-link density. In the transition stage the double bonds present in the polyester chain which is buried inside the microgel undergo intra-molecular cross-linking while those present on the surface reacts with other monomers and microgels. The final stage is the macrogelation stage which takes place by intermolecular microgels and microgel clusters. This is accompanied by a sharp increase in the viscosity. The schematic representation of the curing process is given in Fig. 1.2.

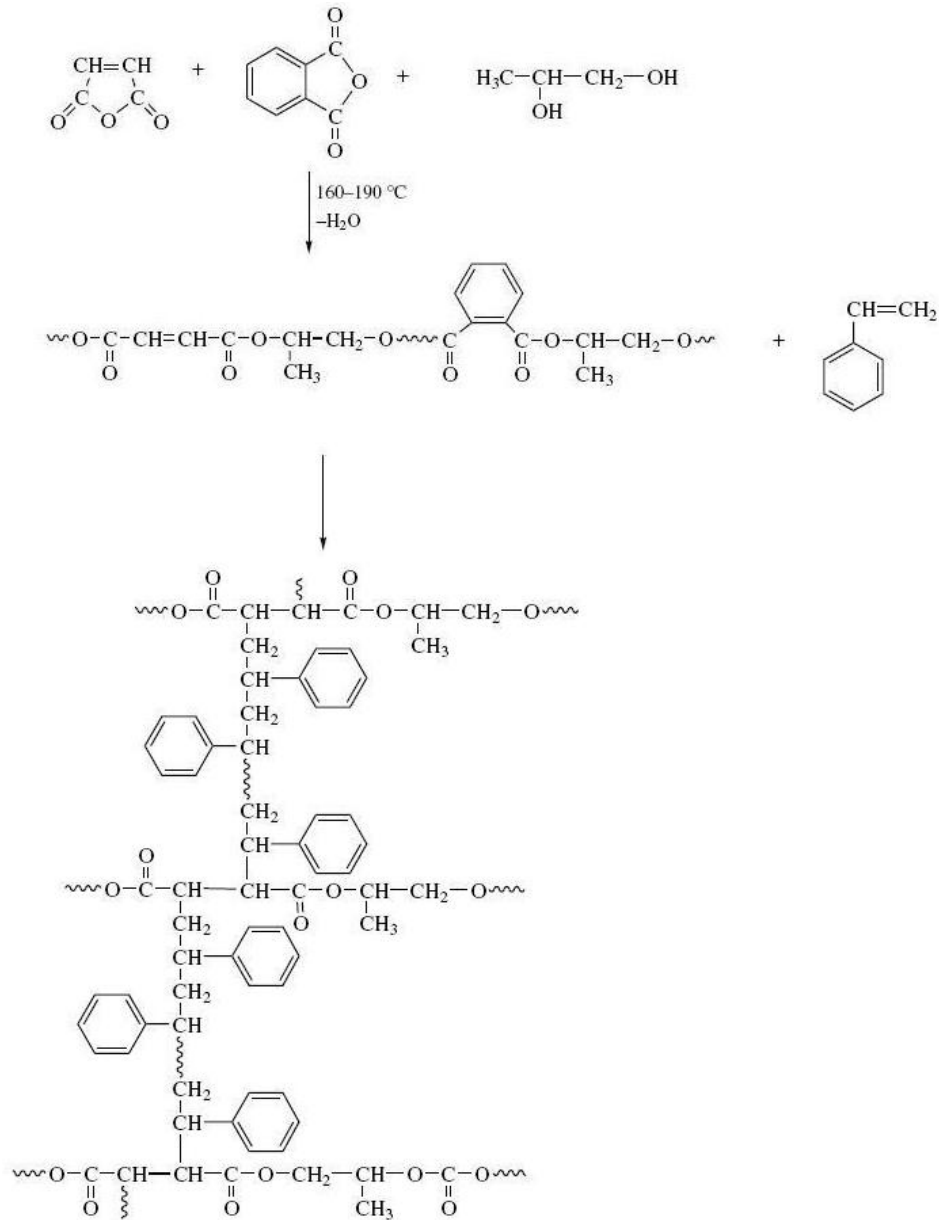


**Fig. 1.2** Polyester cross-linking reaction scheme

Thus, the curing reaction of the UP-styrene system can be described in four steps:

- 1) Intermolecular cross-linking with or without linking through styrene monomers.
- 2) Intramolecular cross-linking with or without linking through styrene monomer.
- 3) Chain branching on the polyester molecule by styrene.
- 4) Free styrene homopolymerization.

By selection of different acids/anhydrides and glycols and changes in the ratio of saturated/unsaturated component and the reactive diluent, the nature of the final network can be varied significantly to meet different performance requirements.

### **1.1.1 Classification of polyester resins**

Based on the structure unsaturated polyester resin can be divided into six major types as given in Table 1.1 [9-11]. Ortho resins are called general purpose resins which are highly cost efficient formed by single step condensation reaction. They possess good overall performance. Isophthalic and terephthalic resins are formed by the two step condensation reaction which possesses increased chemical resistance and toughness compared to ortho resins. Their cost is higher than that of ortho resins. Improved thermal performance was obtained in the case of bisphenol A resin because of the hardness and rigidity imparted by bisphenol A backbone. Chlorendics provide enhanced flame retardant property to polyester backbone which gives self-extinguishing polyesters. Vinyl ester resins are formulated to obtain low styrene emission resins, automotive grades

with high tensile strength and heat deflection temperature, hybrid grades that balance performance and economy, materials for corrosion resistance and marine applications.

**Table 1.1** Classification of UP resins

S.No	Type	Diacid monomer	Diol monomer
1	Phthalic resin	Phthalic anhydride, maleic anhydride or fumaric acid	Propylene glycol
2	Isophthalic resin	Isophthalic acid, maleic anhydride or fumaric acid	Propylene glycol
3	Terephthalic resin	Terephthalic acid, maleic anhydride or fumaric acid	Propylene glycol
4	Bisphenol A fumarates	Fumaric acid	Bisphenol A
5	Chlorendics	Chlorendic anhydride (tetra bromo/tetrachlorophthalic anhydride) or chlorendic acid, maleic anhydride or fumaric acid	Propylene glycol
6	Vinyl ester resin	Acrylic acid or methacrylic acid	Diglycidyl ether of bisphenol A or epoxy of phenol novolac type or epoxy based on tetrabromo bisphenol A

### 1.1.2 Modifications of polyester resins

Several modifications have been done in order to improve the impact resistance, fracture toughness, mechanical and electrical properties of unsaturated polyester resins. Toughness of the resins can be improved by incorporating flexible units in the back bone such as long-chain diols (e.g., DEG, dipropylene glycol, triethylene glycol) or long-chain saturated

acids (e.g., adipic acid). Thermoplastic elastomers, liquid rubbers and vegetable oil based derivatives can also be used as toughening agent for unsaturated polyester resin.

Polyester composite materials are opened new routes for polymer formulations and have allowed the manufacture of new products with optimal properties for special applications [12]. Using natural filler to reinforce the composite materials offers the following benefits like strength and rigidity, light weight, environmental friendly, economical, renewable, and abundant resource [13, 14]. Several authors have reported the use of natural fibers such as palmyra [15], sisal [16], banana [17], oil palm [18], henequen [19], jute [20], hemp [21] and wood pulp [22] as reinforcements in polymer matrixes. However, they have the disadvantage of degradation by moisture, poor surface adhesion to hydrophobic polymers, non-uniform filler sizes, and not being suitable for high temperature application. Carbon black, silica, clay and glass fibers are the fillers which are commonly used to reinforce polyester resin for commercial applications. Recently the incorporation of nanofillers in polymer matrices has gained great attention due to their extra ordinary mechanical, chemical and electrical properties when compared to conventional fillers.

## **1.2 Nanofillers**

Nanofillers, especially those based on carbon nanotubes and graphene, have received a great attention recently for the preparation of polymer composites. Nanofillers possess at least one dimension in the nanometer range i.e 1-100 nm. Based on their physical geometry they can



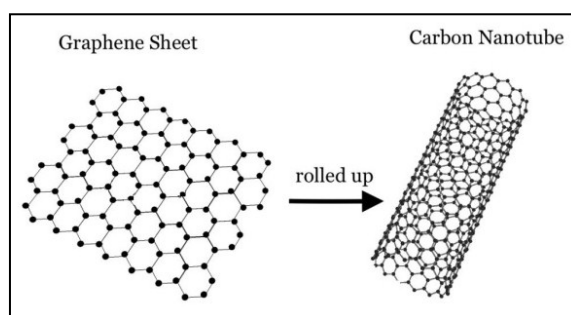
be classified into zero dimensional (0D), one dimensional (1D) and two dimensional (2D) nano fillers.

- 0D nanofillers: Here three dimensions are in the nanometer range e.g. zinc oxide, silica, carbon black etc.
- 1D nanofillers: which show two dimensions in the nanometer range and third is larger as in the case of carbon nanotubes (CNTs). They usually found in the form of fibers, cylinders or rods like CNTs, carbon nanofibers, cellulose whiskers, gold or silver nanotubes.
- 2D nanofillers: They usually possess the structure of layers or sheets in which only one dimension is in the nanometer range. Layered silicates, layered double hydroxides and layered graphene flakes are the common examples which is having thickness in the nanometer range.

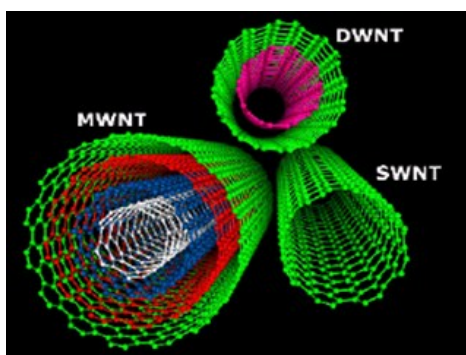
### **1.2.1 Carbon nanotubes (CNTs)**

Carbon nanotubes have been the research focus in both academia and industry since their discovery in 1990s by Sumio Iijima [23-25]. These are cylindrical nanostructures with remarkable and unique mechanical, electrical, optical and thermal properties. Nanotubes are members of fullerene family which possess long, hollow tube like structure with the walls formed by one atom thick sheets of carbon, called graphene (Fig. 1.3 (a)). Based on the number of rolled layers of graphene, CNTs can be classified into three major types. If a single sheet of graphene is rolled into a seamless cylinder it is called single-walled carbon nanotubes (SWCNTs). If

only two concentrically rolled graphene sheets are present it is called double walled carbon nanotubes (DWCNTs). If the structure consists of two or more concentric cylindrical layers it is termed as multi-walled carbon nanotubes (MWCNTs). The structures are presented in Fig. 1.3 (b).



(a)



(b)

**Fig. 1.3** (a) Rolling up of graphene sheets to form CNTs and (b) structures of CNTs

There are two models that can be used to describe MWCNTs, Russian doll model and Parchment model. In Russian doll model graphene sheets are arranged in concentric cylinders i.e. one SWCNT in a large SWCNT. In the Parchment model a single sheet of graphite is rolled in around itself resembling a rolled newspaper. The Russian doll model is

the commonly used one. MWCNTs are cheaper than SWCNTs and economically it is more preferred.

Different methods are used to synthesize CNTs which include arc discharge [26, 27], laser ablation [28], plasma torch [29, 30] and chemical vapor deposition [31, 32]. The properties of CNTs are given in Table 1.2.

**Table 1.2** Properties of SWCNTs and MWCNTs [33-35]

Properties	SWCNTs	MWCNTs
Specific gravity (g/cm <sup>3</sup> )	0.8-1.3	1.8-2.6
Elastic Modulus (TPa)	~1	0.3-1
Strength (GPa)	50-500	10-60
Resistivity ( $\mu\Omega$ cm)	5-50	5-50
Electrical conductivity (S/cm)	10 <sup>2</sup> -10 <sup>6</sup>	10 <sup>3</sup> -10 <sup>5</sup>
Thermal conductivity (W m <sup>-1</sup> K <sup>-1</sup> )	3000-6000	2000-3000
Thermal stability	550-650°C in air; 2800°C in vacuum	550-650°C in air; 2800°C in vacuum
Specific surface area	~400-900 m <sup>2</sup> /g	~200-400 m <sup>2</sup> /g

### 1.2.1.1 Modification of carbon nanotubes

CNTs are considered to be a good candidate for the preparation of polymer nanocomposites. However it is difficult to achieve a homogeneous dispersion of CNTs in polymer matrix. Carbon nanotubes have strong tendency to agglomerate via their huge surface area which is thermodynamically stabilized by numerous  $\pi$ - $\pi$  interactions and Van der Waals forces [36, 37]. Therefore homogeneous dispersion of CNTs in polymer matrix is the key factor to enhance the properties of nanocomposites. Physical and chemical methods are employed for controlling the dispersion of CNTs in polymers. Physical methods include

direct mixing, mechanical stirring and ultrasonication. Chemical methods include covalent (chemical functionalization) and non-covalent (addition of surfactant) functionalization [38, 39].

#### **1.2.1.1.a Covalent functionalization**

In this type of functionalization functional groups are attached on the surface of carbon nanotubes by chemical reaction which involves the formation of covalent bond between CNT and functional groups. The oxygen containing functional groups could be introduced by mechanical, chemical and electrochemical routes [40, 41]. After these harsh treatments CNTs can be effectively purified and the oxygen containing functional groups, mainly carboxyl and hydroxyl have been found to decorate the graphitic surface. These functional groups facilitate the exfoliation of CNT bundles and increase the solubility in polar media. Thus the unique mechanical and electrical properties of CNTs can be transferred to the properties of CNT-polymer composites.

The commonly used acid and/or air oxidation at elevated temperature for CNTs have been well documented in previous studies. Hu et al. and Martinez et al. studied the effect of hot nitric acid on CNTs which reveals the efficient removal of metallic impurities and amorphous carbon [40, 41]. Ziegler et al. studied the effect of Sulphuric acid/H<sub>2</sub>O<sub>2</sub> mixture (piranha) on CNTs. Piranha was found to attack existing damage sites producing significant side wall damage at elevated temperature [42]. Kim et al. treated MWCNTs with ammonium hydroxide/ H<sub>2</sub>O<sub>2</sub> mixture and prepared epoxy-CNT nanocomposite with enhanced electrical properties [43].

Different types of characterization techniques are used to identify the functional groups present on carbon nanotubes. The techniques and their limitations are summarized in Table 1.3 [44].

**Table 1.3** Applications and limitations of techniques used to analyze the structure and surface chemistry of CNTs

Analytical technique	Information provided/strengths	Limitations	Overview of technique (References)
IR	Functional group identification	Not quantitative, some IR modes are too weak to be observed	[45], [46]
XPS	Surface composition and, in principal, information about functional groups	Requires relatively large amounts of sample (~5 mg), peak-fitting is often ambiguous and over interpreted	[45], [46]
Chemical derivatization	Direct quantification of targeted functional groups	Not all function groups can be derivatized	[46]-[48]
Boehm titrations	Quantification of protic functional groups	Does not provide information on aprotic functionalities. Requires large amounts of sample (>10 mg)	[49]
TGA and TPD	Concentration of organic species attached to CNTs	Requires large amount of sample (>10 mg). Data interpretation is often subjective.	[50]
EELS and NEXAFS	Surface composition and functional groups identification	Can be difficult to implement for routine analysis	[51]
TEM	Images of CNTs, observation of sidewalls. CNT diameter, length, and dispersion state can also be determined. Chemical analysis by EDX is also often available in TEMs	CNTs are susceptible to damage from the high-energy electron beam. Sample preparation and drying can result in ambiguous analysis	[45], [51]
Raman spectroscopy	$I_D:I_G$ band ratios can provide a metric of sidewall damage or purity	$I_D:I_G$ band ratio can be misinterpreted or misleading	[45], [46]

### 1.2.1.1.b Non-covalent functionalization

Non covalent functionalization includes the absorption of surfactants, polymers or biological macromolecules on the surface of CNTs [52]. Noncovalent functionalization of CNTs with polymers is an effective way to disperse the tubes in aqueous and non-aqueous solvents without damaging their unique structure and thus preserving their intrinsic properties.  $\pi$ - $\pi$  interaction between CNTs and polymers are considered to be the fundamental mechanism behind non-covalent functionalization. Different functionalization methods are schematically represented in Fig. 1.4 [53].

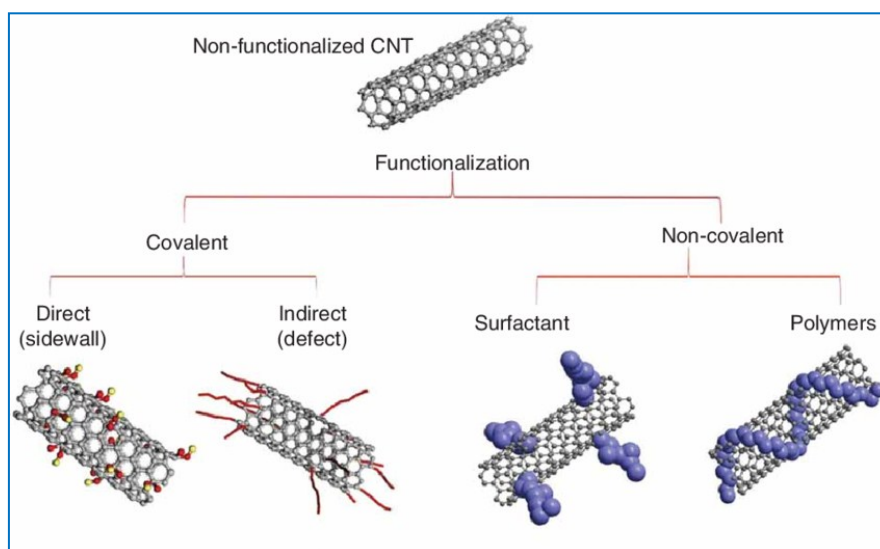


**Fig. 1.4** Different methods for functionalization of CNTs

## 1.2.2 Graphene nanoplatelets

Graphene is described as a sheet of single layer of carbon atoms tightly bound in a hexagonal honeycomb lattice. Graphite is formed by the stacking of graphene sheets on the top of each other with an

interplanar spacing of 0.335 nm which are held together by van der Waals forces (Fig. 1.5). Graphene is the thinnest material known to man with one atom thick, the lightest material known, the strongest compound discovered and the best conductor of heat at room temperature with good electrical conductivity.

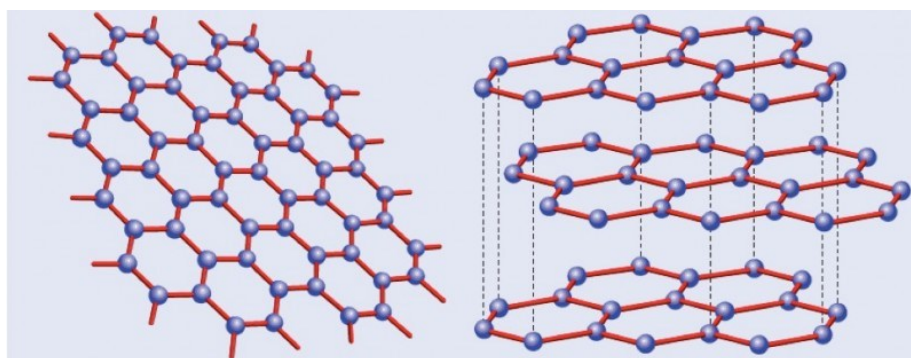


**Fig. 1.5** Structure of graphene and graphite

Several methods have been reported for the exfoliation of graphite into graphene which can be divided into two types: the top-down approach and the bottom-up approach. In the first method graphene layers are separated from stacked graphite by overcoming the van der Waals forces [54]. The bottom-up approach implements carbon molecules as building blocks; typically carbon molecules are obtained from alternative sources [55]. The most common method exercised initially after the discovery of graphene is micro-mechanical cleavage of graphite which is also called Scotch-tape, drawing or peel-off method [56]. After that chemical vapour deposition (CVD) is used as a viable alternative technique [57, 58].

A widely accepted method is the exfoliation of graphite to graphene oxide (GO) which gives high production yield, making the process cost effective and scalable [59, 60]. Graphene nanoflakes can be obtained from GO by chemical reduction method. Moreover electrochemical exfoliation, ball milling and ultrasonication are comes under top-down approach.

Graphene exhibit excellent mechanical, electrical and optical properties with extraordinary strength and flexibility. These properties of graphene can be utilized in various applications like flexible transparent electrodes, touch screen, solar cells, high speed electronics, analog high frequency devices, sensors, photo detectors, capacitors and gas barriers etc. The properties are summarized in Table 1.4.

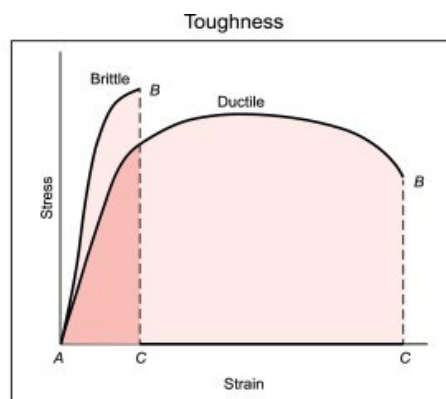
**Table 1.4** Properties of graphene

Property	Value	Comparison with other materials	References
Breaking strength	42 N/m	More than 100 times greater than steel	[61]
Elastic limit	~20%		[62]
Carrier mobility at room temperature	200,000 cm <sup>2</sup> V <sup>-1</sup> S <sup>-1</sup>	More than 100 times higher than SI	[63]
Thermal conductivity	~5000 Wm <sup>-1</sup> K <sup>-1</sup>	More than 100 times higher than Cu	[64]
Maximum current density	>10 <sup>8</sup> A/cm	~100 times larger than Cu	[65]
Optical absorption coefficient	2.3 %	~50 times higher than GaAs	[66]



### 1.3 Toughening agents

Various studies are reported in the area of polymer nanocomposites in order to develop polymers with high cross-link density, high glass transition temperature, high modulus and strength. But with increase in the cross-link density brittleness also increases due to poor resistance to crack initiation and propagation. So improving the fracture toughness of these polymer composites is very important. The addition of toughening agents to a polymer matrix usually increases the overall ductility of the polymer over a wide range of temperature but also improves the resistance to notch sensitivity and toughness, reduces water absorption etc. The toughness of a material depends on the energy of dissipation or energy absorbed in the fracturing part. It can be controlled by introducing a second phase particles in the polymer matrix. Incorporating rubber domains in to the polymer matrix [67-69], modification by thermoplastics [70, 71] and high modulus particulates [72] etc. are the common methods employed for the toughness enhancement of thermosetting polymers.



Toughness = the ability to absorb energy up to fracture  
= the total area under the strain-stress curve up to fracture

**Fig. 1.6** Toughness from stress-strain curve

### 1.3.1 Vegetable oil derivatives as toughening agents

In the past decade there is a growing trend to incorporate natural oils and their derivatives into thermosetting polymers in order to fabricate bio-based polymer systems with improved properties. Soybean oil, linseed oil, castor oil, palm oil and tung oil are the commonly used vegetable oils for toughness enhancement in thermosetting polymers. The unique molecular structure, bio-degradability and low cost are the advantages of these bio-systems compared to conventional modifiers. Mehta et al. in 2004 reported the use of methyl esters of soybean oil for the impact strength modification of polyester resins. They observed 90% enhancement in the impact strength for the modified resin compared to unmodified ones [73]. Ghorui et al. utilized 5 wt% of maleated castor oil as a biomodifier in UPR/fly ash composites and observed about 52% improvement in impact strength [74]. Liu et al. used tung oil triglycerides for the modification of DCPD terminated polyester resins and 373% improvement in impact strength by the addition of 14.8 wt% oil [75].

### 1.3.2 Toughening mechanism

The blends of vegetable oil and polymer matrix form semi immiscible systems as in the case of elastomeric additive toughening process. After curing the oil phase provided the rubbery structure. It acts as a toughening agent which absorbs the impact energy and delays the catastrophic failure. The major toughening mechanism observed in thermosetting polymers are shear yielding and crazing of the polymer matrix and cavitation of the rubber phase. Either a single mechanism or a combination of different mechanism may happen depending on the polymer systems. By the incorporation of a

rubbery phase in thermosets, phase separated morphology is obtained which further results in the formation of microcracks after curing. These microcracks or micro voids helps in the dissipation of impact energy and reduce the crack propagation. The typical mechanism observed in rubber toughened epoxies is shown in Fig. 1.7 [76].

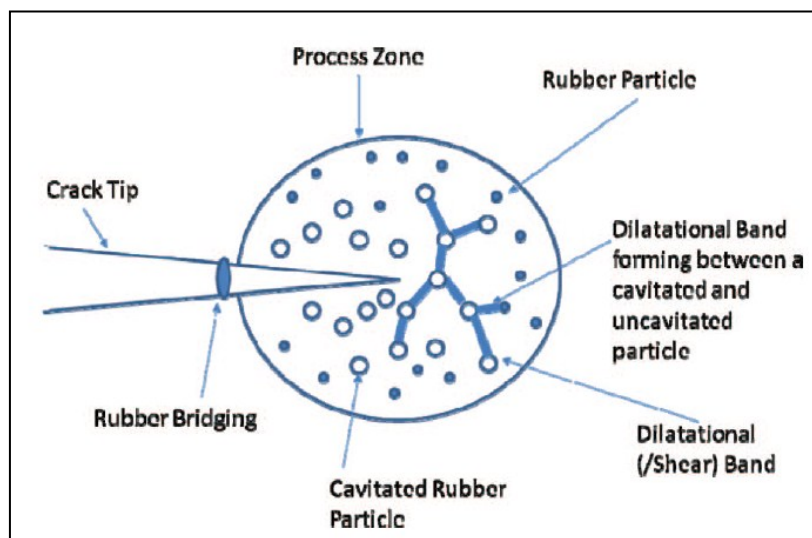


**Fig. 1.7** Rubber toughening mechanism

### 1.3.3 Rubber seed oil (RSO)

Rubber tree (*Hevea brasiliensis*) is economically cultivated for the production of latex as a source of natural rubber in various parts of the country. Kerala is the leading rubber plantation state in India which accounts to 92% of countries total natural rubber production. Natural rubber is extensively used in many applications and products in various fields. But the rubber seed has not yet received a serious attention. However RSO is utilized for bio diesel production [77-80] and bio lubricant preparation [81, 82]. RSO is an unsaturated triglyceride made of

fatty acid chains attached to glyceride unit which is extracted from rubber seeds by different methods (Fig. 1.8). It consists of saturated fatty acids like palmitic acid and stearic acid and unsaturated fatty acids like oleic acid, linoleic acid and linolenic acid. The functional groups present on RSO can be properly utilized which makes this non-edible oil a good candidate for toughening of polymers.



**Fig. 1.8** (a) Rubber seeds and (b) rubber seed oil

#### **1.4 Unsaturated polyester resin/carbon nanotube composites**

Carbon nanotubes due to their inherent mechanical, thermal and electrical properties can be employed for the preparation of polymer nanocomposites. Till 2007 there is no reported work in the literature on the processing and properties of CNT/polyester systems. Seyhan et al. in 2007 reported some critical aspects related to the processing of CNT/UPR nanocomposites [83]. They compared 3-roll-milling and sonication technique for the processing of CNT/UPR system and their study revealed that 3-roll-milling is the more adequate technique for the dispersion of CNTs in the polymer matrix compared to sonication and direct mixing. In another study Sayhan et al. reported the rheological properties of polyester-

vinyl ester resin suspensions containing multi-walled carbon nanotubes with and without amine functionalization. Amine functionalized MWCNT composite showed higher storage modulus and  $T_g$  values [84].

Battisti et al. reported the preparation of electrically conductive UPR/MWCNT nanocomposites by triple-roll milling and shear mixing technique [85]. The composites exhibited a percolation threshold at 0.026 wt% loading of nanotubes. The cured composite exhibited a maximum conductivity of 0.13 S/m for 0.3 wt% loading. The thermal properties of CNT/polyester nanocomposites were reported by Ciupagea et al. They observed an increasing trend for specific heat and co-efficient of thermal expansion with increase in MWCNT content. The mechanical properties of MWCNT/polyester nanocomposites were investigated by Shokrieh et al and Makki et al. MWCNT at low weight fractions improved the tensile and flexural properties of polyester resin [86, 87].

Thostenson et al. investigated the use of calendaring approach for the dispersion of MWCNT in vinyl ester resin for the fabrication of CNT/vinylester composites [88]. They obtained an electrical percolation threshold below 0.1 wt% of CNT loading. The solution dispersion and casting method were utilized for the preparation of MWCNT/UPR nanocomposites by Moshiul Alam et al. and thermo-mechanical properties of the composite were investigated [89]. MWCNTs are pre-dispersed in THF solvent before processing. An enhancement in tensile strength,  $T_g$  and stiffness is observed for the nanocomposites compared to neat resin. A comparative study on the properties of UPR, MWCNT-UPR and THF-MWCNT UPR was conducted by Beg et al. The THF-MWCNT-UPR

composite exhibited highest viscosity, thermal stability and improved mechanical properties compared to other systems [90]. The pre-dispersion of MWCNT in THF enhanced the homogeneous dispersion of MWCNT in UPR matrix. Moreover they reported the formation of hydrogen bond between MWCNTs and UPR which was supported by FTIR spectra (Fig. 1.9). A detailed study on the fracture behaviour of MWCNT reinforced polyester nanocomposites is reported by Moshiul Alam et al [91]. A rough surface is observed in the case of MWCNT UPR composite which gives a ductile nature while the smooth surface of UPR accounts for its brittle nature. Thus the pre-dispersed MWCNT in THF interact well with UPR forming a rough surface morphology which finally improves the fracture behaviour of UPR.

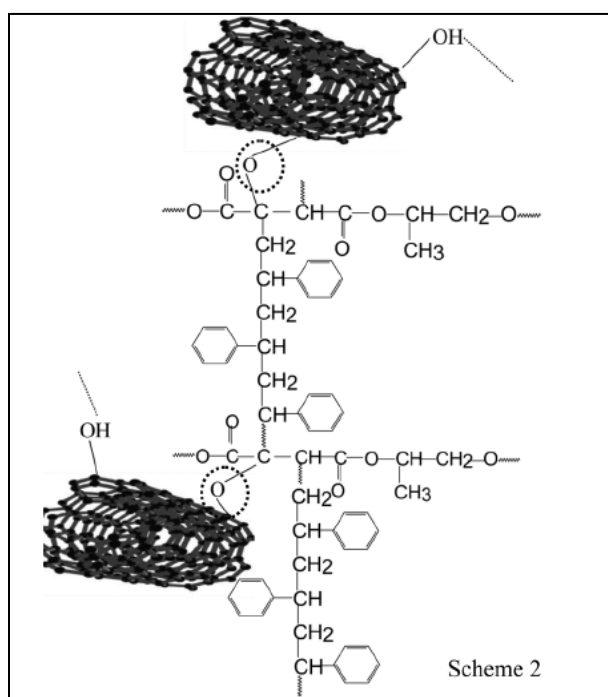


**Fig. 1.9** Interaction between MWCNT and UPR [90]

## 1.5 Unsaturated polyester resin/reduced graphene oxide (rGO) composites

Glass fiber reinforced unsaturated polyester resin has been utilized for decades in many applications including automotive and construction due to their low cost and ease of processing. However their mechanical strength and thermal stability is low compared to other thermosetting resins. Moreover its insulating nature hinders its application in many areas. Several type of fillers like clay, silicates, carbon nanofibers and CNTs have been incorporated in order to improve the properties of polyester resin. Only a few works are reported on rGO/UPR composites. Bora et al. reported the preparation of rGO/UPR composite films with improved mechanical strength, thermal stability and antibacterial activity. GO was prepared from natural graphite by modified Hummers method. GO was reduced using hydrazine hydrate to produce rGO. The fabrication process is illustrated in Fig. 1.10 [92].

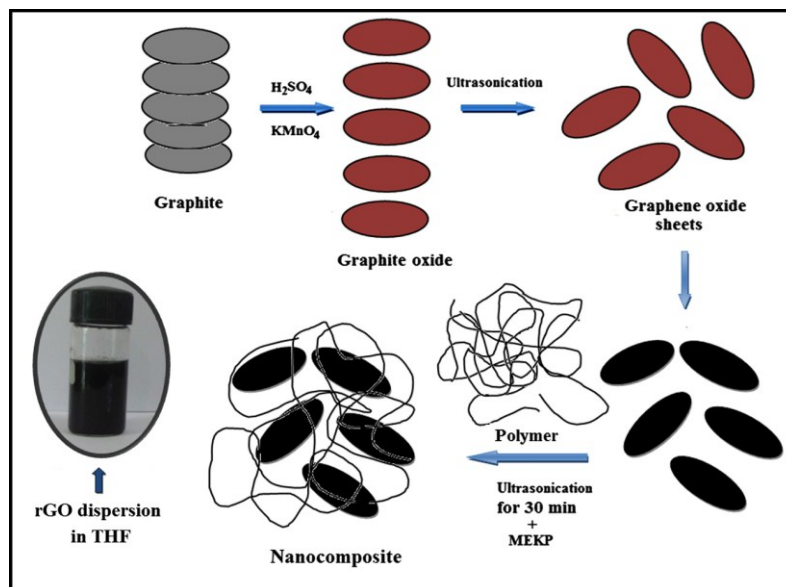


**Fig. 1.10** Fabrication process of rGO/UPR composites

About 123% increase in tensile strength and 87% increase in tensile modulus was obtained for 3 wt% rGO loading. The composite showed significant antibacterial activity towards five different kinds of bacterial strains, which altogether offers new opportunities for the development of new range of materials.

Swain et al. used graphene nano sheets (GNS) in order to improve the mechanical and electrical properties of UP resins. About 52% improvements in tensile strength and 92% improvement in flexural strength was obtained for 0.05 % GNS concentration [93]. The curing dynamics and network formation of cyanate ester resin/GO nanocomposites was studied by Wang et al. by means of differential scanning calorimetry (DSC) [94]. The incorporation of GO into the resin showed a strong catalytic effect on the curing of polyester resin. Yu et al. prepared epoxy/GO composites and got improved thermal conductivity, elastic modulus and tensile strength [95]. Liu et al. reported a novel route to prepare PE/GR composites via simultaneous dispersion and thermo-reduction of GO during in-situ melt polycondensation. The composite showed a significant improvement in tensile strength and elongation at break [96]. Bindu Sharmila et al. prepared microwave exfoliated reduced graphene oxide (MERGO) from natural graphite and fabricated MERGO-epoxy nanocomposite by *in-situ* polymerization. At 0.25 phr MERGO loading the nanocomposites exhibited 32%, 103% and 85% improvement in tensile, impact and flexural strength [97] respectively. A remarkable increase in the dielectric properties and conductivity is also obtained for the nanocomposites.



The chemically/thermally reduced graphene (rGO) sheets exhibits inferior electrical transport and mechanical properties when compared with pure graphene due to the restacking of layers because of the van der Waals interactions. Recently, graphene nanosheets decorated with nanoparticle (nanohybrids) have been extensively investigated to preserve some unique properties of graphene. Among these, silver nanoparticles received great attention because of its unique optical, electrical and thermal conductivity properties. They provide an efficient way to solve the separation problem of graphene since they can act as spacers to keep the layers separated and efficiently suppress the restacking of GNS [98].

Luan et al. reported the synergistic effect of 1D Ag nanowires and 2D chemically reduced graphene on epoxy resin [99]. The newly developed nanocomposites exhibited enhanced electrical, thermal and mechanical properties. About 50% improvement in the break strength was observed for the composite. Chen et al. reported the fabrication of epoxy resin based thermal interfacial materials by the incorporation of silver decorated graphene nanosheets. Effective thermal conductive networks are formed by the synergistic effect of Ag and GNS. SEM images of Ag GNS samples with different Ag loadings are shown in Fig. 1.11 [100].

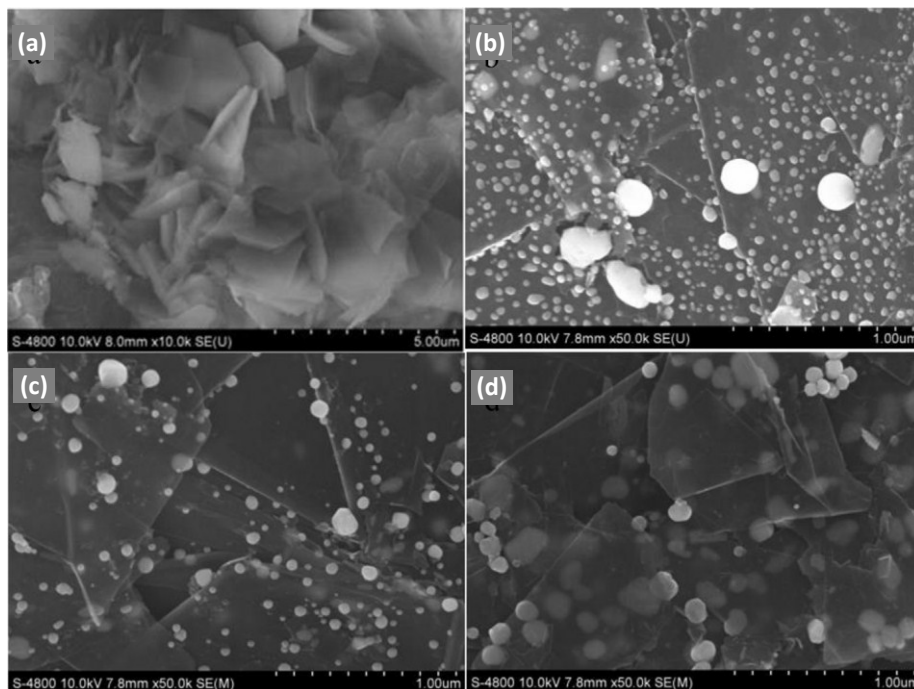


**Fig. 1.11** SEM images of Ag-GNS samples with different Ag loading (a) 0 mol% (b) 0.5 mol% (c) 1.0 Mol% and (d) 1.5 mol%.

## 1.6 Vegetable oil modified unsaturated polyester resins

Bio-based polymer systems are well preferred over petroleum based polymers while considering the environmental factors. The modification of UP resins with functionalized vegetable oils could be of intense research in future. Miyagawa et al. utilized epoxidised methyl linseedate (EML) for the modification of UP resin. The bio-based systems exhibited low storage modulus and cross-link density compared to neat resin but the heterogeneous surface morphology imparts enhanced impact strength for the system. This is due to the fact that the rubbery phase caused greater energy dissipation during crack propagation under impact loading [101].

In another study Miyagawa et al. reported the use of epoxidised methyl soyate (EMS) for the modification of UP resin. In this case although phase separation was observed the izod impact strength value was constant with changing amount of EMS [102].

Haq et al. studied the thermo-physical properties of nanoclay reinforced epoxy/EMS blends. They observed that addition of EMS increased the toughness and decreased the stiffness and the decrease can be compensated by nanoclay addition. UPR composites with improved stiffness-toughness balance produced hybrid multifunctional nanocomposites [103]. Das et al. used tung oil as a toughening agent in UP resins. Here in addition to impact strength, the flexural strength, breaking energy and strain percentage also improved which is quite different from rubber toughened plastics [104]. Haq et al. studied the synergistic effect of UPR/EML blends and nanoclay. Reduction in mechanical and transient properties can be recovered by the addition of nanoclay [105].

Liu et al. developed tung oil based monomer for the preparation of rigid thermosetting polymers. Maleinated tung oil pentaerythritol (TOPERMA) was polymerized with styrene. This can be a potential substitute for petroleum products [106]. Later Liu et al. studied the structure property relationship of TOPERMA with different styrene contents. They observed a phase separated morphology due to the incompatibility of TOPERMA and styrene. The matrix of TOPERMA with 33% styrene exhibited good toughness stiffness balance. Liu et al. in 2014 developed bio based unsaturated polyester resin containing highly

functionalized castor oil (COPERMA) [107]. COPERMA was mixed with 35% styrene before blending with UPR. The UPR/COPERMA system exhibited better thermal and mechanical properties when the amount of COPERMA resin was up to 10 wt%. At 20 wt% the tensile strength and storage modulus decreased gradually but not as much as reported in other systems. But other properties like cross-link density and impact strength were improved.

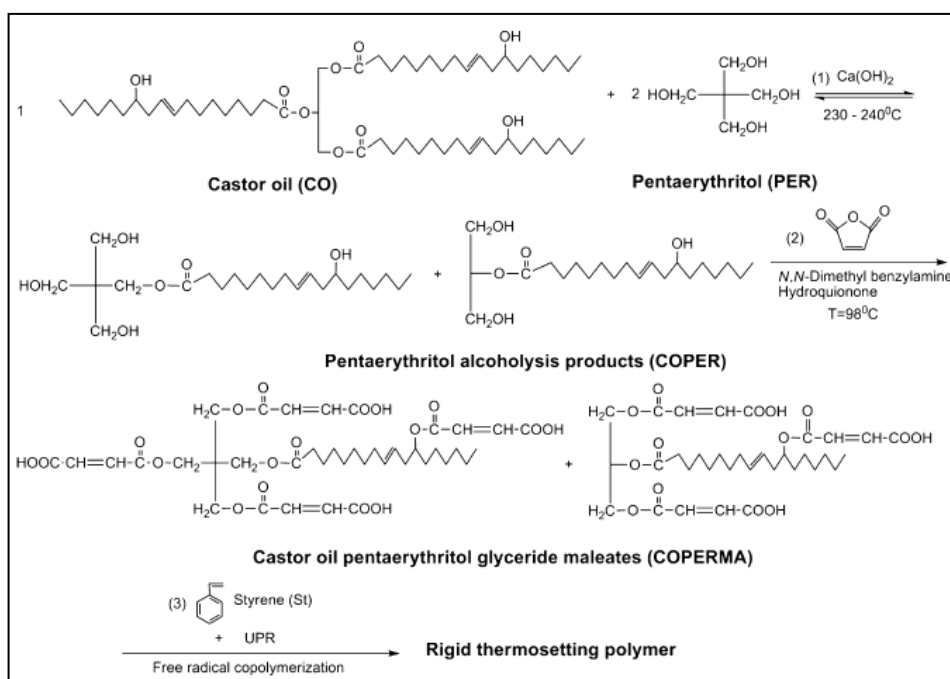


**Fig 1.12** Reaction scheme for the synthesis of COPERMA from castor oil triglyceride and its copolymerization with UPR and styrene [107].

Based on the above observations and literature survey unsaturated polyester resin can be modified using several methods in order to enhance its mechanical, thermal and electrical properties. In all these cases the

homogeneous dispersion of fillers and additives is the key factor which enhances the final properties of the thermosetting polymer [108]. The polymer matrix filler interfacial interaction plays a crucial role in tuning the properties of the polymer composite. It depends on filler nature, shape and concentration. The interaction can be enhanced by increasing the specific contact area between fillers and matrix, i. e., by reducing the filler particle size. Considering this factor nanofillers are preferred over micro and macro fillers to reinforce the polyester systems [109-112]. Moreover the amount of nanofillers used is very less compared to micro and macro fillers. A new elastic contribution is obtained from this nanofillers, which slows down the chain mobility, enhances the glass transition temperature by increasing the rigid phase volume fraction [113-117].

### **1.7 Scope and objective of the work**

Two types of modifications are proposed on unsaturated polyester resin in order to improve its mechanical, thermal and electrical properties. First method is development of polymer nanocomposites based on UPR and nanofillers and second is development of a blend based on UPR and vegetable oil derivative. Multi-walled carbon nanotubes (MWCNTs) and reduced graphene oxide (rGO) are the fillers selected for the preparation of unsaturated polyester resin based nanocomposites. Fatty acid methyl esters (FAMES) prepared from rubber seed oil (RSO) is selected as a vegetable oil derivative for preparing the blend. The first modification is focused on the improvement of mechanical and dielectric properties of polyester resin by the incorporation of rigid and stiff nanofillers while the second modification focused on the impact strength and toughness

properties of polyester resin by adding vegetable oil derivative. Stiffness and toughness are the two important factors to be considered in the case of UPR when it is employed for commercial structural applications and we propose to address both these properties in this study.

The specific objectives of the present work are

- To functionalize MWCNT using maleic anhydride and to study its effect on the unsaturated polyester resin in comparison to unmodified MWCNT.
- To develop UPR/MWCNT nanocomposites by solution dispersion technique.
- To prepare reduced graphene oxide (rGO) from natural graphite by water assisted modified Hummers method.
- To prepare silver nanoparticle decorated rGO (rGO-Ag) nanohybrid and its effect on unsaturated polyester resin in comparison to rGO.
- To develop UPR/rGO and UPR/rGO-Ag nanocomposites by solution dispersion technique.
- To investigate the mechanical and dielectric properties of UPR/MWCNT and UPR/rGO/rGO-Ag nanocomposites
- To prepare fatty acid methyl esters from RSO by two step transesterification process.
- To develop UPR/RSO FAME blends.
- To investigate the static and dynamic mechanical properties of UPR/FAMEs of RSO blends.

## References

- [1] Elliott, J. (2016). Polyester resins, unsaturated, *Chemical Economics Handbook*, London: I H S Markit.
- [2] Kazmierski, C. (2013). Growth opportunities in the Indian composites unsaturated polyester resin markets, Texas: Lucintel.
- [3] Thostenson, E. T. (1983). *Composite design guide*, New York: Center for composite materials, University of Delaware.
- [4] Berins, M. L. (1991). *SPI Plastics engineering handbook of the society of plastic industry*, Verlag: Springer, 74-77.
- [5] Baskaran, M., Sarojadevi, C.T., Viyakumar, J. (2011). Unsaturated polyester nanocomposites filled with nano alumina. *Mater. Sci.*, 46, 4864-4871.
- [6] Riew, C. K., Rowe, E. H., Siebert, A. R. (1976). Rubber toughened thermosets. *Toughness and brittleness of plastics, Advanced Chemistry*, Chapter: 154, 326-343.
- [7] Yang, Y. S., Lee, L. J. (1988). Rheokinetic studies of unsaturated polyester resins. *Polym. Process Eng.*, 5, 327-356.
- [8] Hsu, C. P., Lee, L. J. (1993). Chemorheological analysis of unsaturated polyester-styrene copolymerization. *Polymer*, 34, 4495-4506.
- [9] Gündüz, G., Öztürk, S. (1994). Flame retardancy and mechanical properties of 1, 3 propylene glycol based unsaturated polyester. *Polym. Plast. Technol. Eng.*, 33, 245-252.
- [10] Mapleston, P. (1993). Vinyl ester: Performance upgrades fit many markets. *Mod. Plast.*, 70, 40-41.
- [11] Sagi-Mana, D., Narkis, M., Siegmann, A., Joseph, R., Dodiuk, H. (1998). The effect of marine environment on a vinyl ester resin and its highly filled particulate quartz composites. *J. Appl. Polym. Sci.*, 69, 2229-2234.
- [12] George, J., Sreekala, M.S., and Thomas, S. (2001). A Review on Interface Modification and Characterization of Natural Fiber Reinforced Plastic Composites. *Polym. Eng. Sci.*, 41, 1471–1485.

- [13] Herrera-Franco, P.A., Valadez-Gonzalez, Cervantes, U.C.M. (1997). Development and characterization of a HDPE–Sand–Natural Fiber Composite. *Compos. Part B: Eng.*, 28B, 331–343.
- [14] Maulida, A., Nasir, M., and Khalil, H.P.S.A. (2000). Hybrid Composites Based on Natural Fiber. *Proceedings of Symposium on Polymeric Materials*. Penang: USM Press, 216–219.
- [15] Manikandan, V., Ponnambalam, S. G., Thomas, S., Velmurugan, R. (2004). Mechanical properties of short and uni-directional palmyra fiber reinforced composite. *Int. J. Plast. Technol.*, 205–216.
- [16] Luyt, A. S., Malunka, M. E., Krump, H. (2005). Composites of low density polyethylene and short Sisal fibers: the effect of wax addition and peroxide treatment on thermal properties. *Thermochim. Acta*, 426, 101–107.
- [17] Pothan, L. A., Oommen, Z., Thomas, S. (2003). Dynamic mechanical analysis of banana fiber reinforced polyester composites. *Compos. Sci. Technol.*, 63, 283-293.
- [18] Sreekala, M. S., Kumaran, M. G, Joseph, R., Thomas, S., (2001). Stress relaxation behaviour in composites based on short oil-palm fibers and phenol formaldehyde resin. *Compos. Sci. Technol.*, 61, 1175–88.
- [19] Herrera-Franco, P.J., Valadez-Gonzalez, A. (2004). Mechanical properties of continuous natural fiber-reinforced polymer composites. *Compos. A: Appl. Sci. Manuf.*, 35, 339–45.
- [20] Pratheep, K. A., Singh, R. P., Sarwdie B. D. (2005). Degradability of composites prepared from ethylene–propylene copolymer and jute fiber under accelerated aging and biotic environment. *Mater. Chem. Phys.*, 92, 458–69.
- [21] Aziz, S. H., Ansel, M. P. (2004). The effect of alkalization and fiber alignment on the mechanical and thermal properties of Kenaf and hemp bast fiber composites. *Compos. Sci. Technol.*, 64, 1219–30.
- [22] Espert, A., Vilaplana, F., Karlsson, S. (2004). Comparision of water absorption in natural cellulosic fibers from wood and one year crops in polypropylene composites and its influence on their mechanical properties. *Compos. A: Appl. Sci. Manuf.*, 35, 1267–76.



- [23] Iijima, S. (1991). Helical microtubules of graphitic carbon. *Nature*, 354, 56–8.
- [24] Saito, R., Sato, K., Oyama, Y.,... Dresselhaus, M. S. (2005). Cutting lines near the Fermi energy of single-wall carbon nanotubes. *Phys. Rev. B.*, 72, 1-4.
- [25] Cheng, M. (2002). *Preparation, structure, properties and applications of carbon nanotubes*. Beijing: Chemical Industry Publishing House.
- [26] Sharma, R., Sharma, A. K., Sharma, V. (2015). Synthesis of carbon nanotubes by arc discharge and chemical vapor deposition method with analysis of its morphology, dispersion and functionalization characteristics. *Cogent Eng.*, 2, 1-8.
- [27] Ebbesen, T. W., Ajayan, P. M. (1992). Large-scale synthesis of carbon nanotubes. *Nature*, 358, 220–222.
- [28] Guo, T., Nikolaev, P., Thess, A., Colbert, D., Smalley, R. E. (1995). Catalytic growth of single-walled nanotubes by laser vaporization. *Chem. Phys. Lett.*, 243, 49–54.
- [29] Smiljanic, O., Stansfield, B.L., Dodelet, J.-P., Serventi, A., Désilets, S. (2002). Gas-phase synthesis of SWNT by an atmospheric pressure plasma jet. *Chem. Phys. Lett.*, 356, 189–193.
- [30] Smiljanic, O. (2008). *US Patent No. US20080226536A1*. Retrieved from <http://patents.google.com/patent/US20080226536A1/en>.
- [31] Walker Jr., P. L., Rakszawski, J. F., Imperial, G. R. (1959). Carbon formation from carbon monoxide-hydrogen mixtures over iron catalysts. I. Properties of carbon formed. *J. Phys. Chem.*, 63, 133–140.
- [32] José-Yacamán, M., Miki-Yoshida, M., Rendón, L., Santiesteban, J. G. (1993). Catalytic growth of carbon microtubules with fullerene structure. *Appl. Phys. Lett.*, 62, 657-659.
- [33] Diaz, E., Ordonez, S., Vega, A. (2007). Adsorption of volatile organic compounds onto carbon nanotubes, carbon nanofibers, and high surface-area graphites. *J. Colloid Interface Sci.*, 305, 7–16.

- [34] Ma, P.C., Siddiqui, N.A., Marom, G., Kim, J.K. (2010). Dispersion and functionalization of carbon nanotubes for polymer-based nanocomposites: a review. *Compos. A: Appl. Sci. Manuf.*, 41, 1345–1367.
- [35] Xie, X. L., Mai, Y.W., Zhou, X. P. (2005). Dispersion and alignment of carbon nanotubes in polymer matrix: a review. *Mat. Sci. Eng. R.*, 49, 89–112.
- [36] Breton, Y., Dresarmot, G., Salvetat, J. P., Bonnamy, S. (2004). Mechanical properties of multiwall carbon nanotubes/epoxy composites: influence of network morphology. *Carbon*, 42, 1027–30.
- [37] Sun, C. H., Yin, L. C., Li, F., Lu, G. Q., Cheng, H. M. (2005). Van der Waals interactions between two parallel infinitely long single-walled nanotubes. *Chem. Phys. Lett.*, 403, 343–346.
- [38] Hilding, J., Grulke, E. A., Zhang, Z. G., Lockwood, F. (2003). Dispersion of Carbon Nanotubes in Liquids. *J. Disp. Sci. Tech.*, 24, 1-41.
- [39] Mackay, M. E., Tuteja, A., Duxbury, P. M., Hawker, C. J., Van Horn, B., Guan, Z., Chen, G., Krishnan, R. S. (2006). General strategies for nanoparticle dispersion. *Science*, 311, 1740 – 43.
- [40] Hu, H., Zhao, B., Itkis, M.E., Haddon, R. C. (2003). Nitric acid purification of single-walled carbon nanotubes. *J. Phys. Chem. B.*, 107, 13838–42.
- [41] Martinez, M.T., Callejas, M. A., Benito, A.M., Cochet, M., Seeger T., Anson A. (2003) Sensitivity of single-wall carbon nanotubes to oxidative processing: structural modification, intercalation and functionalization. *Carbon*, 41, 2247–56.
- [42] Ziegler, K. J., Gu, Z., Peng, H., Flor, E. L., Hauge, R. H., Smalley, R. E. (2005). Controlled oxidative cutting of single-walled carbon nanotubes. *J. Am. Chem. Soc.*, 127, 1541–7.
- [43] Kim, Y. J., Shin, T.S., Choi, H.D., Kwon, J.H., Chung, Y.C., Yoon, H.G. (2005). Electrical conductivity of chemically modified multiwalled carbon nanotube/epoxy composites. *Carbon*, 43, 23–30.

- [44] Wepasnick, K. A., Smith, B. A., Bitter, J. L., and Fairbrother, D. H. (2010). Chemical and structural characterization of carbon nanotube surfaces. *Anal. Bioanal. Chem.*, 396, 1003-1014.
- [45] Brundle, C. R., Evans, C.A., Wilson, S. (1992). *Encyclopedia of materials characterization*. Stoneham: Butterworth-Heinemann.
- [46] Vickerman, J. C. (1997). *Surface analysis: The principal techniques*, 1st edn. Chichester : John Wiley & Sons.
- [47] Povstugar, V. I., Mikhailova, S. S., Shakov, A. A. (2000). Chemical derivatization techniques in the determination of functional groups by X-ray photoelectron spectroscopy. *J. Anal. Chem.*, 55, 405–416.
- [48] Xing, Y., Dementev, N., Borguet, E. (2007). Chemical labeling for quantitative characterization of surface chemistry. *Curr. Opin. Solid State Mater. Sci.*, 11, 86–91.
- [49] Boehm, H. P., Diehl, E., Heck, W., Sappok, R. (1964). Surface oxides of carbon. *Angew Chem. Int. Edit.*, 3, 669–677.
- [50] Speyer, R.F. (1994). *Thermal analysis of materials*. New York: Marcel Dekker.
- [51] Kirkland, A. I., Hutchison, J. L. (eds) (2007). *Nanocharacterisation*. Cambridge : The Royal Society of Chemistry.
- [52] Cheng, J., Fernando, K. A. S., Veca, L.M., Sun, Y.P., Lamond, A. I., Lam, Y.W., Cheng, S.H. (2008). Reversible accumulation of PEGylated single-walled carbon nanotubes in the mammalian nucleus. *ACS Nano*, 2, 2085–2094.
- [53] Kaimi, M., Solati, N., Amiri, M., Mirshekari, H., Mohamed, E., Taheri, M., Hamblin, M. R. (2015). Carbon nanotubes part I: preparation of a novel and versatile drug-delivery vehicle. *Expert Opin. Drug Deliv.*, 12, 1071-1087.
- [54] Edwards, R. S., & Coleman, K. S. (2013). Graphene synthesis: relationship to applications. *Nanoscale*, 5, 38-51.

- [55] Warner, J. H., Schaffel, F., Bachmatiuk, A., Rummeli, M. H. (2012). *Graphene: Fundamentals and emergent applications*, Oxford : Elsevier.
- [56] Novoselov, K. S., Geim, A. K., Morozov, S. V., Jiang, D. A., Zhang, Y., Dubonos, S. V., Firsov, A. A. (2004). Electric field effect in atomically thin carbon films. *Science*, 306, 666-669.
- [57] Dato, A., Radmilovic, V., Lee, Z., Phillips, J., Frenklach, M. (2008). Substrate-free gas-phase synthesis of graphene sheets. *Nano lett.*, 8, 2012-2016.
- [58] Reina, A., Jia, X., Ho, J., Nezich, D., Son, H., Bulovic, V., Kong, J. (2009). Large area, few-layer graphene films on arbitrary substrates by chemical vapor deposition. *Nano lett.*, 9, 30-35.
- [59] Park, S., Ruoff, R. S. (2009). Chemical methods for the production of graphenes. *Nat. nanotechnol.*, 4, 217-224.
- [60] Segal, M. (2009). Selling graphene by the ton. *Nat. nanotechnol.*, 4, 612-614.
- [61] Lee, C., Wei, X., Kysar, J. W., Hone, J. (2008). Measurement of the elastic properties and intrinsic strength of monolayer graphene, *Science*, 321, 385–388.
- [62] Kim, K. S., Zhao, Y., Jang, H., Lee, S. Y., Kim, J. M.,... Hong, B. H. (2009). Large-scale pattern growth of graphene films for stretchable transparent electrodes. *Nature*, 457, 706–710.
- [63] Chen, J. H., Jang, C., Xiao, S., Ishigami, M., Fuhrer, M. S. (2008). Intrinsic and extrinsic performance limits of graphene devices on SiO<sub>2</sub>, *Nat. Nanotechnol.*, 3, 206–209.
- [64] Ghosh, S., Bao, W., Nika, D. L., Subrina, S., Pokatilov, E. P., Lau, C. N., Balandin, A. A. (2010). Dimensional crossover of thermal transport in few-layer graphene. *Nature Mater.*, 9, 555–558.
- [65] Murali, R., Yang, Y., Brenner, K., Beck, T., and Meindl, J. D. (2009). Breakdown current density of graphene nanoribbons. *Appl. Phys. Lett.*, 94, 243114.

- [66] Nair, R. R., Blake, P., Grigorenko, A. N., Novoselov, K. S., Booth, T. J., Stauber, T., Geim, A. K. (2008). Fine structure constant defines visual transparency of graphene. *Science*, 320, 1308.
- [67] Maspoch, M. L. L., Martinez, A. B. (1998). Toughening of unsaturated polyester with rubber particles, Part I: morphological study. *Polym. Eng. Sci.*, 38, 282–289.
- [68] Salamone, J.C. (1996). *Polymeric Materials Encyclopedia. In: Unsaturated Polyester Resins (Toughening with Liquid Rubber)*. Boca Raton, FL: CRC Press, 8489.
- [69] Roy, P. K., Iqbal, N., Kumar, D., Rajagopal, C. (2014). Rubber toughening of unsaturated polyester with core–shell poly(siloxane)-epoxy microspheres. *Polym. Bull.*, 71, 2733–2748.
- [70] Ray, D. (2008). Modification of the dynamic damping behavior of unsaturated polyester resin. *J. Reinf. Plast. Compos.*, 27, 1525–1532.
- [71] Salamone, J. C. (1998). *Concise polymeric materials encyclopedia. In: unsaturated polyester resins (Toughening with Elastomers)*. Boca Raton, FL: CRC Press, 8486.
- [72] Ahmadi, M., Moghbeli, M. R., Shokrieh M. M. (2012). Unsaturated polyester-based hybrid nanocomposite: fracture behavior and tensile properties. *J. Polym. Res.*, 19, 1-12.
- [73] Mehta, G., Mohanty, A. K., Misra, M., Drzal, L. T. (2004). Biobased resin as a toughening agent for biocomposites. *Green Chem.*, 6, 254-258.
- [74] Ghorui, S., Bandyopadhyay, N. R., Ray, D., Sengupta, S., Kar, T. (2011). Use of maleated castor oil as biomodifier in unsaturated polyester resin/fly ash composites. *Ind. Crops Prod.*, 34, 893–899.
- [75] Liu, C., Li, J., Lei, W., Zhou, Y. (2014). Development of biobased unsaturated polyester resin containing highly functionalized castor oil. *Ind. Crops Prod.*, 52, 329–337.
- [76] Huang, Y., Kinloch, A.J. (1992). Modelling of the toughening mechanisms in rubber modified epoxy polymers: 2. A quantitative description of the microstructure fracture property relationships. *J. Mater. Sci.*, 27, 2763–2769.

- [77] Onoji, S. E., Iyuke, S. E., Igbafe, A. I., Nkazi, D. B. (2016). Rubber seed oil: A potential renewable source of biodiesel for sustainable development in sub-Saharan Africa. *Energy Convers. Manage.*, 110, 125–134.
- [78] Ramadhas, A. S., Jayaraj, S., Muraleedharan, C. (2005). Biodiesel production from high FFA rubber seed oil. *Fuel*, 84, 335-340.
- [79] Atabani, A. E., Silitonga, A. S., Ong, H. C., Mahlia, T. M. I., Masjuki, H. H., Badruddin, I. A., Fayaz, H. (2013). Non-edible vegetable oils: A critical evaluation of oil extraction, fatty acid compositions, biodiesel production, characteristics, engine performance and emissions production. *Renew. Sust. Energ. Rev.*, 18, 211–245.
- [80] Takase, M., Zhao, T., Zhang, M., Chen, Y., Liu, H., Yang, L., Wu, X. (2015). An expatiated review of neem, jatropha, rubber and karanja as multipurpose non-edible biodiesel resources and comparison of their fuel, engine and emission properties. *Renew. Sust. Energ. Rev.*, 43, 495–520.
- [81] Aravind, A., Nair, P. K., Joy, M. L. (2016). Physio-chemical characterization of rubber seed oil (*Hevea brasiliensis*)-A biodegradable lubricant substitute. *Technol. Lett.*, 3, 20-24.
- [82] Kamalakar, K., Rajak, A. K., Prasad, R. B. N., Karuna, M. S. L. (2013). Rubber seed oil-based biolubricant base stocks: A potential source for hydraulic oils. *Ind. Crops Prod.*, 51, 249– 257.
- [83] Seyhan, A. T., Gojny, F. H., Tanoglu, M., Schulte, K. (2007). Critical aspects related to processing of carbon nanotube/unsaturated thermoset polyester nanocomposites. *Eur. Polym. J.*, 43, 374–379.
- [84] Seyhan, A. T., Gojny, F. H., Tanoglu, M., Schulte, K. (2007). Rheological and dynamic-mechanical behavior of carbon nanotube/vinyl ester–polyester suspensions and their nanocomposites. *Eur. Polym. J.*, 43, 2836–2847.
- [85] Battisti, A., Skordos, A. A., Partridge, I. K. (2009). Percolation threshold of carbon nanotubes filled unsaturated polyesters. *Compos. Sci. Technol.*, 69, 1516–1520.

- [86] Shokrieh, M. M., Saeedi, A., Chitsazzadeh, M. (2013). Mechanical properties of multi-walled carbon nanotube/polyester nanocomposites. *J. Nanostructure Chem.*, 3, 1-5.
- [87] Makki, M. S. I., Abdelaal, M. Y., Bellucci, S., Salam, M. A. (2014). Multi-walled carbon nanotubes/unsaturated polyester composites: mechanical and thermal properties study. *Fuller. Nanotub. Car. Nanostr.*, 22, 820-833.
- [88] Erik, T. T., Saeed, Z., Tsu-Wei, C. (2009). Processing and electrical properties of carbon nanotube/vinyl ester nanocomposites. *Compos. Sci. Technol.*, 69, 801–804.
- [89] Moshiul Alam, A. K. M., Beg, M. D. H., Yunus, R. M. (2015). Influence of carbon nanotubes on the thermo-mechanical properties of unsaturated polyester nanocomposites. *IOP Conf. Ser.: Mater. Sci. Eng.*, 78, 012023.
- [90] Beg, M. D. H., Moshiul Alam, A. K. M., Yunus, R. M., Mina, M. F. (2015). Improvement of interaction between pre-dispersed multiwalled carbon nanotubes and unsaturated polyester resin. *J. Nanopart. Res.*, 17, 1-13.
- [91] Moshiul Alam, A. K. M., Beg, M. D. H., Yunus, R. M. (2016) Micro structure and fractography of multiwalled carbon nanotube reinforced unsaturated polyester nanocomposites. *Polym. Compos.*, 38, E462-E471.
- [92] Bora, C., Bharali, P., Baglari, S., Dolui, S. K., Konwar, B. K. (2013). Strong and conductive reduced graphene oxide/polyester resin composite films with improved mechanical strength, thermal stability and its antibacterial activity. *Compos. Sci. Technol.*, 87, 1–7.
- [93] Sarojini, S. (2013). Synthesis and Characterization of Graphene Based unsaturated polyester resin composites. *Trans. Electr. Electron. Mater.*, 14, 53-58.
- [94] Wang, X. (2012). Cyanate ester resin/graphene nanocomposite: Curing dynamics and network formation, *Eur. Polym. J.*, 48, 1034-1041.
- [95] Yu, A. (2007). Graphite nanoplatelet-epoxy composite thermal interface materials, *J. Phys. Chem. C*, 111, 7565-7569.

- [96] Liu, K. (2011). Preparation of polyester/reduced graphene oxide composites *via in situ* melt polycondensation and simultaneous thermo-reduction of graphene oxide, *J. Mater. Chem.*, 21, 8612-8617.
- [97] Bindu Sharmila, T.K., Nair, A. B., Abraham, B. T., Sabura Beegum, P. M., Thachil, E. T. (2014). Microwave exfoliated reduced graphene oxide epoxy nanocomposites for high performance applications. *Polymer*, 55, 3614-3627.
- [98] Li, Z., Wang, D., Zhang, M., Zhao, L. (2014). Enhancement of thermal conductivity of polymer composites with Ag-graphene hybrids as fillers. *Phys. Status Solidi A*, 211, 2142-2149.
- [99] Luan, V. H., Tien, H. N., Cuong, T. V., Kong, B. S., Chung, J. S., Kim, E. J., Hur, S. H. (2012). Novel conductive epoxy composites composed of 2-D chemically reduced graphene and 1-D silver nanowire hybrid fillers. *J. Mater. Chem.*, 22, 8649-8653.
- [100] Chen, L., Zhao, P., Xie, H., Yu, W. (2016). Thermal properties of epoxy resin based thermal interfacial materials by filling Ag nanoparticle-decorated graphene nanosheets. *Compos. Sci. Technol.*, 125, 17-21.
- [101] Miyagawa, H., Mohanty, A.K., Burgueno, R., Drzal, L.T., Misra, M. (2006). Development of biobased unsaturated polyester containing functionalized linseed oil. *Ind. Eng. Chem. Res.*, 45, 1014-1018.
- [102] Miyagawa, H., Mohanty, A.K., Burgueno, R., Drzal, L.T., Misra, M. (2007). Novel biobased resins from blends of functionalized soybean oil and unsaturated polyester resin. *J. Polym. Sci. Polym. Phys.*, 45, 698-704.
- [103] Haq, M., Burgueno, R., Mohanty, A.K., Misra, M. (2009). Bio-based unsaturated polyester/layered silicate nanocomposites: characterization and thermo-physical properties. *Compos. Part A.*, 40, 540-547.
- [104] Das, K., Ray, D., Banerjee, C., Bandyopadhyay, N.R., Mohanty, A.K., Misra, M. (2011). Novel materials from unsaturated polyester resin/styrene/tung oil blends with high impact strengths and enhanced mechanical properties. *J. Appl. Polym. Sci.*, 119, 2174-2182.



- [105] Haq, M., Burgueno, R., Mohanty, A.K., Misra, M. (2011). Bio-based polymer nanocomposites from UPE/EML blends and nanoclay: development, experimental characterization and limits to synergistic performance. *Compos. Part A.*, 42, 41–49.
- [106] Liu, C., Yang, X., Cui, J., Zhou, Y., Liu, H. (2012). Tung oil based monomers for thermosetting polymers; synthesis, characterization and copolymerization with styrene. *Bioresources*, 7, 447-463.
- [107] Liu, C.G., Li, J., Lei, W., Zhou, Y.H. (2014). Development of biobased unsaturated polyester resin containing highly functionalized castor oil. *Ind. Crops Prod.*, 52, 329–337.
- [108] Leblanc, J. L. (2002). Rubber filler interactions and rheological properties in filled compounds. *Prog. Polym. Sci.*, 27, 627-687.
- [109] Ehrburger-Dolle, F., Hindermann-Bischoff, M., Livet, F., Bley, F., Rochas, C., Geissler, E. (2001). Anisotropic ultra-small-angle x-ray scattering in carbon black filled polymers. *Langmuir*, 17, 329-334.
- [110] Zou, H., Wu, S., Shen, J. (2008). Polymer/silica nanocomposites: preparation, characterization, properties, and applications. *Chem. Rev.*, 108, 3893-3957.
- [111] Bokobza, L. (2007). Multiwall carbon nanotube elastomeric composites: A review. *Polymer*, 48, 4907-4920.
- [112] Heinrich, G., Klüppel, M., Vilgis, T. A. (2002). Reinforcement of elastomers. *Curr. Opin. Solid State Mater. Sci.*, 6, 195-203.
- [113] Cassagnau, P. (2008). Melt rheology of organoclay and fumed silica nanocomposites. *Polymer*, 49, 2183-2196.
- [114] Dutta, N. K., Choudhury, N. R., Haidar, B., Vidal, A., Donnet, J. B., Delmotte, L., Chezeau, J. M. (1994). High resolution solid-state nmr investigation of the filler-rubber interaction: 1. High speed 1H magic-angle spinning nmr spectroscopy in carbon black filled styrene-butadiene rubber. *Polymer*, 35, 4293-4299.

- [115] Berriot, J., Montes, H., Lequeux, F., Long, D., Sotta, P. (2002). Evidence for the shift of the glass transition near the particles in silica-filled elastomers. *Macromolecules*, 35, 9756-9762.
- [116] Zhu, Z., Thompson, T., Wang, S. Q., von Meerwall, E. D., Halasa, A. (2005). Investigating linear and nonlinear viscoelastic behavior using model silica-particle-filled polybutadiene. *Macromolecules*, 38, 8816-8824.
- [117] Maier, P. G., Goritz, D. (1996). Molecular interpretation of the Payne effect. *Kaut. Gummi Kunst.*, 49, 18-21.
- [118] Sarvestani, A. S. (2008). Modeling the solid-like behavior of entangled polymer nanocomposites at low frequency regimes. *Eur. Polym. J.*, 44, 263-269.

.....✂.....

---

The details of materials used, processing methods adopted and characterization techniques employed for the present work are described in this chapter.

---

## **2.1 Materials**

### **2.1.1 Unsaturated polyester resin (UPR)**

General purpose grade terephthalic unsaturated polyester resin (solid) with monomers terephthalic acid, maleic anhydride and propylene glycol was kindly provided by Riotech Industries, Pala, kerala. The obtained polyester solid is dissolved in styrene to make unsaturated polyester resin as per the requirement. The specifications are given in Table 2.1.

**Table 2.1** Characteristics of UPR

Acid number	20-30 mg KOH/g
Styrene content	35-37%
Specific gravity at 25°C	1.08-1.19
Viscosity at 25°C	4-4.7 Pa.s
Refractive index at 25°C	1.519-1.543
Gel time	~ 4min

### 2.1.2 Fillers and modifying agents

Multi-walled carbon nanotubes and natural graphite are the fillers used for the modification of unsaturated polyester resins. Rubber seed oil is used as a bio-based modifier for UPR.

#### 2.1.2.1 Multi-walled carbon nanotubes (MWCNTs)

The carbon nanotubes were supplied by Bayer Material Science AG (Leverkusen, Germany) as MWCNT Baytube<sup>R</sup> 150P. The specifications are given in Table 2.2.

**Table 2.2** Characteristics of MWCNTs

Carbon purity	>95
Number of walls	13-15
Outer mean diameter	13-16 nm
Inner mean diameter	4 nm
Length	8 µm
Bulk density	150 Kg/m <sup>3</sup>

#### 2.1.2.2 Graphite fine powder

About 98% extra pure graphite fine powder insoluble in water was purchased from Loba Chemie Pvt Ltd, Mumbai. The specifications are given in Table 2.3.

**Table 2.3** Characteristics of graphite fine powder

C (M. W.)	12.01
Carbon (min)	98%
Fe	0.4% max
S	0.1%
P	Traces
Ash content	0.7%
Particle size	60 mesh

### 2.1.2.3 Rubber seed oil (RSO)

Crude rubber seed oil was purchased from Vignesh Trader, Virudhunagar, Tamilnadu, India. The specifications are given in Table 2.4.

**Table 2.4** Characteristics of crude rubber seed oil

Colour	Dark brown
Specific gravity at 25°C	0.913
Density at 25°C	0.861 g/cm <sup>3</sup>
Acid number	41.26 mg KOH/g of oil
Iodine value	120.75 g I <sub>2</sub> /100 g oil
Saponification value	271.8 mg KOH/g of oil
Refractive index at 25°C	1.46

## 2.1.3 Chemicals

### 2.1.3.1 Chemicals for the processing of UP resins

#### Styrene

Commercial grade styrene monomer was supplied by Riotech Industries, Pala, kerala.

### **Cobalt octoate**

About 6% cobalt octoate in mineral spirit (commercial grade) was provided by Sharon Engineering Enterprises, Kochi, which was used as a promoter.

### **Methyl ethyl ketone peroxide (MEKP)**

The initiator MEKP with 8% active oxygen was provided by Sharon Engineering Enterprises, Kochi

### **THF**

Tetrahydrofuran was supplied by Merck life science Pvt. Ltd. Mumbai, with purity > 99.0%.

### **2.1.3.2 Chemicals for functionalisation of MWCNTs**

#### **Maleic anhydride (MA)**

MA was purchased from Loba Chemie Pvt. Ltd., Mumbai. The specifications are given in Table 2.5.

**Table 2.5** Characteristics of maleic anhydride

M. W.	98.06%
Purity	9.0%
Melting point	51-53°C

#### **Ethyl acetate**

Ethyl acetate was supplied by Spectrochem, Mumbai, with purity 99.5% and boiling range 76.5-77.5°C.

#### **Conc. HNO<sub>3</sub>**

Analytical grade Conc. HNO<sub>3</sub> (69%) was purchased from Merck Specialities Pvt Ltd, Mumbai with assay 68-70%.

### **Conc. HCl**

Analytical grade Conc. HCl (35%) was purchased from Merck Specialities Pvt Ltd, Mumbai.

### **Sodium bicarbonate**

LR grade NaHCO<sub>3</sub> was purchased from Merck Specialities Pvt Ltd, Mumbai with 99.0% assay.

### **Sodium hydroxide**

NaOH with assay > 97% was provided by Merck life science Pvt. Ltd, Mumbai.

### **2.1.3.3 Chemicals used for the modification of natural graphite**

#### **Conc. H<sub>2</sub>SO<sub>4</sub> (98%)**

Analytical grade Conc. H<sub>2</sub>SO<sub>4</sub> was purchased from Merck Specialities Pvt Ltd, Mumbai.

#### **Potassium permanganate (KMnO<sub>4</sub>)**

KMnO<sub>4</sub> with purity > 98.5% was purchased from Merck life science Pvt. Ltd, Mumbai.

#### **Hydrogen peroxide**

30% H<sub>2</sub>O<sub>2</sub> solution with assay 29-32% was provided by Merck life science Pvt. Ltd, Mumbai.

#### **Silver nitrate**

AgNO<sub>3</sub> was supplied by Spectrochem Pvt. Ltd., Mumbai. It was with about 99.9% purity.

### **Vit-C (L-Ascorbic acid)**

About 99.5% pure L-Ascorbic acid was purchased from Spectrochem Pvt. Ltd., Mumbai with a specific optical rotation  $[\alpha]_D^{20}$  +20.5° to +21.5° (10% aqueous solution).

### **25% NH<sub>3</sub> solution**

Ammonia solution with assay > 25% was purchased from Merck Specialities Pvt Ltd, Mumbai

### **2.1.3.4 Chemicals used for the preparation of FAMES of RSO**

#### **Partially sulfonated polystyrene (PSS) catalyst**

PSS was synthesized from expanded polystyrene waste (EPS) by a partial sulfonation reaction [1]. This is used as a heterogeneous acid catalyst for the esterification reaction. The specification of PSS is given in Table 2.6.

**Table 2.6** Characteristics of PSS catalyst [2]

Degree of sulfonation (x)	0.27
Ion exchange capacity	2.07 meq/g
T <sub>g</sub> (from DSC)	121°C
Thermal degradation temperature	401°C
Percentage water absorption	>1200%

## **2.2 Experimental methods**

Mechanical stirring and sonication are the physical methods employed for dispersing nanofillers/additives in unsaturated polyester resin.



### 2.2.1 Mechanical stirring

The mechanical stirrer (1MLH) used in this study was purchased from Remi Sales and Engineering Ltd., Mumbai with a speed up to 1200 rpm. The stirring capacity is 1Ltrs with a PTFE coated stirring paddle.

### 2.2.2 Ultrasonication

The dispersions of nano fillers in polymer matrix were achieved by ultrasonication. Both horn sonicator and bath sonicator were used in this study (Fig. 2.1 (a) and (b)). The horn sonicator used is Sonics VCX-750 Vibra Cell Ultra Sonic Processor with a cylindrical tip of 13mm end cap diameter which is operated at 40% amplitude with a maximum power of 750W. The bath sonicator used is BRANSON 1510E-MT which is operating at 70W power and 42 kHz frequency.

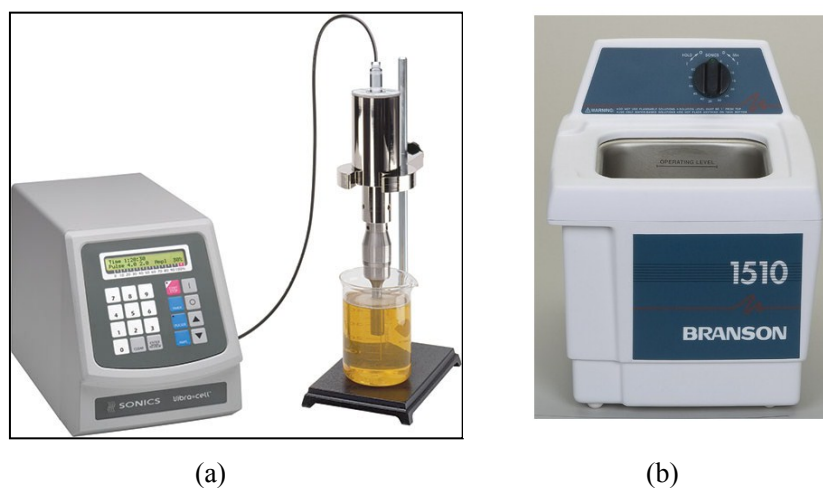


**Fig. 2.1** (a) Horn sonicator and (b) bath sonicator

### **2.2.3 Direct mixing dispersion technique and molding**

For the dispersion of nanoparticles in polyester resin THF is used as a solvent. Nanoparticles are first dispersed in THF and sonicated to obtain fine dispersion. It is then directly mixed with UPR (solid) by mechanical stirring and sonication. After achieving good dispersion THF is removed from the mixture by heating. After the removal of THF the mixture is mixed with styrene & initiator and transferred to Teflon molds for curing.

## **2.3 Characterization techniques**

### **2.3.1 UV-Vis spectroscopy**

The UV-Vis absorption spectrum was recorded on a Thermo Scientific™ Evolution™ 300 UV-Vis spectrophotometer in the range 200-800 nm. Absorption of UV-Vis radiation is associated with excitation of electrons from lower to higher energy levels. Excitation takes place from bonding to anti-bonding molecular orbitals and/or non-bonding to anti-bonding molecular orbitals. A non-bonding orbital is a lone pair which is present in oxygen, nitrogen or halogen. The oxidized MWCNTs and graphene oxides were characterized by their specific absorption in the UV-Vis range. The aqueous dispersion of samples was prepared with the help of ultrasonication.

### **2.3.2 Fourier Transform Infrared Spectroscopy (FTIR)**

FTIR spectral analysis is a powerful tool for structural characterization. FTIR spectroscopy is employed to identify the various functional groups present in oil derivatives and modified nanofillers. This gives an insight into the structural aspects of nanofillers and oil derivatives at room

temperature. The instrument used is Thermo Nicolet, Avatar 370 model IR spectrometer with  $4\text{cm}^{-1}$  resolution in transmittance mode. The spectral range was taken as  $4000\text{-}400\text{ cm}^{-1}$ .

### 2.3.3 Boehm titrations

The quantitative evaluation of oxygen containing functional groups on MWCNTs can be evaluated using Boehm titration method. The amount of carboxyl and total acidic sites present on the carbon surface can be analyzed by titration method. About 5 mg of the sample was reacted with certain amount of  $\text{NaHCO}_3$  and  $\text{NaOH}$ .  $\text{NaHCO}_3$  neutralizes only the carboxyl groups while  $\text{NaOH}$  neutralizes carboxyl, lactone and phenolic groups. The unreacted portion was neutralized with  $\text{HCl}$  and the amount of excess  $\text{HCl}$  was determined using titrating it with  $\text{NaOH}$  solution [3, 4].

### 2.3.4 Nuclear Magnetic Resonance Spectroscopy (NMR)

NMR spectroscopy is a nondestructive tool for the identification of oil derivatives. In the present study  $^1\text{H}$ NMR spectrum was recorded on Bruker, AV 400-AVANCE III FT-NMR spectrometer operating at proton resonance frequency of 400 MHz. The sample was dissolved in deuterated chloroform ( $\text{CDCl}_3$ ) ( $\delta=7.26\text{ ppm}$ ) containing a small amount of tetramethyl silane (TMS) as an internal standard ( $\delta=0\text{ ppm}$ ). About 30 mg of sample was dissolved in 1 mL of  $\text{CDCl}_3$  and spectra were recorded at  $25^\circ\text{C}$ .

### 2.3.5 GC-MS Analysis

The fatty acid methyl esters (FAMES) contents of RSO were determined by gas chromatography, model GC-7890A coupled with mass

spectrometer, model MS-5975c MSD (Agilent Technologies) (Fig. 2.2). Separation was performed on a capillary column DB-5MS (30m × 250 μm × 0.25 μm of film thickness). The carrier gas was Helium with flow rate of 1.1 mL/min. The column temperature was programmed from 100 to 250°C at the rate of 5°C /min. The temperature of both injector and detector was set at 250°C. A sample volume of 0.1 μL RSO in hexane was injected using a split mode with the split ratio of 1:10. The mass spectrometer was set to scan in the range of  $m/z$  50-550 with electron impact (EI) mode of ionization.

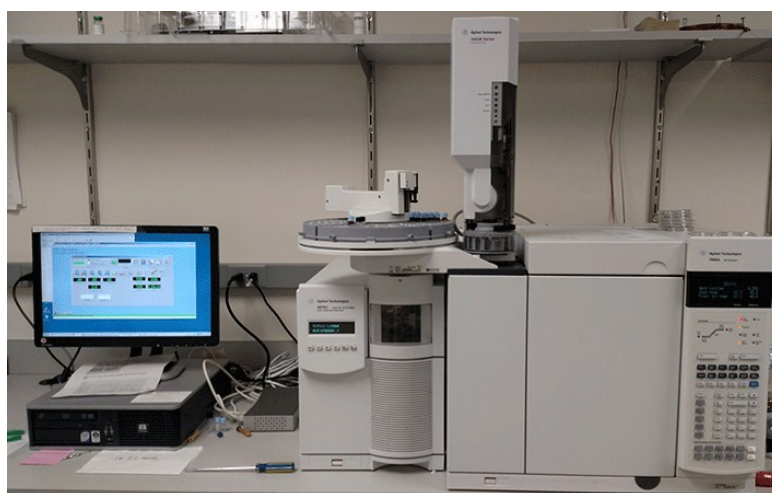


**Fig. 2.2** GC-MS (GC coupled with mass spectrometer)

### **2.3.6 X-Ray Diffraction Technique (XRD)**

XRD is an effective method for determining the crystal structure and chemical phase composition of materials. Crystalline materials are composed of atoms arranged in a regular ordered pattern in three dimensions. The 'd spacing' is defined as the distance between adjacent

planes. The orientation and interplaner spacing ( $d$ ) of these lattice planes are defined by three integers  $h, k, l$  called Miller Indices. The  $(hkl)$  designate a crystal face or family planes throughout a crystal lattice. X-ray is a form of electromagnetic radiation which interact with the crystal planes producing diffraction patterns which contains information about atomic arrangements within the crystal. The diffraction process can be explained by Bragg's equation,  $n\lambda = 2d \sin\theta$ , where  $n$  is an integer,  $\lambda$  is the wavelength of X-rays used and  $d$  is the interplannar spacing

The XRD patterns were recorded using X-Ray Diffractometer, Bruker, D8 Advance model, employing Cu  $K_{\alpha}$  radiation ( $\lambda = 1.54 \text{ \AA}$ ) as radiation source and Ni filter operating at 30 kV and 20 mA at a  $2\theta$  scan speed of  $10^\circ/\text{min}$ . The samples were scanned in the range of  $3-80^\circ$  at an increment step of scanning  $0.020^\circ$ .

### 2.3.7 Raman spectroscopy

In Raman spectroscopy vibrational modes are identified by measuring the energy of scattered photons generated from the sample when it is exposed to intense laser light. Typical Raman spectra of MWCNTs consist of two bands designated as G-band and D-band. G-band or graphitic band originated from highly ordered CNT sidewalls, while the D-band or defect band is due to the disordered structure in the sidewalls. The ratio between these two bands ( $I_D:I_G$ ) gives a quantitative measure of defect density present on the CNT sidewall.

Raman spectra of P-MWCNT and MA-MWCNT were recorded with Horiba Jobin Yvon Lab Ram HR system at a resolution of  $2 \text{ cm}^{-1}$  by using excitation of  $514.5 \text{ nm}$  by Argon ion laser.

### **2.3.8 Inductively Coupled Plasma Atomic Emission Spectrometer (ICP-AES)**

The concentration of silver decorated on rGO sheets were analyzed by ICP-AES. The atomic spectrum emitted by a sample is used to determine its elemental composition in this instrument. The wavelength at which emission occurs identifies the element, while the intensity of the emitted radiation quantifies its concentration. The analysis was carried out on ICP-AES model Thermo Electron IRIS INTREPID II XSP DUO, axial and radial view instrument with a spectral range of 165 to 1000 nm with a detection limit of ppb level.

### **2.3.9 Mechanical properties**

#### **2.3.9.1 Tensile properties**

The ability to resist breaking under tensile stress is one of the most important and widely measured properties of materials used in structural applications. The force per unit area (MPa or psi) required to break a material in such a manner is the ultimate tensile strength or tensile strength at break. The tensile modulus is the ratio of stress to elastic strain in tension. A high tensile modulus means that the material is rigid - more stress is required to produce a given amount of strain. The ultimate elongation of an engineering material is the percentage increase in length that occurs before it breaks under tension.

Tensile properties were evaluated using Shimadzu Autograph AG-1 series universal testing machine equipped with a 10 kN load cell capacity at a displacement rate of 5 mm/min at room temperature as per ASTM D 638 on dumb-bell shaped specimens (Fig. 2.3). The gauge length between the jaws

at the start of each test was fixed to 100 mm. A minimum of ten samples were tested in each composite and the average results were recorded.

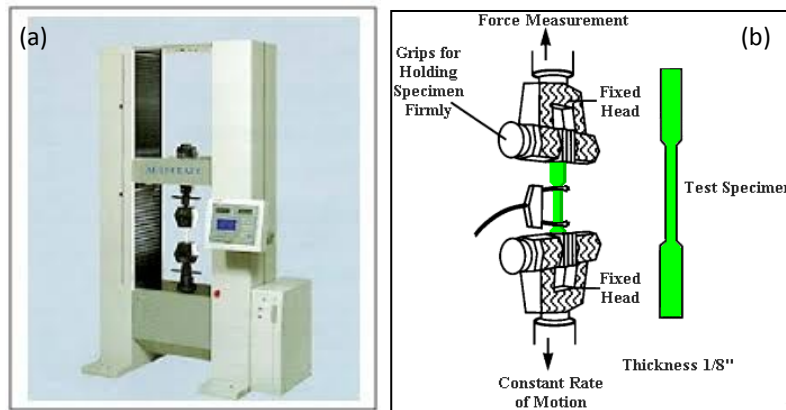


Fig. 2.3 (a) Universal testing machine and (b) testing of specimen

### 2.3.9.2 Flexural properties

Flexural strength means the ability of the material to withstand bending forces applied perpendicular to its longitudinal axis. Flexural modulus is used as an indication of material's stiffness when flexed.

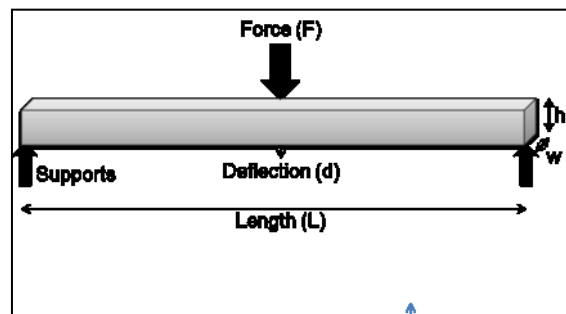


Fig. 2.4 Flexural measurement

For a 3-point test of a rectangular beam behaving as an isotropic linear material, where  $w$  and  $h$  are the width and height of the beam,  $I$  is

the second moment of area of the beam's cross-section,  $L$  is the distance between the two outer supports, and  $d$  is the deflection due to the load  $F$  applied at the middle of the beam, the flexural modulus;

$$E_{bend} = L^3 F / 4wh^3 d \dots\dots\dots (2.1)$$

From elastic beam theory

$$d = L^3 F / 48IE \dots\dots\dots (2.2)$$

and for rectangular beam

$$I = \frac{1}{12} wh^3 \dots\dots\dots (2.3)$$

Flexural test was conducted by three point loading system using Shimadzu AG-1 series universal testing machine equipped with a 10 kN load cell capacity at a speed of 5 mm/min according to ASTM D 790, using rectangular bar shaped samples at room temperature. The rectangular specimens were placed on a three-point bending apparatus with two supports spanning 40 mm from each other and loaded by means of a loading nose midway between the supports until failure. A minimum of six samples were tested in each case and the average results were recorded.

### 2.3.9.3 Impact strength

The impact strength is calculated as the ratio of impact absorption to test specimen cross-section. Toughness is dependent upon temperature and the shape of the test specimen. The area under the stress-strain curve is directly proportional to the toughness of the material. The unnotched rectangular specimen is fixed vertically in the base of the machine, a



pendulum swings on its course, released and strikes the sample, and the impact energy is directly read from the machine.

$$\text{Impact strength} = \text{Impact energy (J)}/\text{Thickness (m)}$$

The impact strength of the samples were measured on a Resil Impact Analyzer (Junior) as per ASTM D 256-88 specifications (Fig. 2.5). The specimens were tested on the impact tester having 4J capacity hammer and striking velocity of 2.9m/sec. All specimens were casted in Teflon molds having the same dimensions. A minimum of six specimens were tested for each composition.



**Fig. 2.5** Resil Impactor (Junior)

#### **2.3.9.4 Dynamic mechanical analysis**

Dynamic mechanical analysis is a technique which is used to characterize the materials. A sinusoidal stress is applied and the strain in the material is measured, allowing one to determine the complex

modulus. The temperature of the sample or the frequency of the stress are often varied, leading to variations in the complex modulus; this approach can be used to locate the glass transition temperature of the material, as well as to identify transitions corresponding to other molecular motions.

The dynamic mechanical properties were measured with a TA Instruments DMA Q 800 (Fig. 2.6 (a)). The Q800 Dynamic Mechanical Analyzer is a precision instrument designed to measure viscoelastic properties, such as modulus and damping of rigid and soft solid materials. The tests were carried out by temperature sweep method at a constant frequency of 1 Hz. Data were collected from ambient to 150°C at a scanning rate of 3°C/min. The dynamic storage modulus ( $E'$ ), loss modulus ( $E''$ ) and tan delta ( $E''/E'$ ) values of the samples were obtained. The instrument is operating in the three-point bending mode (Fig. 2.6 (b)).

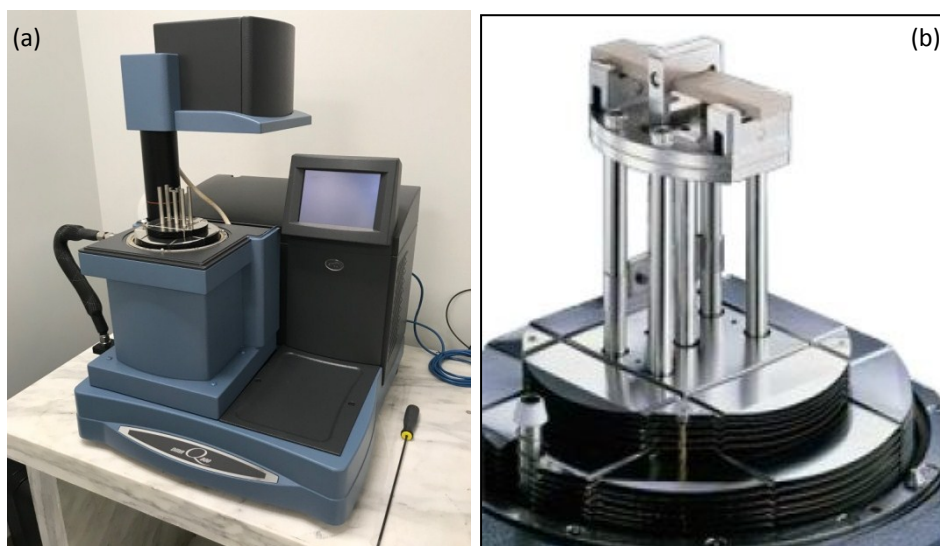


**Fig. 2.6** (a) DMA Q 800 & (b) 3-point-bend dual cantilever

### 2.3.10 Morphological properties

The morphological properties of the nanofillers and composites were characterized by electron microscopic techniques. An electron microscope is a microscope that uses a beam of accelerated electrons as a source of illumination. The interaction of electron beam with sample is depicted in Fig. 2.7. SEM and TEM are the generally used techniques.

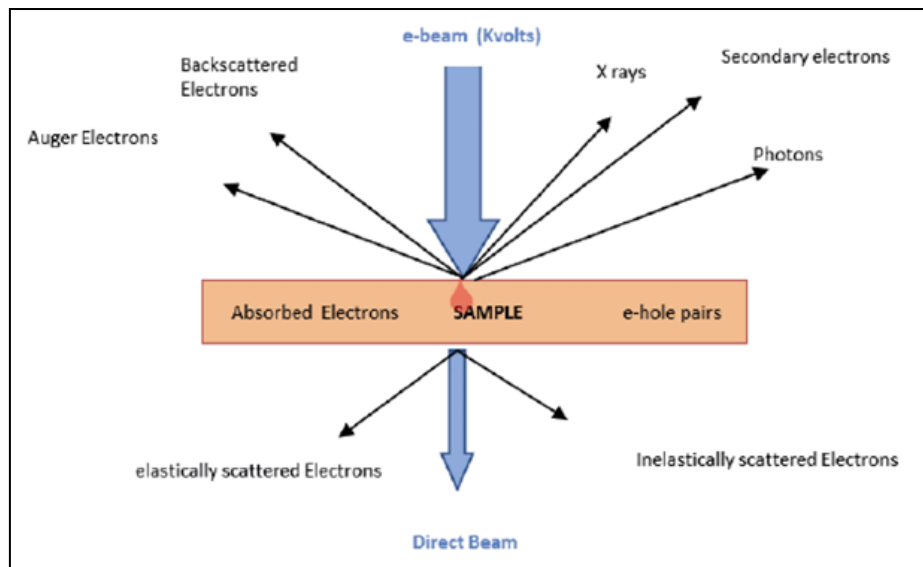


**Fig. 2.7** Interaction of electron beam with sample

#### 2.3.10.1 Scanning Electron Microscopy (SEM)

Scanning electron microscope is a type of electron microscope that takes the images of a sample by scanning the surface with processed beam of electrons. The electrons interact with atoms in the sample, producing various signals that contain information about the sample's surface topography and composition. The electron beam is scanned in a raster scan pattern, and the beam's position is combined with the detected signal to produce an image.

SEM can achieve resolution better than 1 nanometer. In conventional SEM specimens can be observed in high vacuum. SEM is focused on the detection of secondary electrons emitted by atoms excited by the electron beam. By scanning the sample and collecting the secondary electrons that are emitted using a special detector, an image displaying the topography of the surface is created.

The morphology of fractured surfaces of neat UP resin and UPR composites were observed with a JEOL Model JSM 6390 LV scanning electron microscope (SEM) instrument with 20 kV accelerating voltage. The failure surfaces of specimens were coated with Au thin films having a thickness of a few nanometers to make them conductive.

#### **2.3.10.2 Transmission Electron Microscopy (TEM)**

Transmission electron microscopy (TEM) is a microscopy technique in which a high energy beam of electrons is transmitted through an ultra-thin specimen, interacting with the specimen as it passes through. An image is formed from the interaction of the electrons transmitted through the specimen.

High resolution transmission electron microscopy (HRTEM) was performed using high resolution transmission electron microscope (HRTEM, JEOL model JEM-2100). For TEM observation aqueous suspensions of nanofillers were sonicated for 15 min to disperse the aggregated particles. The well dispersed suspensions were directly dropped on a copper microgrid and dried before observation. In the case of polyester nanocomposites, the ultra thin TEM sample with a thickness of 70 nm was

cut using a Leica Ultracut UCT Ultramicrotome at room temperature. Microtomed thin sections were collected on 200 mesh copper grids and examined by a JEM 2100 TEM at 200 kV in a bright field mode.

### **2.3.11 Thermo gravimetric analysis (TGA)**

TGA is a method which is widely adopted to study the thermal properties of polymers. TGA aims at the investigation of pyrolysis and thermal degradation of solids<sup>5</sup>. It monitors the mass of a sample as a function of temperature or time while the substance is subjected to a controlled temperature programme<sup>6</sup>. The integral (TGA) and derivative (DTG) thermo gravimetric curves give information about thermal stability and extent of degradation of the polymeric material.

Approximately 5-10mg of each of the cured samples were subjected to thermo gravimetric analysis using a TGA Q-50 Thermal Analyser (TA Instruments) in a nitrogen atmosphere at a heating rate of 20 °C /min from room temperature to 800 °C. The nitrogen gas flow rate was maintained at 40–60 cm<sup>3</sup>/min.

### **2.3.12 Dielectric properties**

A dielectric material is an electrical insulator that can be polarized by an applied electric field. When a dielectric is placed in an electric field, electric charges do not flow through the material as they do in an electrical conductor but only slightly shift from their average equilibrium positions causing dielectric polarization. Because of dielectric polarization, positive charges are displaced in the direction of the field and negative charges shift in the opposite direction. This creates an internal electric field that

reduces the overall field within the dielectric itself. If a dielectric is composed of weakly bonded molecules, those molecules not only become polarized, but also reorient so that their symmetry axes align to the field. The dielectric permittivity is the measure of capacitance that is encountered when forming an electric field in a particular medium. More specifically, permittivity describes the amount of charge needed to generate one unit of electric flux in a particular medium. Dielectric loss quantifies a dielectric material's inherent dissipation of electromagnetic energy (e.g. heat). It can be parameterized in terms of either the loss angle  $\delta$ .

Dielectric and AC conductivity measurements were carried out in the frequency range 40Hz to 30MHz using Precision Impedance Analyser (Agilent 4294A) with dielectric test fixture 16451B (Fig. 2.). Disc shaped samples with diameter 12mm and thickness 2mm were used for the measurements. The variation of dielectric permittivity, loss tangent and AC conductivity with frequency were recorded. Parallel plate method was employed to measure the dielectric properties of the samples.

AC conductivity was calculated using the formula

$$\sigma = 2\pi f \epsilon_0 \epsilon'' \dots\dots\dots(2.4)$$

where,  $f$  is the frequency in Hz,  $\epsilon_0$  is the permittivity of free space and  $\epsilon''$  is the imaginary part of permittivity

### 2.3.13 EMI shielding measurements

The EMI shielding measurements of the nanocomposites were performed using Agilent Performance Network Analyzer E8362B in the X-band frequency region (8-12 GHz) using waveguides coupled to the vector network analyzer. The rectangular waveguide transmission line technique is used to measure the EMI SE of polyester nanocomposites. A pair of coaxial cables was connected between network analyzer and rectangular waveguide adaptors (WR 90). The sample with dimensions  $2.3 \times 1 \times 0.18$  cm is placed between the two sections of the waveguide for measurement. Fig. 2.8 shows the EMI shielding measurement setup.

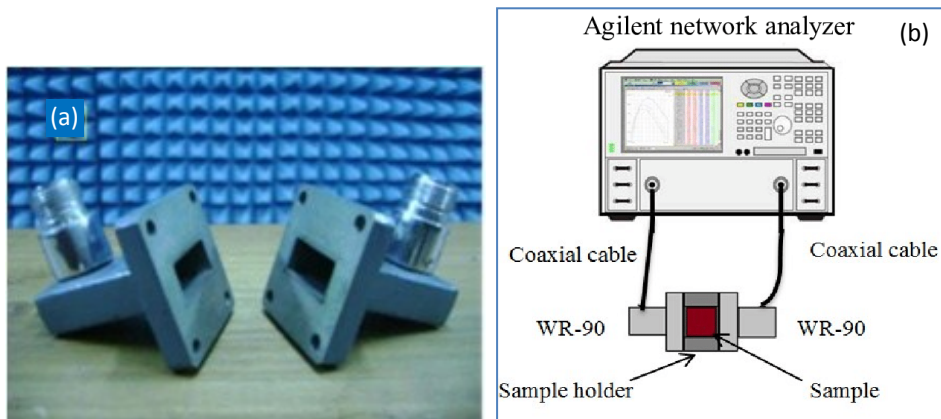


**Fig. 2.8** (a) X-band waveguide & (b) measurement setup for EMI shielding

The scattering parameters (S parameters) were measured in a two port EMI shielding setup. The S parameter which corresponds to reflection is represented as S11 or S22 and for absorption as S21 or S12. Total shielding effectiveness (SE) depends on reflection and absorption as per the equation.

$$SE = SE_R + SE_A \dots\dots\dots (2.5)$$

Where  $SE_R$  is the reflection shielding effectiveness and  $SE_A$  the absorption shielding effectiveness.  $SE_R$  and  $SE_A$  can be expressed as

$$SE_R = -10 \log(1 - S_{11}^2) \dots\dots\dots (2.6)$$

$$SE_A = -10 \log\left(\frac{S_{21}^2}{1 - S_{11}^2}\right) \dots\dots\dots (2.7)$$

Thus the total shielding effectiveness (SE) can be represented as

$$SE = -10 \log (S_{21}^2) \dots\dots\dots (2.8)$$

## References

- [1] Antony, J. V., Kurian, P., Vadakkedathu, N. P. N., Kochimoolayil, G. E. (2014). In situ synthesis of CdS quantum dot-Partially sulfonated polystyrene composite: characterization and optical properties. *Ind. Eng. Chem. Res.*, 53, 2261–2269.
- [2] Suresh, R., Antony, J. V., Vengalil, R., Kochimoolayil, G. E., Joseph, R. (2017). Esterification of free fatty acids in non- edible oils using partially sulfonated polystyrene for biodiesel feedstock. *Ind. Crops Prod.*, 95, 66–74.
- [3] Boehm, H. P., Diehl, E., Heck, W., Sappok, R. (1964). Surface oxides of carbon. *Angew. Chem. Int.*, Edit 3, 669–677.
- [4] Boehm, H. P. (1994). Some aspects of the surface chemistry of carbon blacks and other carbons. *Carbon*, 32, 759-69.

.....❧.....



**UNSATURATED POLYESTER RESIN MULTI-WALLED  
CARBON NANOTUBE COMPOSITES****Contents**

*Part A: Preparation of maleic anhydride functionalized multi-walled carbon nanotubes*

*Part B: Modification of Unsaturated polyester resin with MA functionalized MWCNT*

Multi-walled carbon nanotubes (MWCNTs) have been tried as a modifier in unsaturated polyester resin (UPR). In order to improve the interfacial interaction with the polymer so as to get better dispersion and properties, MWCNT has been functionalized with maleic anhydride (MA). The advantage of this two-step process using MA is that it will not severely damage the CNT frame work as in the case of vigorous acid functionalization. The functionalization was confirmed by Fourier Transform Infra Red spectra (FT-IR), UV-Vis absorption spectra, Raman spectra and Transmission Electron Microscopy (TEM). The nanocomposites were prepared by mechanical stirring and ultrasonication. The good dispersion of MA-MWCNT in UPR was confirmed by TEM analysis. Considerable improvement in mechanical, electrical and electromagnetic interference shielding (EMI) properties was observed for the nanocomposite even at very low filler loading.

## Preparation of maleic anhydride functionalized multi-walled carbon nanotubes

### 3.A.1 Introduction

Carbon nanotubes have drawn much attention in recent years since their discovery in 1991 by Iijima [1], due to their inherent combination of distinctive mechanical, thermal and electrical properties [2, 3]. They are composed of thin tubes of graphene cylinders with diameter in nanometer range, but a length of few microns. Its extraordinary mechanical and electrical properties attract researchers to fabricate nanocomposites with CNTs for different applications [4].

CNTs are more attractive than conventional macro and micro fillers due to their high aspect ratio, low mass density and effective load transfer property [5, 6]. Single, double and multi-walled carbon nanotubes are used for reinforcing polymer matrix. However it is difficult to achieve a homogeneous dispersion of CNTs in polymer matrix. Carbon nanotubes have strong tendency to agglomerate via their huge surface area which is thermodynamically stabilized by numerous  $\pi$ - $\pi$  interactions and Van der Waals forces [7, 8]. Therefore homogeneous dispersion of CNTs in polymer matrix is the key factor to enhance the properties of nanocomposites. Physical and chemical methods are employed for controlling the dispersion of CNTs in polymers. Physical methods include direct mixing, mechanical stirring and ultrasonication. Chemical methods include covalent (chemical functionalization) and non-covalent (addition of surfactant) functionalization [9, 10].

CNTs are incorporated in thermosetting polymers like epoxy to fabricate composite materials for specific applications [11, 12]. In order to get good dispersion of CNTs in thermosetting polymers mechanical stirring, sonication and 3-roll-milling techniques are used. Besides physical approaches, chemical functionalization of the CNT surfaces has done to enhance the degree of dispersion. Chemical functionalization of CNTs is a major area of interest for researchers to develop advanced nanocomposites with special properties. The oxidation of CNTs by chemical methods produces oxygen containing groups, mainly carboxyl and hydroxyl which decorate the CNT surface. This facilitates the exfoliation of bundles and increases the solubility in polymer matrix [13-15]. As a result the unique properties of CNTs can be transferred to the polymer matrix.

Unsaturated polyester resins (UPR) can be modified by MWCNTs to obtain better mechanical and electrical properties. But functionalization has to be done for CNT in order to get better dispersion in resin. Several studies have been reported in which acid and amine functionalized CNTs are used for UPR. In the present study MWCNT has been functionalized with maleic anhydride, a monomer of UP resin. The common acid functionalization using  $H_2SO_4$  may damage the molecular frame work of CNTs [16]. The MA functionalization induces fewer defects compared to  $H_2SO_4$  functionalization. MA functionalization of MWCNTs by a mild two-step reaction process is proposed to be investigated in this study.

## 3.A.2 Experimental

### 3.A.2.1 Preparation of MA functionalized MWCNTs

The MA functionalization was done by a two-step process. In the first step MWCNTs were mixed with Con. HNO<sub>3</sub> and sonicated for 1h. The mixture was refluxed at 130°C for 5h. The solution was cooled diluted with water and filtered through PTFE membrane filter (0.2µm pore size) and MWCNTs were dried in vacuum oven at 60°C for 24h. In the second step acid functionalized MWCNTs were reacted with maleic anhydride in ethyl acetate in presence of concentrated HCl at 60°C for 5h (1:3 is the volume ratio of HCl and ethyl acetate). Then MA functionalized MWCNTs were filtered, washed by distilled water until the pH was 7 and dried and labeled as MA-MWCNTs. The pristine MWCNT was labeled as P-MWCNT.

### 3.A.2.2 Characterization

The functionalized MWCNT was quantitatively analyzed by Boehm titration which is used to determine the protic functional groups on MWCNTs. In this the MWCNTs protic groups are neutralized with different bases like NaHCO<sub>3</sub> and NaOH. The quantity of unreacted bases was estimated by titrating it with HCl. The detailed procedure is given in Chapter 2.

Functionalized MWCNTs were characterized by thermo gravimetric analysis (TGA), Fourier transform infrared spectra (FTIR) and UV-Vis absorption spectra. For UV-Vis analysis the samples were dispersed in distilled water and sonicated for 20min. Raman spectra and X-ray diffraction studies (XRD) were used to confirm the MA functionalization

on CNT. The surface morphology of MA-MWCNT was analyzed by high resolution transmission electron microscope (HR-TEM).

### 3.A.3 Results and discussions

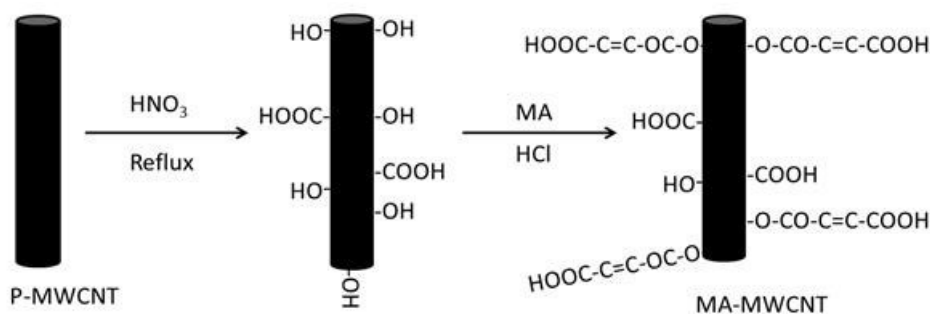


**Fig. 3.A.1** Schematic representation of MA functionalization of MWCNT

$\text{HNO}_3$  treatment introduces polar hydroxyl and carboxyl groups on the surface of MWCNT as shown in Fig. 3.A.1. This acid treated MWCNT when reacted with maleic anhydride in presence of  $\text{HCl}$  gives esters of maleic acid with hydroxyl groups on the surface of MWCNT.

Boehm titration gives the quantitative analysis of functional groups attached on the MWCNT surface [17, 18].  $\text{NaHCO}_3$  only neutralizes the carboxyl groups while  $\text{NaOH}$  neutralizes both carboxyl and hydroxyl groups. The amount of functional groups neutralized per gram of MWCNT is given in Table 3.A.1. An enhancement in the concentration of carboxyl group is observed in the case of MA-MWCNT, from 2.91 mmol/g to 4.71 mmol/g compared to acid treated MWCNTs [19]. This clearly indicates that the hydroxyl groups on acid treated MWCNTs get participated in the esterification reaction with maleic acid in presence of acid.

**Table 3.A.1** Relative concentration of functional groups on CNTs

Sample	-COOH (NaHCO <sub>3</sub> ) mmol/g	-OH & -COOH (NaOH) mmol/g	-OH mmol/g
HNO <sub>3</sub> -MWCNT	2.91	4.76	1.85
MA-MWCNT	4.71	4.99	0.28

The prepared MA-MWCNTs were characterized by FTIR spectra. P-MWCNT shows no significant absorption bands of functional groups other than O-H stretching vibration at 3439 cm<sup>-1</sup> due to the presence of moisture. The HNO<sub>3</sub> treated MWCNT shows characteristic peaks of hydroxyl and carbonyl groups at 3453 and 1714 cm<sup>-1</sup> which indicates -O-H stretching and -C=O stretching respectively [20, 21]. After the MA functionalization a peak at 1744cm<sup>-1</sup> is observed for MA-MWCNT which corresponds to ester linkage on the surface of CNT [22] (Fig. 3.A.2). The peak at 1617-1620 cm<sup>-1</sup> corresponds to -C=C- stretching of graphitic structure.

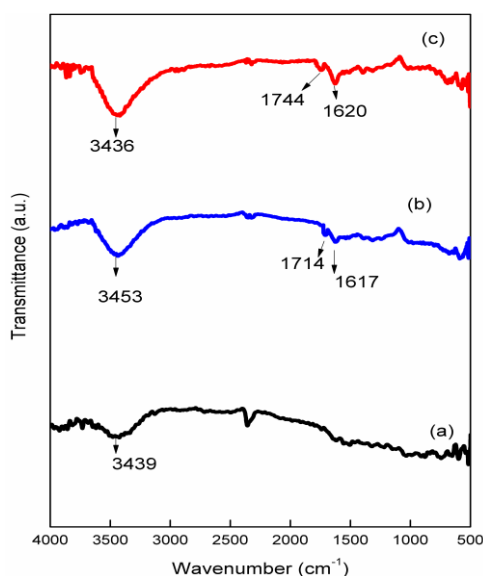


**Fig. 3.A.2** FTIR spectra of (a) P-MWCNT (b) HNO<sub>3</sub> treated MWCNT & (c) MA-MWCNT

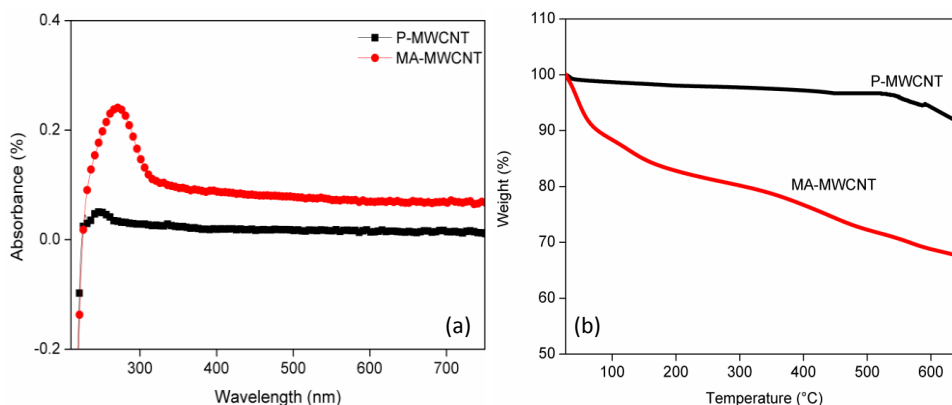


**Fig. 3.A.3** (a) UV-Vis spectra & (b) TGA curves of P-MWCNT and MA-MWCNT.

A significant difference is observed in the UV-Vis absorption spectra of P-MWCNT and MA-MWCNT (Fig.3.A.3 (a)). The absorption peak at 250 nm for P-MWCNT shifted to 270 nm after functionalization. The increase in absorption peak intensity of MA-MWCNT dispersion indicates an enhanced dispersion of functionalized MWCNT in polar solvent compared to non-functionalized MWCNT. This is due to the presence of polar functional groups on the surface of nanotubes which increases the extent of dispersion [23].

The extent of functionalization of MWCNTs is further confirmed by thermo gravimetric analysis. The thermogram of P-MWCNT and MA-MWCNT samples are presented in Fig. 3.A.3 (b). A well graphitized structure oxidizes at a relatively high temperature compared to disordered structure which tends to be oxidized at low temperature. The thermal degradation of MWCNTs is a multi-stage process. An enhanced thermal degradation is observed in the case of MA-MWCNT. The first stage weight loss which is up to 150°C corresponds to the evaporation of

absorbed water. From 150-350°C the second stage weight loss occurs which is due to the removal of carboxyl functional groups. The weight loss from 350-500°C is due to the elimination of hydroxyl groups from MWCNT surface. Finally the weight loss above 500°C is due to the thermal oxidation of remaining disordered carbon [19, 24].

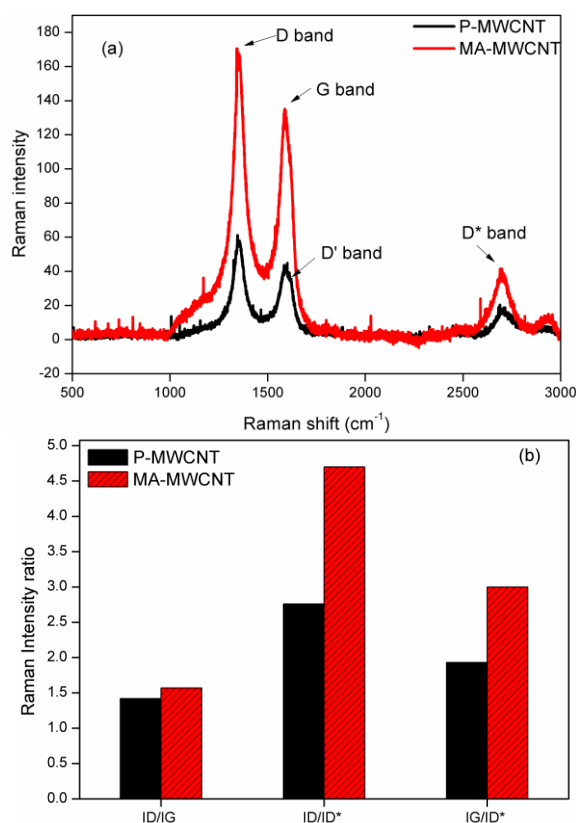


**Fig. 3.A.4** (a) Raman spectra and (b) Raman Intensity ratio of P-MWCNT and MA-MWCNT

Raman spectroscopy is a valuable tool for characterization of MWCNTs [19, 24]. The Raman spectra of P-MWCNT and MA-MWCNT are shown in Fig. 3.A.4 (a). It show three characteristic peaks for all the



samples. The D band at  $\sim 1340\text{ cm}^{-1}$  is due to the presence of amorphous or disordered carbon in the MWCNT sample. It arises from the double resonance Raman scattering process from the non-zero-center phonon mode. D band is activated in the first order scattering process of  $sp^2$  carbons by the presence of defects and by finite size effects, which lower the crystalline symmetry of the quasi infinite lattice. The G band arises from in-plane tangential stretching of C-C bonds in graphene sheets which is in the range  $\sim 1585\text{ cm}^{-1}$ . The third band which also originates from the double resonance induced by defects, appeared as a weak shoulder (at  $\sim 1602\text{ cm}^{-1}$ ) of G band, and is called D' band. At  $\sim 2699\text{ cm}^{-1}$  the second order overtone band occurs which is D\* band.

The ratio of intensity of D and G band ( $I_D/I_G$ ) is a very important factor to analyze the defect level of MWCNT due to functionalization [25].  $I_D/I_G$  value increased from 1.42 to 1.57 after the functionalization due to the presence of more defects. Due to the presence of amorphous carbon type impurities on P-MWCNT, only a slight increase in  $I_D/I_G$  value is observed for MA-MWCNT. In this case we have to consider the D\* band and  $I_D/I_{D^*}$  and  $I_G/I_{D^*}$  is estimated [26]. Fig. 3.A.4 (b) depicts the Raman intensity ratios of P-MWCNT and MA-MWCNT samples. Both ratios significantly enhanced for MA-MWCNT compared to P-MWCNT which confirms the presence of increased number of  $SP^3$  hybridized carbons for MA-MWCNT due to functionalization.

The amorphous nature of functionalized MWCNT is further confirmed by XRD data. Fig. 3.A.5 depicts XRD pattern of P-MWCNT,  $\text{HNO}_3$  treated MWCNT and MA-MWCNT. The main diffraction peaks of graphitic

structures are at 2-Theta = 25.3, 42.6 and 53.6 which corresponds to (002), (101) and (102) plane. The (002) plane indicates the inter layer spacing between adjacent graphitic layers and it appears broaden because of the finite number of layers and of the curvature of each tube. As oxidation increases broadness of the peak also increases due to the formation of amorphous region. Broadness is the indication of lattice distortion due to functionalization [27, 28].

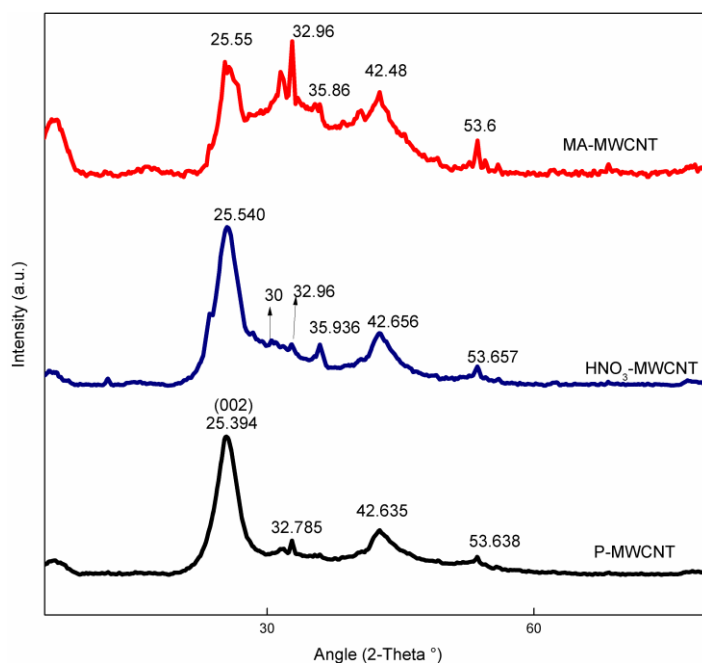


**Fig. 3.A.5** XRD patterns of P-MWCNT, HNO<sub>3</sub>-MWCNT and MA-MWCNTs

The morphological changes on MWCNT samples were investigated by transmission electron microscopy (TEM). Fig. 3.A.6 (a) &(b) indicates P-MWCNTs and (c), (d) & (e) corresponds to MA functionalized MWCNTs. After the two-step oxidation process with nitric acid and maleic anhydride, some bundles exfoliated and tubes curled.

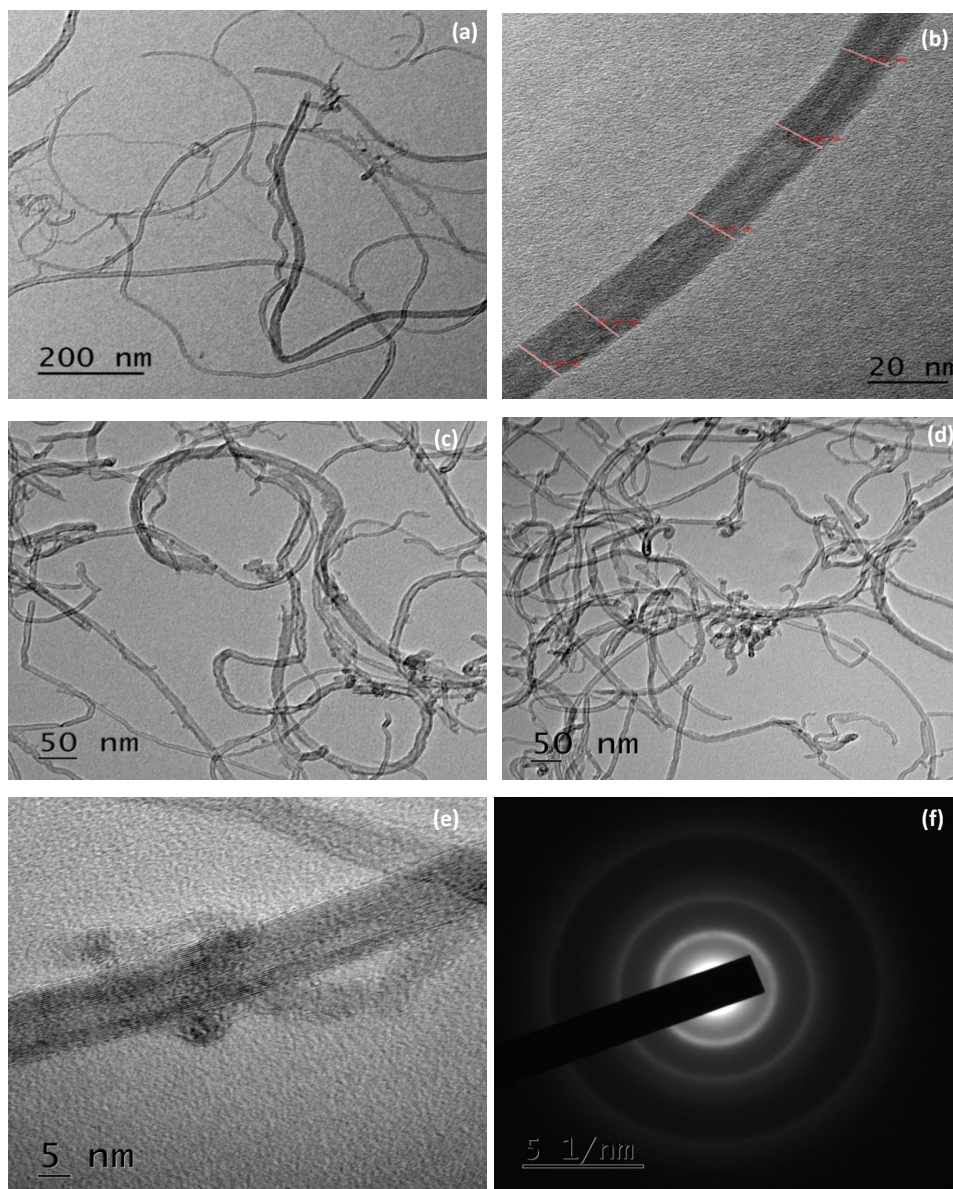


**Fig. 3.A.6** TEM images of (a & b) P-MWCNTs, (c, d & e) MA-MWCNTs & (f) SAED pattern of MA-MWCNTs

The treatment with strong oxidants like nitric acid induces a considerable amount of defects on the structure of MWCNTs. This is

due to the etching of graphitic surface caused by functionalization which leads to shortening of tube length and enhancement in the disordered sites. From the TEM images it is clear that the external walls of P-MWCNTs are structurally more organized when compared to MA-MWCNTs [21, 24].

The selected area electron diffraction pattern (SAED) also confirms the amorphous nature of MA-MWCNTs as shown in Fig. 3.A.6 (f). One advantage of this two-step functionalization is that the defect caused is not severe as in the case of strong  $\text{H}_2\text{SO}_4/\text{HNO}_3$  mixture acid functionalization which is commonly employed for MWCNTs oxidation as shown in Fig. 3.A.7. So this type of functionalization is not very destructive for the tubes and it retain the inherent properties [29, 30] of MWCNTs up to certain extent for further applications.

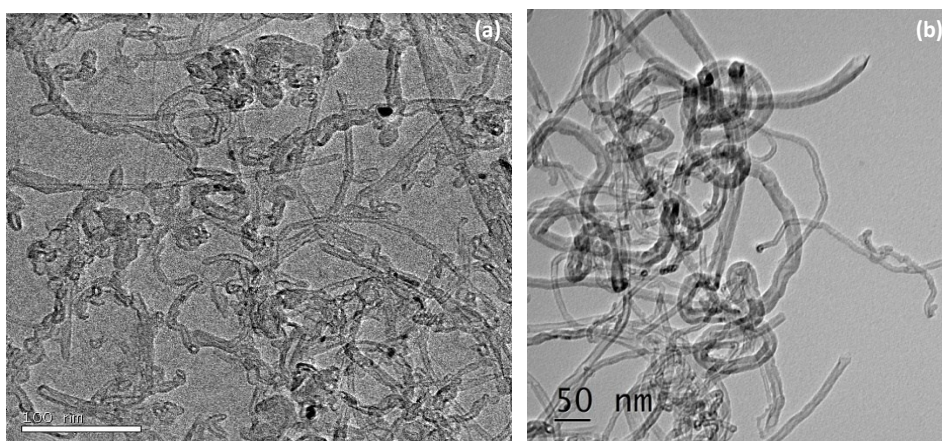


**Fig. 3.A.7** TEM images of (a)  $\text{H}_2\text{SO}_4/\text{HNO}_3$  mixture treated MWCNTs & (b) MA functionalized MWCNTs

### **3.A.4 Conclusions**

The surface modification of MWCNT is done by a two-step functionalization process using Con. HNO<sub>3</sub> and maleic anhydride. The extent of functionalization was quantitatively analyzed by Boehm titration which gives the protic functional groups on the surface of CNTs. FTIR spectroscopy, UV-Vis spectroscopy and thermo gravimetric analysis provide strong evidence for the functionalization. The formation of ester bond on the surface of MA-MWCNT is clearly evident from FTIR spectra. The enhancement in the defect intensity of functionalized MWCNTs was confirmed by analyzing I<sub>D</sub>/I<sub>G</sub> ratio from the Raman spectra. Oxidation with nitric acid followed by MA functionalization under extreme condition increases the defect formation on the CNTs due to shortening of length, as verified by XRD and TEM analysis. Compared to strong acid mixture functionalization, the present process retains the structural integrity of CNTs to certain extent without causing severe damage to the tubes.

### **References**

- [1] Iijima, S. (1991). Helical microtubules of graphitic carbon. *Nature*, 354, 56-58.
- [2] Dresselhaus, M. S., Dresselhaus, G., Avouris, P. (2001). *Carbon nanotubes: synthesis, properties and applications*. Berlin: Springer-Verlag.
- [3] Jonathan, Coleman, N., Khan, U., Gun'ko, Y. K. (2006). Mechanical reinforcement of polymers using carbon nanotubes. *Adv. Mater.*, 18, 689–706.
- [4] De Volder, M. F., Tawfick, S. H., Baughman, R. H., Hart, A.J. (2013). Carbon nanotubes: present and future commercial applications. *Science*, 339, 535-9.

- [5] Kayatin, M. J., Davis, V.A. (2009). Visco-elasticity and shear stability of single-walled carbon nanotube/unsaturated polyester resin dispersions. *Macromolecules*, 42, 6624–6632.
- [6] Gojny, F. H., Wichmann, M. H. G., Kopke, U., Fiedler, B., Schulte, K. (2004). Carbon nanotube reinforced epoxy-composites: enhanced stiffness and fracture toughness at low nanotube content. *Compos. Sci. Technol.*, 64, 2363–2371.
- [7] Breton, Y., Desarmot, G., Salvetat, J. P. (2004). Mechanical properties of multiwall carbon nanotube/epoxy composite: influence of network morphology. *Carbon*, 42, 1027–30.
- [8] Sun, C. H., Yin, L. C., Li, F., Lu, G. Q., Cheng, H. M. (2005). Van der Waals interactions between two parallel infinitely long single-walled nanotubes. *Chem. Phys. Lett.*, 403, 343–346.
- [9] Hilding, J., Grulke, E. A., Zhang, Z. G., Lockwood, F. (2003). Dispersion of Carbon Nanotubes in Liquids. *J. Disp. Sci. Tech.*, 24, 1–41.
- [10] Mackay, M. E., Tuteja, A., Duxbury, P. M., Hawker, C. J., Van Horn, B., Guan, Z., Chen, G., Krishnan, R. S. (2006). General strategies for nanoparticle dispersion. *Science*, 311, 1740 – 43.
- [11] Gojny, F. H., Wichmann, M.H.G., Kopke, U., Fiedler, B., Schulte, K. (2004). Carbon nanotube-reinforced epoxy-composites: enhanced stiffness and fracture toughness at low nanotube content. *Compos. Sci. Technol.*, 64, 2363–2371.
- [12] Martone, A., Formicola, C., Giordano, M. (2010). Reinforcement efficiency of multi-walled carbon nanotube/epoxy nanocomposites. *Compos. Sci. Technol.*, 70, 1154–1160.
- [13] Chen, J., Hamon, M.A., Hu, H., Chen, Y., Rao, A.M., Eklund, P.C. (1998). Solution properties of single-walled carbon nanotubes. *Science*, 282, 95–8.
- [14] Liu, J., Rinzler, A. G., Dai, H., Hafner, J. H., Bradley, R. K., Boul, P.J. (1998). Fullerene pipes. *Science*, 280, 1253–6.
- [15] Kim, M. G., Moon, J.B., Kim, C. G. (2012). Effect of CNT functionalization on crack resistance of a carbon/epoxy composite at a cryogenic temperature. *Compos. Part A*, 43, 1620–1627.

- [16] Park, S. J., Cho, M. S., Lim, S.T., Choi, H. J., Jhon, M. S. (2003). Synthesis and dispersion characteristics of multi-walled carbon nanotube composites with poly(methyl methacrylate) prepared by in-situ bulk polymerization. *Macromol. Rapid Commun.*, 24, 1070–3.
- [17] Boehm, H. P., Diehl, E., Heck, W., Sappok, R. (1964). Surface oxides of carbon. *Angew Chem. Int.*, 3, 669–677.
- [18] Boehm, H. P. (1994). Some aspects of the surface chemistry of carbon blacks and other carbons. *Carbon*, 32, 759-69.
- [19] Datsyuk, V., Kalyva, M., Papagelis, J., Galiotis, C. (2008). Chemical oxidation of multi-walled carbon nanotubes. *Carbon*, 46, 833-840.
- [20] George, N., Julie Chandra C. S., Mathiazhagan, A., Joseph, R. (2015). High performance natural rubber composites with conductive segregated network of multi-walled carbon nanotubes. *Compos. Sci. Technol.*, 116, 33-40.
- [21] Yang, D., Guo, G., Hu, J., Wang, C., Jiang, D. (2008). Hydrothermal treatment to prepare hydroxyl group modified multi-walled carbon nanotubes. *J. Mater. Chem.*, 18, 350-354.
- [22] Jiang, J., Wang, Z., Xu, F., Xu, J. (2014). Effect of functionalization of MWCNTs on the electrical conductivity and mechanical properties of unsaturated polyester resin composites. *Polym. Polym. Compos.*, 22, 209-214.
- [23] Shahnawaza, S., Sohrabi, B., Najafib, M. (2014). The investigation of functionalization role in multi-walled carbon nanotubes dispersion by surfactants, *The 18<sup>th</sup> electronic international conference on synthetic organic chemistry*. Switzerland: MDPI.
- [24] Silva, W. M., Ribeiro, H., Seara, L. M., Silva, G. G. (2012). Surface properties of oxidized and aminated multi-walled carbon nanotubes. *J. Braz. Chem. Soc.*, 23, 1078-1086.
- [25] Yudianti, R., Onggo, H., Sudirman, Yukie Saito, Tadahisa Iwata, Jun-ichi Azuma. (2011). Analysis of Functional Group Sited on Multi-Wall Carbon Nanotube Surface. *Mater. Sci. J.*, 5, 242-247.

- [26] Murphy, H., Papakonstantinou, P., Okpalugo, T. I. T. (2006). Raman study of multi-walled carbon nanotubes functionalized with oxygen groups. *J. Vac. Sci. Technol. B.*, 24, 715 -20.
- [27] Singh, D. K., Iyer, P. K., Giri, P. K. (2008). Functionalization of Carbon nanotubes and study of its optical and structural properties. *Nanotrends: J. Nanotechnol. Appl.*, 4, 55-58.
- [28] Chen, L., Xie, H., Li, Y., Yu, W. (2008). Surface chemical modification of multi-walled carbon nanotubes by a wet-mechanochemical reaction. *J. Nanomater.*, 2008, 1-5.
- [29] Zhang, J., Zou, H., Qing, Q., Yang, Y., Li, Q., Liu, Z., Guo, X., Du, Z. (2003). Effect of chemical oxidation on the structure of single-walled carbon nanotubes. *J. Phys. Chem. B*, 107, 3712-3718.
- [30] Lu, Y. Y., Li, H., Liu, H. Z. (2010). Maleic anhydride functionalization of multi-walled carbon nanotubes by the electron beam irradiation in the liquid media. *Physica E*, 43, 510–514.



## Modification of unsaturated polyester resin with MA functionalized MWCNTs

### 3.B.1 Introduction

Unsaturated polyester resins (UPR) are the most commonly used thermosetting polymer for the production of composite material, mainly glass fibre reinforced plastics (FRP) [1, 2]. They have been utilized in a variety of applications like construction, automotive, marine, aerospace and advanced naval structures [3, 4]. The nonreinforced form of polyester resin is used to make gel coats, automotive repair putty and filler, cultured marbles, adhesives, bowling balls and buttons etc. Low cost, quick curing, light weight, ease of handling and good balance of mechanical, chemical and electrical properties made UP resins commercially important for multifunctional applications [5, 6]. However low impact strength and brittleness limits their use for some advanced engineering applications [7, 8]. So the thermo mechanical properties and load transfer ability is to be improved. To overcome these drawbacks different type of fillers are incorporated in UPR to fabricate filler reinforced composites [9, 10].

Carbon nanotubes (CNTs) have captured the interest of researchers due to their unique mechanical, electrical and physical properties. So there has been considerable research in utilizing CNTs as reinforcement for polymer nanocomposites. Seyhan et al. reported the critical aspects related to the processing of UPR-CNT nanocomposites. They studied the

rheological properties and observed shear thinning behavior for CNT/polyester suspension [11,12]. Battisti et al. prepared electrically conductive polyester nanocomposite with percolation threshold at 0.026 wt% loading of carbon nanotubes [13]. The mechanical and thermal properties of polyester/ MWCNT composites were studied by Makki et al. They observed an enhancement in these properties upon the addition of MWCNTs [14].

The degree of dispersion and interfacial adhesion of CNTs in polymer matrix is a key factor which determines the final properties of the composite. The large surface area and van der Waal's interaction of CNTs restrict their homogeneous dispersion in polymer matrix. So these entangled aggregates are very difficult to separate into individual tubes. Different physical and chemical methods are employed to achieve good dispersion of CNTs in polymer matrix [15]. Physical methods include mechanical stirring, three-roll milling, shear mixing and ultrasonication. Ultrasonication is a popular method which involves direct mixing of nanotubes by the application of ultrasound energy. Besides the physical methods, chemical methods like surfactant modification, surface functionalization and polymer wrapping methods are also used to obtain good adhesion between CNTs and polymer matrix. Surface modification by covalent functionalization is a key area of interest in recent research. Carboxylated, hydroxylated and amine functionalized CNTs are used to fabricate CNT/ polyester nanocomposite. So depending upon the polymer matrix, an effective chemical modification method is required to obtain good dispersion of CNT in polymer without destructing the properties of CNT.

In the present study maleic anhydride (MA) functionalized MWCNTs is proposed to be used to modify UP resins. MA is an important monomer used for the preparation of UP resin. The unsaturation present on MA enables crosslinking reaction between polyester chain and styrene. The hydroxyl and carboxyl groups present on the surface of MA-MWCNTs may improve the interaction between polyester and MWCNTs. Moreover the double bond present in MA may also take part in the cross-linking reaction upon curing. The thermal, mechanical and electrical properties of MWCNT/polyester composites are also proposed to be investigated.

### **3.B.2 Experimental**

#### **3.B.2.1 Preparation of MA-MWCNT/ UPR composites**

About 0.1-1 wt% MA-MWCNTs were mixed with THF solvent maintaining the CNT:THF ratio as 1:25 (w/v). This MA-MWCNT suspension mechanically stirred for 15 minutes by a magnetic stirrer followed by ultrasonication in an ice bath for 1h. After that it is mixed with UPR and stirred for 15min followed by ultrasonication for 40min. This CNT/UPR suspension heated at the boiling temperature of THF (66°C) for 5 min to remove the solvent. To the cooled suspension 0.5 wt% cobalt octoate (promoter) was added and gently stirred for 5min and placed in vacuum to remove the bubbles. About 1.5 wt% MEKP initiator was added to this and stirred. After that this mixture is poured in to Teflon molds and cured at room temperature for 24h followed by post curing at 70°C for 4h. The same procedure was repeated for P-MWCNT/ UPR composites. The detailed procedure was given in Chapter 2.

### **3.B.2.2 Characterization**

The dynamic mechanical properties of the composites were measured using dynamic mechanical analyzer DMA (Model Q 800, TA instruments). The tensile properties were determined using Universal Testing Machine (UTM, 10 kN). The three-point bending flexural test was conducted to analyze bending strength and modulus of the composite on a 10kN UTM machine.

The changes in physical and chemical properties of composites as a function of increasing temperature were measured using Thermo Gravimetric Analysis (TGA). The fractured surfaces of nanocomposites were investigated by Scanning Electron Microscopy (SEM). The dispersion of P-MWCNTs and MA-MWCNTs in UPR was analyzed by Transmission Electron Microscopy (TEM).

The dielectric properties of the samples were measured using Precision Impedance Analyzer (Agilent 4294A) in band width from 40 Hz to 30 MHz. The Electro Magnetic Interference shielding behavior of nanocomposites was studied using Agilent Performance Network Analyzer from 8-12 GHz range in the X-band region.

### **3.B.3 Results and discussions**

The first stage dispersion of MWCNTs in THF is a convenient technique than direct mixing of CNTs in UP resin. The MWCNT aggregates get dispersed quickly in THF than in polyester resin [15, 16]. This finally makes fine dispersion of MWCNTs in resin matrix. The cured samples are shown in Fig. 3.B.1.



Fig. 3.B.1 Cured MA-MWCNT/polyester samples

### 3.B.3.1 Dynamic mechanical properties

Dynamic mechanical analysis is useful in finding the viscoelastic properties such as storage modulus ( $E'$ ), loss modulus ( $E''$ ) and damping factor ( $\tan \delta$ ) of MWCNT/ UPR composites.

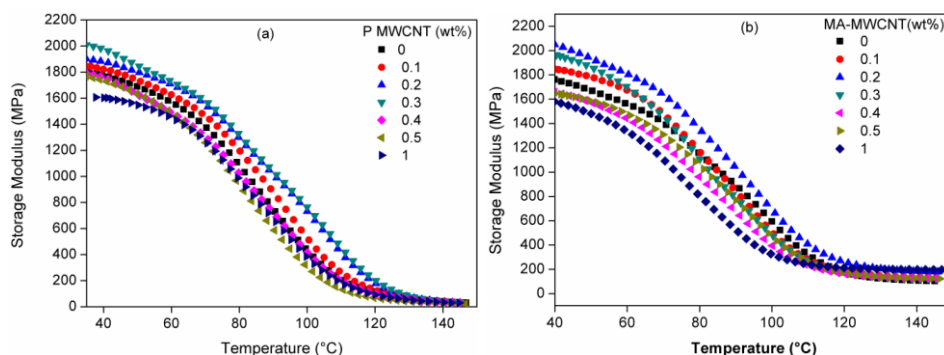


Fig. 3.B.2 Variation of storage modulus of (a) P-MWCNT & (b) MA-MWCNT UPR composites with temperature

The change in storage modulus of the samples as a function of temperature is given in Fig. 3.B.2. In the case of P-MWCNT/UPR

composites, the storage modulus increases significantly up to 0.3 wt% after that it decreases. But in the case of MA-MWCNT/UPR maximum value is shown by 0.2 wt% loading. It clearly indicates that MA functionalization on MWCNT enhances the interfacial interaction with the polyester matrix when compared to P-MWCNTs. The enhanced storage modulus indicates that in the glassy state the motion of polyester chains were restricted by the filler and it is more in the case of MA-MWCNT/UPR composites [17]. This effect is more pronounced in the glass transition region which can be observed from  $\tan \delta$  curves.

**Table 3.B.1** Storage modulus values of P-MWCNT & MA-MWCNT UPR composites

Filler wt%	Storage Modulus at 40°C	
	P MWCNT UPR	MA MWCNT UPR
0	1761	1761
0.1	1821	1862
0.2	1880	<b>2047</b>
0.3	<b>1976</b>	1980
0.4	1759	1661
0.5	1737	1644
1	1604	1593

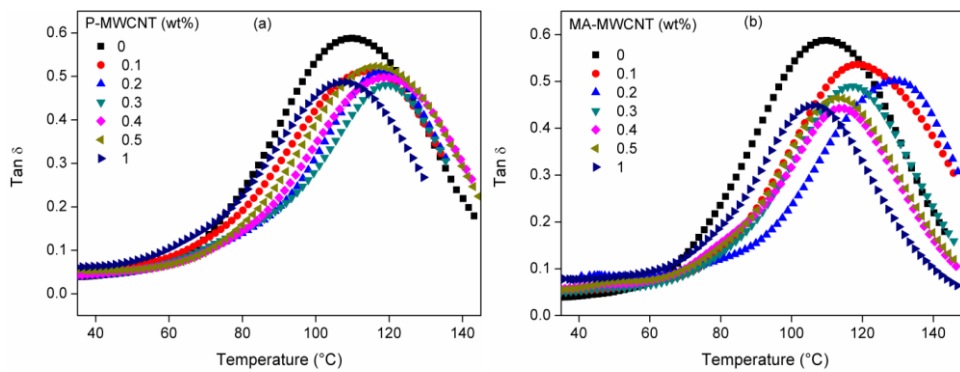


**Fig. 3.B.3** Variation of  $\tan \delta$  curves of (a) P-MWCNT & (b) MA-MWCNT UPR composites with temperature

**Table 3.B.2**  $T_g$  values of P-MWCNT & MA-MWCNT UPR composites from  $\tan \delta$  curve

Filler wt%	$T_g$ values from $\tan \delta$ curve	
	P-MWCNT UPR	MA-MWCNT UPR
0	108	108
0.1	114	118
0.2	117	<b>129</b>
0.3	<b>120</b>	116
0.4	118	114
0.5	113	113
1	107	105

In order to understand the increase of storage modulus at low concentration of CNTs, the DMA curves of  $\tan \delta$  versus temperature was analyzed and the corresponding  $T_g$  values are given in Table 3.B.1. The  $T_g$  occurs at 108°C for neat polyester resin, where as it slightly increases to 114°C, 118°C for P-MWCNT and MA-MWCNT composites respectively. For composites loaded with 0.2 wt% of MA-MWCNT, the  $T_g$  increased to 129°C, which is nearly 20°C higher than neat UPR. So it suggests that  $T_g$  values are higher in which covalent bonded interface interactions are more. The mobility of polymer matrix around the nanotube is reduced due to the presence of CNTs [11]. MA functionalization considerably enhances the interface adhesion between MWCNTs and UPR, which leads to hindered relaxational mobility in the polymer chains in the interfaces [18]. At higher concentration of CNTs, lacking of surrounding entanglement and agglomeration leads to lowering of  $T_g$  and modulus.

### 3.B.3.2 Static mechanical properties

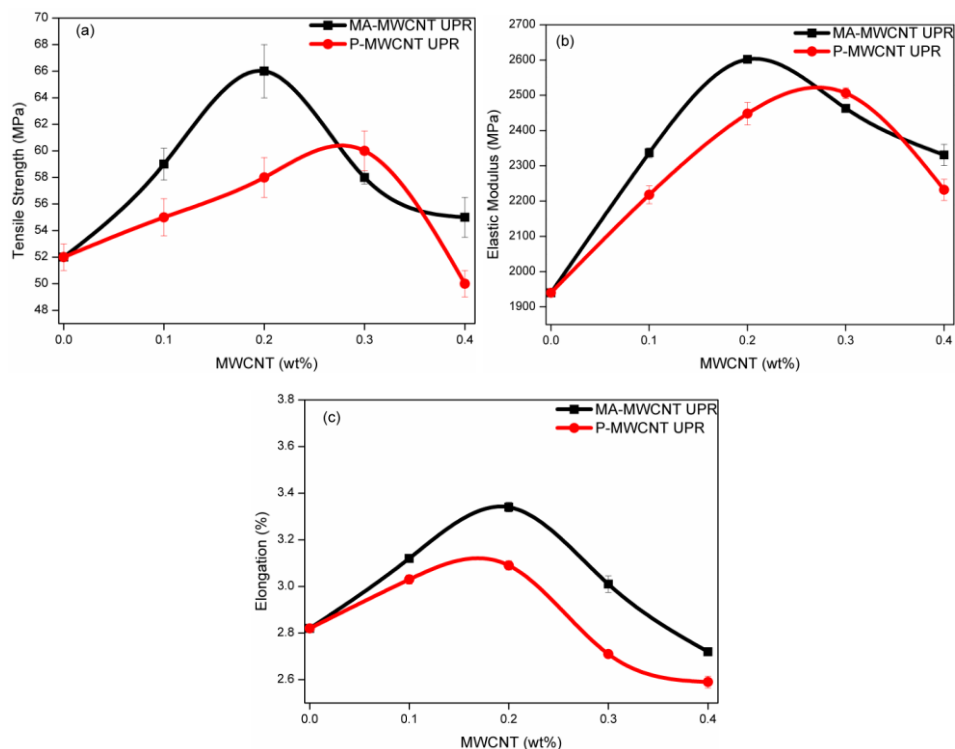


**Fig. 3.B.4** Variation of (a) tensile strength (b) tensile modulus & (c) elongation at break of MWCNT/UPR composites with nanofiller content

A considerable improvement in the tensile strength, modulus and elongation at break is observed for MWCNT/UPR composites (Fig. 3.B.4). Compared to P-MWCNT, MA-MWCNT/UPR composites show higher improvement in the static mechanical properties. Such an increasing trend persists with increase of MA-MWCNT content till 0.2 wt%. At this concentration, the composite achieved about 21%, 25% and 12% increase in tensile strength, modulus and % of elongation



respectively compared to neat UPR. The MA functionalization enhances the dispersion of MWCNT in UP resin which enabled an efficient load transfer in the system. The slight increase in the elongation at break value indicates that MWCNT not only enhances the mechanical strength but also imparts plastic deformation behaviour in the nanocomposite [16]. At high loading of CNTs, the major problem is agglomeration of nanotubes which acts as stress concentrations and thus decreases the mechanical properties [19]. More over at high concentration of MWCNT, the viscosity of the polyester resin increases considerably which further resulted in processing difficulties of the nanocomposite [14]. Thus it is concluded that MA-MWCNTs improve the mechanical properties of the polyester resin at low weight fractions.

The flexural properties follow the same trend as observed in the case of tensile properties. Flexural strength and modulus increases with MWCNT loading and the maximum values are obtained for 0.2 wt% MA-MWCNT. MA-MWCNT provides better interface interaction with the polymer matrix compared to non-functionalized MWCNTs. About 26%, 40% and 17% improvement in flexural strength, modulus and deformation is observed for 0.2 wt% MA-MWCNT UPR composite (Fig. 3.B.5). Considering the impact strength of composite, about 30% improvement is observed for 0.2 wt% loading of MA-MWCNTs (Fig. 3.B.5 (d)). At lower concentration of fillers the distribution is homogeneous and stress transfer takes place in an effective manner. At higher loading agglomeration is observed and effective stress transfer will not take place which further reduces the mechanical properties [20].

More over the increase in viscosity of the liquid resin causes non homogeneous distribution of nano fillers.

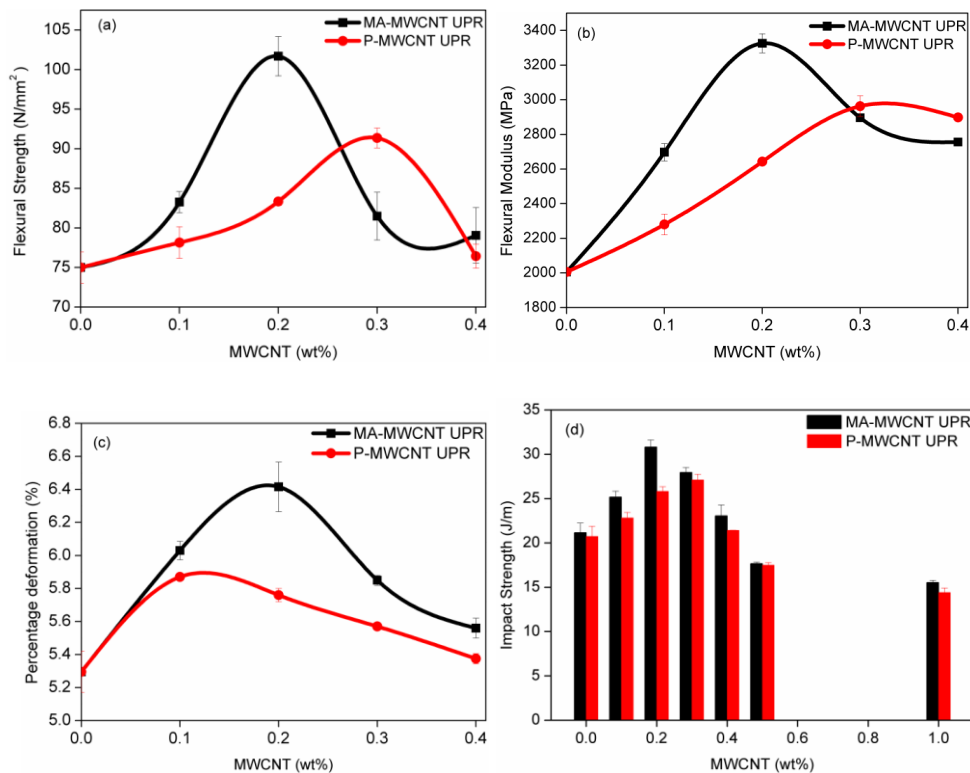


**Fig. 3.B.5** Variation of (a) flexural strength (b) Modulus (c) % deformation and (d) impact strength of P-MWCNT/MA-MWCNT UPR composites with nanofiller content

### 3.B.3.3 Thermo gravimetric analysis

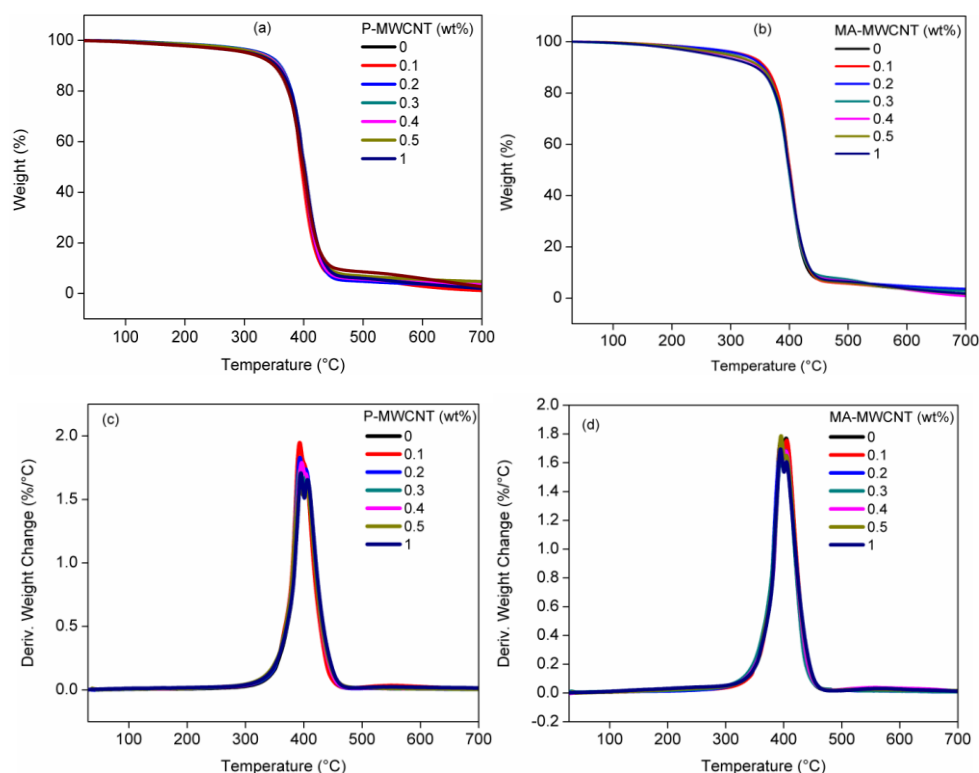


**Fig. 3.B.6** Thermogram [(a) and (b)] and differential thermogram [(c) and (d)] of P-MWCNT/MA-MWCNT UPR composites

The thermal properties of P-MWCNT/MA-MWCNT UPR nanocomposites were studied and the results are given in Fig. 3.B.6. It is observed that all the nanocomposites show comparable thermal stability with a single step degradation process. This may be attributed to the decomposition of cross-linked polyester network. A significant enhancement in the thermal stability is not observed since the amount of MWCNTs used is very small.

### 3.B.3.4 Morphological properties

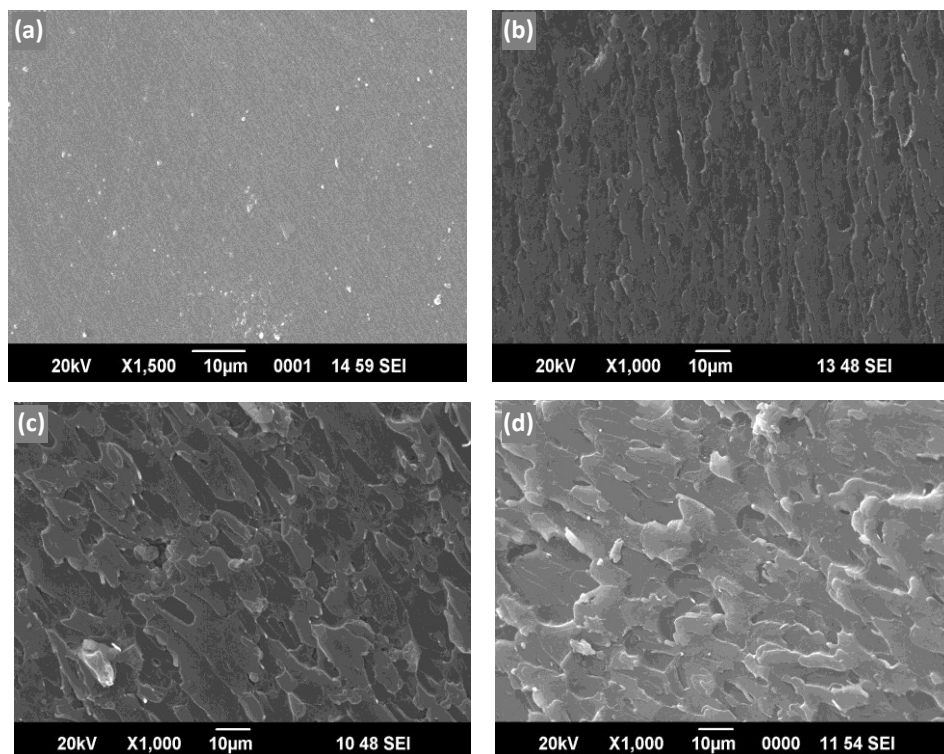


**Fig. 3.B.7** SEM micrographs of (a) Neat UPR (b) 0.3% P-MWCNT UPR (c) 0.1% MA-MWCNT UPR and (d) 0.2% MA-MWNT UPR.

Fig. 3.B.7 illustrates SEM micrographs of fractured surfaces of neat UPR and MWCNT/UPR nanocomposites. The neat UPR shows flat, smooth and featureless morphology but nanocomposite shows rough and patterned morphology. 0.3% P-MWCNT UPR composite shows rough morphology but the roughness is very less compared to MA-MWCNT UPR composites. A very clear patterned fracture surface is obtained in the case of 0.2% MA-MWCNT UPR composite which indicates good wetting of CNTs in the polymer matrix. This strongly suggests that by

means of MA functionalization and solvent mixing the MWCNTs are homogeneously dispersed to some extent in UPR matrix [16, 21].

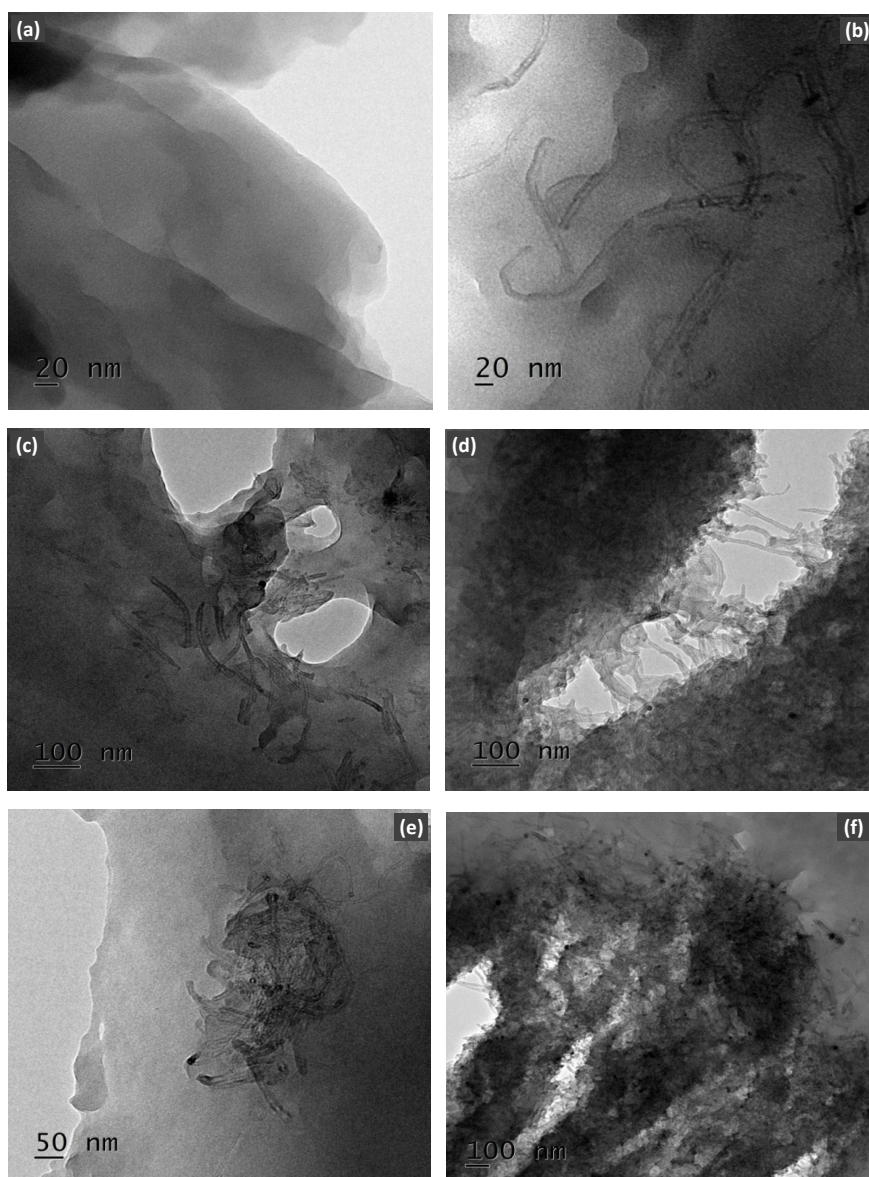


**Fig.3.B.8** TEM images of (a) Neat UPR and MWCNT/UPR composites with (b) 0.1% MA-MWCNT (c) 0.2% MA-MWCNT (d) 0.4% MA-MWCNT (e) 0.2% P-MWCNT and (f) 0.4% P-MWCNT.

The TEM micrographs of UPR and MWCNT-UPR nanocomposites are shown in Fig. 3.B.8. MWCNTs with MA functionalization exhibited better dispersion in the polymer matrix as seen from the images. At higher concentration agglomeration is observed and it is high in the case of P-MWCNT composite which is caused by their high surface area. From the morphological studies it is clear that MA functionalization improves the dispersion of MWCNTs in polyester matrix which finally gives good mechanical properties. These findings are similar to the results reported earlier [12].

### **3.B.3.5 Dielectric properties**

The dielectric permittivity and loss tangent values of MWCNT/UPR composites are depicted in Fig. 3.B.9 &10. Only a slight increase in these values is observed in the case of P-MWCNT UPR while the value increases at lower frequency and decreases at higher frequency for MA-MWCNT UPR composites. The dipole moment and charge carriers can freely move within the MWCNT-UPR nanocomposites at low frequencies and they follow the varying electromagnetic field. But at higher frequencies the charge carriers and dipoles become unable to follow the variations of the applied field which will decrease the dielectric permittivity and loss. In addition to this, Maxwell-Wagner-Sillars (MVS) polarization for the heterogeneous systems also plays significant role in improving the dielectric constant. It is associated with the accumulation of charges between insulator-conductor interfaces and can be characterized by the frequency dependence of dielectric constant at low frequency range. At lower filler loading of MA-MWCNT the dielectric constant is almost

independent of frequency indicating that there is no plentiful accumulation of interfacial charges inside the nanocomposite.

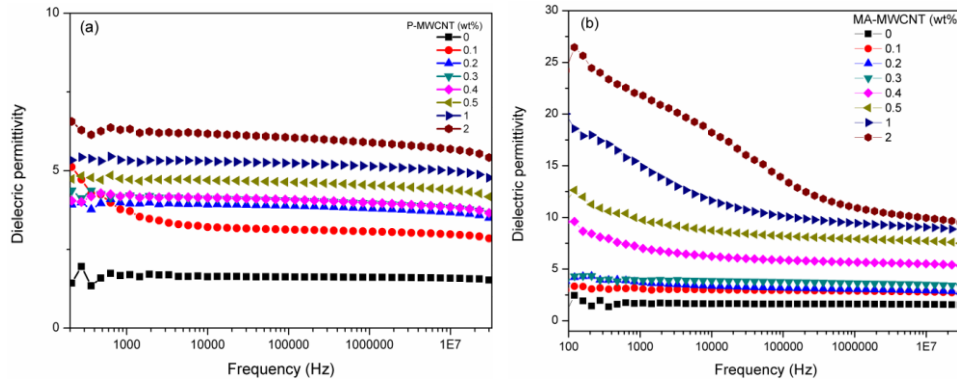


**Fig. 3.B.9** Dielectric permittivity as a function of frequency for (a) P-MWCNT and (b) MA-MWCNT UPR composites

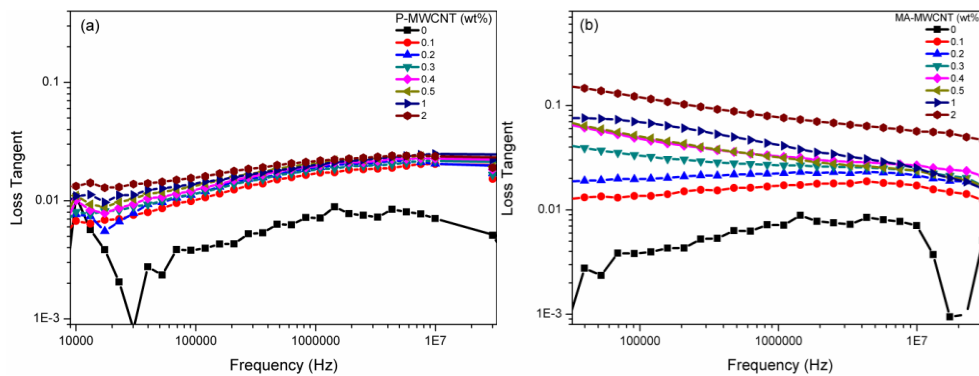


**Fig. 3.B.10** Loss tangent as a function of frequency for (a) P-MWCNT and (b) MA-MWCNT UPR composites

After a certain concentration, a sudden increase in dielectric constant is observed at lower frequencies. This indicates that a lot of charges were blocked at the interfaces which make a remarkable contribution to dielectric permittivity at low frequency range. However at high frequency

the dielectric permittivity was contributed by micro capacitance structure model (frequency independent model) so that the values are in a steady form [22, 23]. Thus the conductor- insulator layer formed between MWCNT and polyester enhances the dielectric properties of the nanocomposite compared to neat UPR.

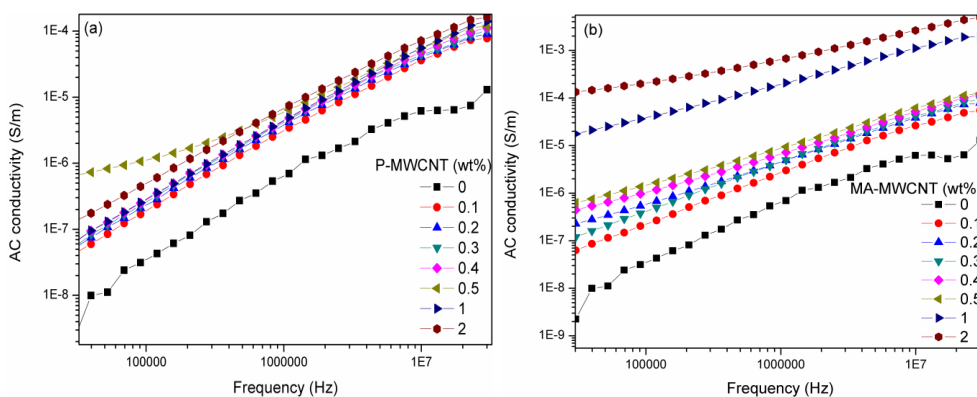


**Fig. 3.B.11** Plot of AC conductivity as a function of frequency for (a) P-MWCNT and (b) MA-MWCNT UPR composites

The variation of AC conductivity with MWCNT loading is depicted in Fig. 3.B.11. It is calculated from dielectric permittivity and dielectric loss by using the equation  $\sigma_{AC} = 2\pi f \epsilon_0 \epsilon' \tan\delta$ . Where  $\epsilon_0$  corresponds to permittivity of vacuum,  $\epsilon'$  is the real permittivity and  $f$  is the frequency at room temperature. The neat polyester resin shows a purely capacitive behaviour at all frequencies. The AC conductivity is increasing with increase in frequency for P-MWCNT and MA-MWCNT composites. At lower frequencies conduction will be provided by the displacement currents associated with the dipole moment whereas at higher frequencies it is due to the presence of induced surface currents within the material which is created by the application of external electric field. The



conductivity ( $\sigma$ ) reached a value of  $4.68 \times 10^{-9}$  and  $7.18 \times 10^{-5}$  for 2 wt% P-MWCNT and MA-MWCNT loading at frequency 1 kHz. At 10 MHz the value for  $\sigma$  is  $7.47 \times 10^{-6}$  and  $6.77 \times 10^{-4}$  for 2 wt% P-MWCNT and MA-MWCNTs. The MA-MWCNT UPR nanocomposite shows considerable enhancement in the  $\sigma$  value due to better dispersion in the polymer matrix. The quality of filler dispersion is a critical factor which governs the conductivity enhancement [24, 25].

### **3.B.3.6 EMI shielding effectiveness**

The EMI shielding measurements of MWCNT polyester nanocomposites were carried out in the X-band (8-12 GHz) region using wave-guide coupled to a ZVB20 network analyzer. MWCNT- polymer nanocomposites with good conductive network and dielectric properties can be used as micro wave absorbers and electromagnetic shielding materials for both civil and military applications. The EMI shielding properties of MWCNT filled nanocomposites depends on intrinsic electrical conductivity of CNTs, interaction between CNTs, polymer matrix-CNT interaction, CNT agglomeration, thickness of the sample and frequency of the microwave. The shielding effectiveness (SE) is a number that quantifies the amount of attenuation of electromagnetic wave. The total EMI SE is defined as  $SE(\text{dB}) = \log(P_I/P_T)$ , where  $P_I$  and  $P_T$  are the power of incident and transmitted electromagnetic wave respectively [26, 27]. The SE of MWCNT-UPR composite is shown in Fig. 3.B.12 (a) and (b). The value of SE for neat UPR is very low because of its insulating nature. As the concentration of MWCNTs increases shielding efficiency

also increases. In all the composites the SE decreases with increase in frequency.

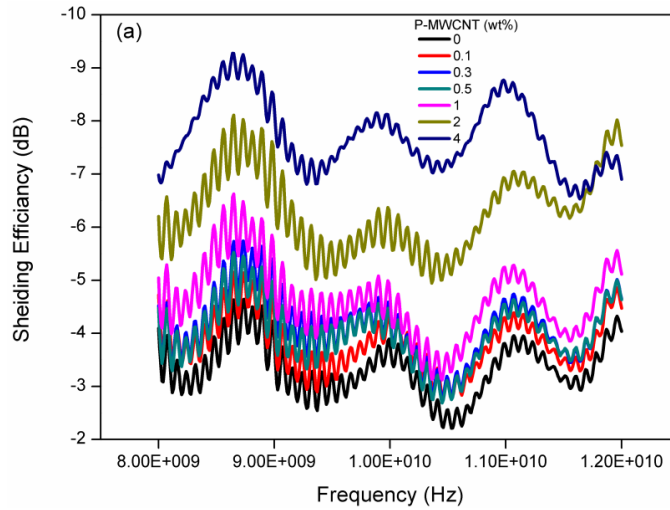


Fig. 3.B.12 (a) Variation of SE with frequency for P-MWCNT/UPR composites

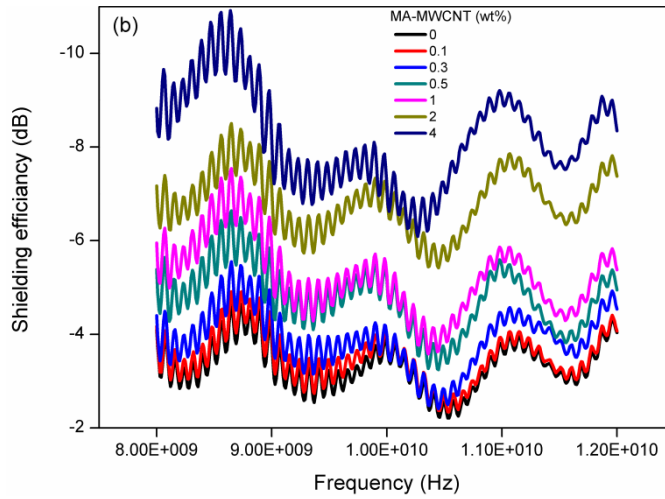


Fig. 3.B.12 (b) Variation of SE with frequency for MA-MWCNT/UPR composites

Compared to P-MWCNT UPR composite, MA-CNT UPR composite shows high SE value. At 8.6 GHz, SE reaches a value of 10.9 dB and 9.2 dB for 4 wt% loading of MA-MWCNT and P-MWCNT respectively. The enhancement of the EMI SE is mainly attributed to formation of conducting networks by MWCNTs in the insulating polyester matrix, which will interact with the incident radiation and it is attenuated by reflecting and scattering many times between conductor-insulator interfaces thus hindering the escape of wave from the material [28]. Though high SE values are required for certain applications, composites with SE value in this range can be used for static dissipation of charges [29, 30].

The decrease in SE with increase in frequency can be described by the effect of interfacial polarization. The frequency dependent dielectric properties of MWCNT-UPR composites can enhance the SE. As the MWCNT content increases, accumulation of charges at the interface also increases, which considerably improve the dielectric loss thus enhances the shielding efficiency. As the frequency increases the dielectric properties of the composites was dominated by micro capacitance structure model (frequency independent). Thus the effect of interfacial polarization decreases at higher frequency which further decreases the SE.

### **3.B.4 Conclusions**

Unsaturated polyester resins were modified by P-MWCNT and MA-MWCNTs at different loadings through solvent dispersion and sonication methods. The dispersion of MWCNTs in polyester matrix has been investigated by TEM analysis. Improved mechanical properties are obtained for the MA-MWCNT UPR composites compared to P-MWCNT

UPR composites. Considerable enhancement in storage modulus and  $T_g$  values are observed for the nanocomposites. About 25%, 40% and 30% increase in tensile, flexural modulus and impact strength is observed for the MA-MWCNT UPR composite at 0.2 wt% loading. Thermogravimetric analysis reveals comparable thermal stability for all the composites. The fracture surface morphology by SEM analysis supports the dispersion of MWCNTs in polyester matrix. The dielectric permittivity, dielectric loss and AC conductivity of UP resins are improved by the incorporation of MWCNTs. Moreover MA functionalization on CNTs significantly improved the homogeneous dispersion of CNTs in polyester matrix which further improves the mechanical and dielectric properties. These MWCNT-UPR nanocomposites with improved SE property can be used as EMI shielding materials.

## Reference

- [1] Boenig, H. V. (1964). *Unsaturated polyesters: structure and properties*, Amsterdam: Elsevier.
- [2] Grayson, M., Eckroth, D. (1982). *Encyclopedia of chemical technology*, 3rd ed., Vol 18, New York: John Wiley & Sons.
- [3] Puglia, D., Biagiotti, J., Kenny, J. M. (2005). A review on natural fibre-based composites-Part II, *J. Nat. Fibers*, 1, 23-65.
- [4] Baley, C., Perrot, J. Y., Davies, P., Bourmaud, Grohens, Y. (2006). Mechanical properties of composites based on low styrene emission polyester resins for marine applications. *Appl. Compos. Mater.*, 13, 1–22.
- [5] Berins, M. L. (1991). *SPI Plastics engineering handbook of the society of plastic industry*, 5<sup>th</sup> edition, Verlag: Springer.

- [6] Baskaran, M. Sarojadevi, C.T. Viyakumar, J. (2011). Unsaturated polyester nanocomposites filled with nano alumina. *Mater. Sci.*, 46, 4864-4871.
- [7] Hameed, A., Islam, M., Ahmad, I., Mahmood, N., Saeed, S., Javed, H. (2015). Thermal and mechanical properties of carbon nanotube/epoxy nanocomposites reinforced with pristine and functionalized multi-walled carbon nanotubes. *Polym. Compos.*, 36, 1891.
- [8] Singh, N. K., Singh, K. K. (2015). Mechanical behavior of glass/epoxy composite laminate with varying amount of MWCNTs under different loadings. *Polym. Compos.*, 36, 1786.
- [9] Mehta, G., Mohanty, A. K., Misra, M., Drzal, T. (2004). Effect of novel sizing on the mechanical and morphological characteristics of natural fiber reinforced unsaturated polyester resin based bio-composites. *J. Mater. Sci.*, 39, 2961 – 2964.
- [10] Sreenivasan, V. S., Ravindran, D., Manikandan, V., Narayanasamy, R. (2011). Mechanical properties of randomly oriented short Sansevieria cylindrical fibre/polyester composites. *Mater. Des.*, 32, 2444–2455.
- [11] Seyhan, A. T., Gojny, F. H., Tanoglu, M., Schulte, K. (2007). Rheological and dynamic-mechanical behavior of carbon nanotube/vinyl ester–polyester suspensions and their nanocomposites. *Eur. Polym. J.*, 43, 2836–2847.
- [12] Seyhan, A. T., Gojny, F. H., Tanoglu, M., Schulte, K. (2007). Critical aspects related to processing of carbon nanotube/unsaturated thermoset polyester nanocomposites. *Eur. Polym. J.*, 43, 374–379.
- [13] Battisti, A., Skordos, A. A., Partridge, I. K. (2009). Percolation threshold of carbon nanotubes filled unsaturated polyesters. *Compos. Sci. Technol.*, 69, 1516–1520.
- [14] Makki M. S. I., Abdelaal, M. Y., Bellucci, S., Salam, M. A. (2014). Multi-walled carbon nanotubes/unsaturated polyester composites: mechanical and thermal properties study, *Fuller. Nanotub. Car. N.*, 22, 820-833.

- [15] Moshiul Alam, A. K. M., Beg, M. D. H., Yunus, R. M. (2015). Influence of carbon nanotubes on the thermo-mechanical properties of unsaturated polyester nanocomposites. *IOP Conf. Ser.: Mater. Sci. Eng.*, 78, 012023.
- [16] Beg, M. D. H., Moshiul Alam, A. K. M., Yunus, R. M., Mina, M. F. (2015). Improvement of interaction between pre-dispersed multi-walled carbon nanotubes and unsaturated polyester resin. *J. Nanopart. Res.*, 17, 1-13.
- [17] Chen, L., Chai, S., Liu, K., Ning, N., Gao, J., Liu, Q., Chen, F., Fu, Q. (2012). Enhanced epoxy/silica composites mechanical properties by introducing graphene oxide to the interface. *ACS Appl. Mater. Interfaces*, 4, 4398–4404.
- [18] Wang, L., Wang, K., Chen, L., Zhang, Y., He, C. (2006). Preparation, morphology and thermal/mechanical properties of epoxy/nanoclay composite. *Compos. Part A*, 37, 1890–1896.
- [19] Shokrieh, M. M., Saeedi, A., Chitsazzadeh, M. (2013). Mechanical properties of multi-walled carbon nanotube/polyester nanocomposites. *J. Nanostruct. Chem.*, 3, 1-5.
- [20] Bindu Sharmila, T.K., Nair, A. B., Abraham, B. T., Sabura Beegum, P. M., Thachil, E. T. (2014). Microwave exfoliated reduced graphene oxide epoxy nanocomposites for high performance applications. *Polymer*, 55, 3614-3627.
- [21] Murarescu, M., Dima, D., Andrei, A. G., Circiumaru, A. (2014). Synthesis of polyester composites with functionalized carbon nanotubes by oxidative reactions and chemical deposition. *Dig. J. Nanomater. Biostruct.*, 9, 653 – 665.
- [22] Dang, Z. M., Wang, L., Yin, Y., Zhang, Q., Lei, Q. Q. (2007). Giant dielectric permittivities in functionalized carbon-nanotube/ electroactive-polymer nanocomposites. *Adv. Mater.*, 19, 852.
- [23] He, F., Lau, S., Chan, H. L., Fan, J. (2009). High dielectric permittivity and low percolation threshold in nanocomposites based on poly(vinylidene fluoride) and exfoliated graphite nanoplates. *Adv. Mater.*, 21, 710-715.

- [24] Brosseau, C. (2002). Generalized effective medium theory and dielectric relaxation in particle-filled polymeric resins. *J. Appl. Phys.*, 91, 3197–204.
- [25] Mdarhri, A., Carmona, F., Brosseau, C., Delhaes, P. (2008). Direct current electrical and microwave properties of polymer-multi-walled carbon nanotubes composites. *J. Appl. Phys.*, 103, 054303.
- [26] Kim, H. M., Kim, K., Lee, C. Y., Joo, J., Cho, S. J., Yoon, H. S. (2004). Electrical conductivity and electromagnetic interference shielding of multi-walled carbon nanotube composites containing Fe catalyst, *Appl. Phys. Lett.*, 84, 589–91.
- [27] Huang, Y. L., Yuen, S. M., Ma, C. C. M., Chuang, C. Y., Yu, K. C., Teng, C. C. T., Tien, H. W., Chiu, Y. C., Wua, S. Y., Liao, S. H., Weng, F. B. (2009). Morphological, electrical, electromagnetic interference (EMI) shielding, and tribological properties of functionalized multi-walled carbon nanotube/poly methyl methacrylate (PMMA) composites. *Compos. Sci. Technol.*, 69, 1991–1996.
- [28] Yan, D. X., Pang, H., Li, B., Vajtai, R., Xu, L., Ren, P. G., & Li, Z. M. (2015). Structured Reduced Graphene Oxide/Polymer Composites for Ultra-Efficient Electromagnetic Interference Shielding. *Adv. Funct. Mater.*, 25, 559-566.
- [29] Dhawan, S. K., Singh, N., & Rodrigues, D. (2003). Electromagnetic shielding behaviour of conducting polyaniline composites. *Sci. Technol. Adv. Mater.*, 4, 105 -113.
- [30] Liu, Z., Bai, G., Huang, Y., Ma, Y., Du, F., Li, F. (2007). Enhanced dielectric constants and shielding effectiveness of, uniformly dispersed, functionalized carbon nanotube composites. *Carbon*, 45, 821–7.







**UNSATURATED POLYESTER RESIN- REDUCED GRAPHENE OXIDE COMPOSITES****Contents**

*Part A: Preparation of silver decorated reduced graphene oxide nanohybrids*

*Part B: Modification of Unsaturated polyester resin with rGO-Ag nanohybrids*

Water assisted modified Hummers method is adopted for the oxidation of natural graphite to hydroxyl and epoxide rich graphene oxide. rGO and rGO-Ag nano fillers were synthesized from GO by chemical reduction method using Vit-C as a reducing agent. The formation of silver decorated reduced graphene oxide is confirmed by FT-IR, XRD and UV-Vis analysis. TEM micrograph shows that nano sized silver nano particles are homogeneously distributed in the graphene oxide layers. RGO/rGO-Ag UPR composites were prepared and mechanical and dielectric properties were investigated. Enhanced mechanical properties are observed for the nano hybrid composite compared to rGO composite. Ag nano particles acting as spacers between graphene oxide sheets and preventing its restacking upon reduction may be the reason for this.

## Preparation of silver decorated reduced graphene oxide nanohybrids

### 4.A.1 Introduction

Owing to its remarkable physical properties and to the perspective of unique applications, in recent years graphene has emerged as a subject of intense research [1, 2]. Graphene nano sheets, a nano structure of carbon material exhibit unique structure of two-dimensional sheet composed of  $sp^2$  bonded carbon atoms with one atom thickness [3]. They possess large surface area and strong interaction towards metals [4, 5]. These properties make them as a supporting material for dispersing the metal nano particles on their surfaces. This type of metal graphene nano hybrids shows extra ordinary electrical and thermal conductivity, thermal stability and excellent mechanical properties [6, 7]. But practically these properties cannot be utilized because upon drying the graphene dispersion these sheets were tend to agglomerate like other dispersion of nano material with high aspect ratios. Thus the advantage caused by the ultra-high surface area of two dimensional nano sheets is lost. So graphene nano sheets behave like ordinary graphite sheets with low surface area [8].

Several studies have been reported recently in which introduction of metal nano particles to graphene dispersion which causes exfoliation of graphene sheets [8, 9]. The metal nano particle acts as a “spacer” between the graphene sheets which increases the distance between graphene layers to several nanometers there by making the faces of graphene accessible even in the dry state. Thus the unique properties exhibited by two

dimensional graphene are retained when it is dispersed in to polymer matrices.

Silver nano particles have received a great attention because of their unique optical properties, electrical and thermal conductivity and surface plasmon resonance [10, 11]. For graphene polymer composites one important feature of graphene metal nano particle is that they provide an efficient way to solve the separation problem of graphene sheets since these nano particle act as spacers between graphene layers which keeps the adjacent nano sheets separated and efficiently suppress the restacking of graphene layers. In addition these bridged metal nano particles promotes interfacial interaction between graphene sheets and polymer matrices. So this type of graphene-metal nano hybrids should be an attractive candidate which can be used for the preparation of high performance polymer composites.

In the present study graphene oxide (GO) is proposed to be prepared from natural graphite by water assisted modified Hummers method. RGO/rGO-Ag nano fillers are proposed to be prepared from GO by reduction using Vit-C as a reducing agent. The morphology and crystal structure of rGO-Ag hybrids are investigated by transmission electron microscopy (TEM), XRD and FTIR analysis.

## **4.A.2 Experimental**

### **4.A.2.1 Preparation of silver nano particle decorated reduced graphene oxide nanohybrids**

Hybrid nano fillers were prepared by two step process. In the first step graphene oxide (GO) were prepared from natural graphite by modified Hummer's method. In the second step GO is reduced in

presence of silver nitrate by using Vit-C as reducing agent to form silver decorated reduced graphene oxide (rGO-Ag).

#### **4.A.2.1.a Water assisted oxidation of graphite (G) to graphene oxide (GO)**

4mL water was mixed with ice cooled con.H<sub>2</sub>SO<sub>4</sub> (46mL) in an ice bath at temperature <10°C with mechanical agitation [12]. Graphite powder (1g) was added to this solution by maintaining the temperature <10°C. To this suspension KMnO<sub>4</sub> (3g) was added slowly in order to keep the temperature <20°C followed by 30 min stirring. The whole reaction system was transferred to a 40°C oil bath and vigorously stirred for 2 h. After the oxidation the product was slowly poured in to 300mL ice water mixture under agitation to keep the temperature <10°C and it is stirred for 20 min. 7mL H<sub>2</sub>O<sub>2</sub> (50%) was then added drop wise and the colour of the solution changed from dark brown to yellow. Afterward the suspension was kept undisturbed for overnight to settle down the GO. It was then centrifuged washed with distilled water and dried in an oven.

#### **4.A.2.1.b Preparation of rGO and rGO-Ag from GO**

The rGO-Ag and rGO nano fillers were prepared by chemical reduction method. In typical procedure 100mg of GO mixed with 50mL DI water and it is sonicated for 1h to form a stable GO colloid. About 20mg of AgNO<sub>3</sub> was added to this solution and the mixture was vigorously stirred for 30min. To this about 1.5g Vit-C was added with adjusting the p<sup>H</sup> value to 10 by adding 2-3 drops of 25% NH<sub>3</sub> solution. The above solution was refluxed at 95°C for 6 h. The rGO-Ag nanohybrids were filtered, washed and dried in a vacuum oven at 55°C. For comparison rGO was prepared using the same procedure by excluding AgNO<sub>3</sub> [13].

#### **4.A.2.2 Characterization**

The characteristic peaks of graphite, GO and rGO were analyzed by UV-Vis spectrophotometer. Fourier transform infrared spectra (FTIR) were used to analyze the functional groups present on the nanofillers. The extent of functionalisation was studied by Thermo gravimetric analysis (TGA). X-Ray diffraction (XRD) patterns of the samples were recorded on a Bruker AXS D8 Advance X-Ray powder diffractometer.

The morphologies of the graphite sheets before and after oxidation were investigated by Scanning electron microscopy (SEM). The microstructure of G, GO and rGO-Ag was analyzed by Transmission electron microscopy (TEM). In order to find out the Ag concentration on rGO-Ag sample ICP-AES analysis was carried out. About 5mg of the samples were digested in con. HNO<sub>3</sub> and make up to 50 mL.

#### **4.A.3 Results and discussion**

GO can be prepared by the oxidation and exfoliation of natural graphite. In the present study a modified Hummers method is adopted for the preparation of GO with heavy oxidation and structural integrity, in which a certain amount of water is added to the reaction system. This water assisted oxidation produces more hydroxyl and epoxide rich GO sheets when compared to generally employed Hummers method, in which carboxyl rich GO sheets are dominating. The GO obtained by water assisted oxidation is highly soluble in water indicating the presence of polar groups on the surface of graphite sheets.

The second step is the reduction of GO and  $\text{AgNO}_3$  using Vit-C as a reducing agent. Commonly hydrazine hydrate or hydrazine is employed for the reduction of GO. But it is highly poisonous and explosive and the reaction is environmentally unsafe especially when large quantities are involved. As a green approach Vit-C (ascorbic acid), a natural antioxidant is employed for the reduction. Several studies have been reported in which Vit-C is used as a reducing agent. These findings suggest that Vit-C is an ideal substitute for hydrazine in large scale production of solution-processable graphene [14-16]. The schematic representation of the process is presented in Fig. 4.A.1.

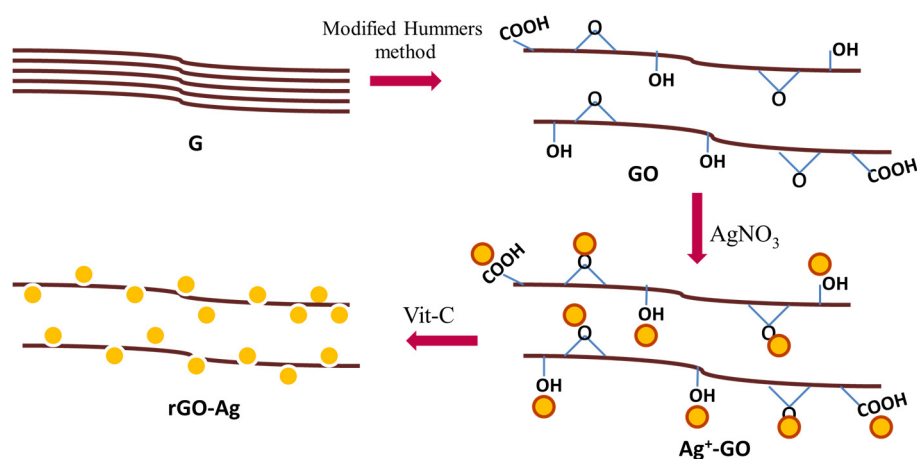


**Fig. 4.A.1** Schematic representation for the preparation of rGO-Ag nano hybrids

Vit-C specifically attacks the epoxy and hydroxyl groups present on GO. After reduction L-ascorbic acid is converted to L-dehydroascorbic acid (Fig. 4.A.2). Since the solvent is water the pH of the dispersion is adjusted to ~9-10 by using 25% ammonia solution. It promotes the colloidal stability of the graphene oxide sheets through electrostatic repulsion.

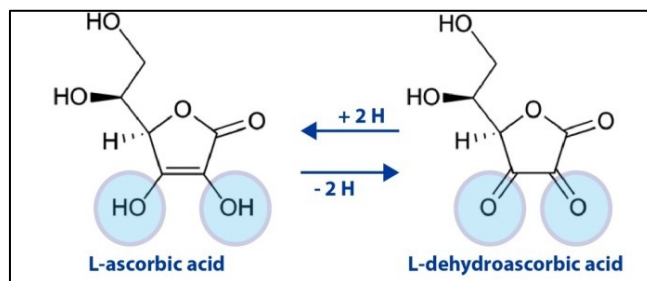


Fig. 4.A.2 Oxidation reduction mechanism in Vit-C.

The UV-Vis absorption spectra of the aqueous dispersion of G, GO, rGO and rGO-Ag is shown in Fig. 4.A.3. The GO exhibits strong absorption peak at 232 nm corresponding to  $\pi$ - $\pi^*$  transition of aromatic C=C bonds. There is a shoulder peak at 294 nm due to n- $\pi^*$  transition of C=O bonds. A distinctive surface plasmon resonance band of silver is observed at  $\sim$ 405 nm in the absorption spectra of rGO-Ag which indicates the presence of Ag nano particles on the rGO sheets. After the reduction the  $\pi$ - $\pi^*$  transition in GO redshifts to 264 nm due to the reduction of GO to rGO [17, 18].

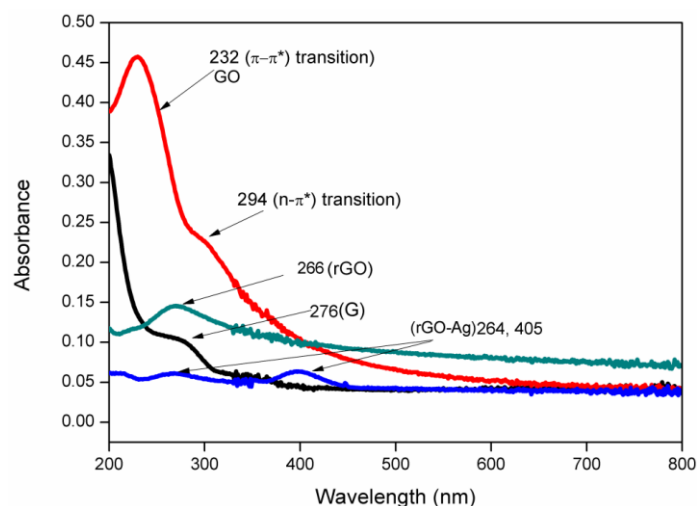
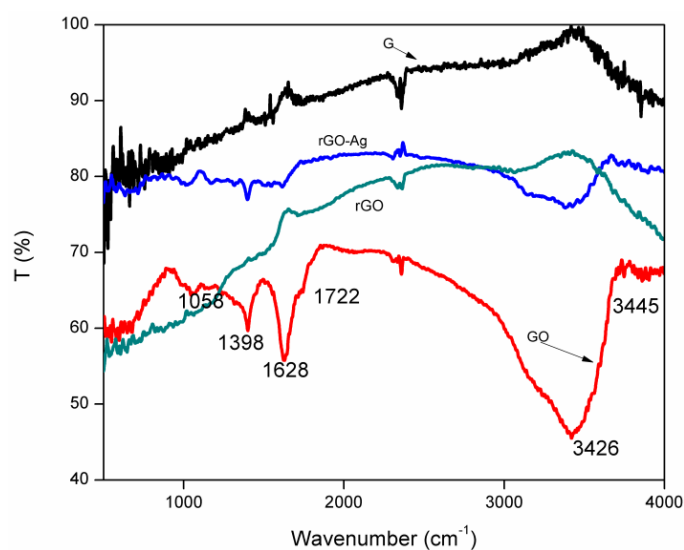


Fig. 4.A.3 UV-Vis spectra of G, GO, rGO and rGO-Ag.

The extent of oxidation can be further analyzed by FTIR spectroscopy. In the case of GO the graphs show the stretching of hydroxyl peaks (C-OH) at  $3426\text{ cm}^{-1}$ , carbonyl stretching (C=O) at  $1722\text{ cm}^{-1}$ , -C-O stretching (coupled with -O-H bending deformation) at  $1398\text{ cm}^{-1}$  and -C-O-C- bond of epoxide at  $1058\text{ cm}^{-1}$ . The peak at  $1628\text{ cm}^{-1}$  corresponds to skeletal vibration of graphite sheets. No significant bands are observed in the case of graphite while rGO-Ag shows a peak at  $3426\text{ cm}^{-1}$  which indicates that some hydroxyl peaks are still present on the surface of rGO after the reduction (Fig. 4.A.4). The peak at  $1628\text{ cm}^{-1}$  is also observed in the case of rGO-Ag which indicates that the structural integrity of graphite sheets are preserved up to some extent after reduction [19].



**Fig. 4.A.4** FT-IR spectra of G, GO, rGO and rGO-Ag



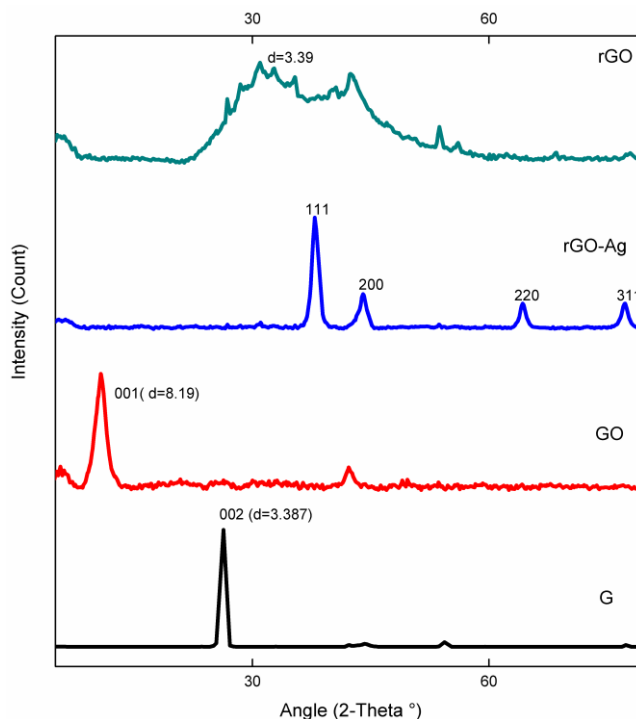


**Fig. 4.A.5** XRD pattern of G, GO, rGO and rGO-Ag

Fig. 4.A.5 shows the XRD pattern of G, GO, rGO and rGO-Ag. G shows a diffraction peak at  $26.1^\circ$  which correspond to basal spacing of ( $d_{002}$ ) of  $3.38 \text{ \AA}$ . After the oxidation GO exhibit  $d_{001}$  reflection of  $8.19 \text{ \AA}$  at  $2\text{-Theta } 10.72^\circ$ . The increase in the d-spacing value from  $3.38 \text{ \AA}$  to  $10.72 \text{ \AA}$  indicates that interlayer distance of graphite oxide is expanded due to the formation of oxygen functionalities. These functional groups facilitate the subsequent exfoliation of layers by weakening the van der Waals forces between layers. For rGO-Ag hybrid sheet the peak of graphite oxide disappears and characteristic peaks of silver metal is obtained as per JCPDS number 04-0783. The characteristic diffraction peaks of rGO-Ag are Ag (111), Ag (200), Ag (220) and Ag (311) which

suggest that metallic Ag nano particles are formed on the layers of rGO. However only the peaks of Ag nano particles are observed while no rGO/GO peaks are detected in the XRD pattern of rGO-Ag nano hybrids. This can be explained by the fact that the crystal growth of Ag nano particle between the layers of rGO destroys the regular layer stacking pattern of rGO after the reduction process. No additional diffraction peaks are obtained other than Ag indicating the high purity of Ag nano particles. Thus the formation of crystalline, fcc, metallic Ag nano particles are observed on the rGO layers by investigating XRD pattern [20].

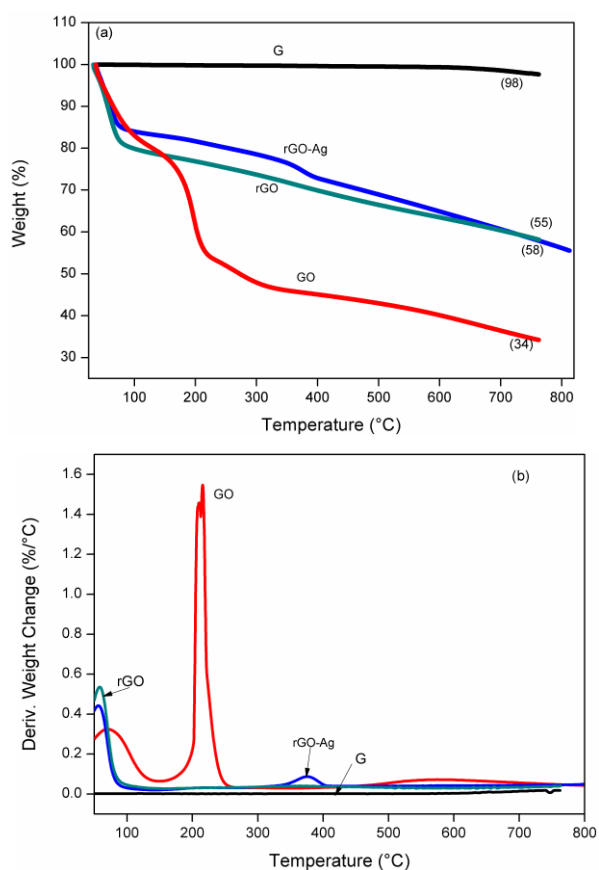


**Fig. 4.A.6** (a) TGA and (b) DTG curves of G, GO, rGO and rGO-Ag.

The thermogravimetric analysis and corresponding differential thermal analysis curves are depicted in Fig. 4.A.6. It is clear from the curves that natural graphite shows a good thermal stability up to 800°C. But GO is thermally unstable and weight reduction starts below 100°C due to the removal of water molecules. Major weight reduction occurs at ~200°C due to the pyrolysis of labile oxygen containing functional groups. From 450-650°C thermal decomposition of graphitic structure take place. After reduction some functional groups are still present on the surface of rGO-Ag and rGO which is understood from the residue value obtained in the TGA curve. Thus TGA studies further support the oxidation and reduction of graphite and graphene oxide [21- 23].

The morphology of nano fillers was analyzed using SEM and is presented in Fig. 4.A.7. A multi-layer stacked structure is observed in the case of graphite. After oxidation the stacked sheets are separated due to the presence of oxygen functionalities between graphite layers. Thus an exfoliated morphology is observed in the case of GO. After reduction restacking occurs and some exfoliation is still present due to the presence of functional groups on rGO. The SEM micrograph of rGO-Ag shows homogeneous distribution of Ag nano particles on rGO layers. The oxygen containing functional groups on GO sheets supply chemical active centers for Ag deposition [24]. So Ag nano particles are well separated with each other and distributed randomly on GO sheets which are further confirmed by TEM analysis [25, 26].

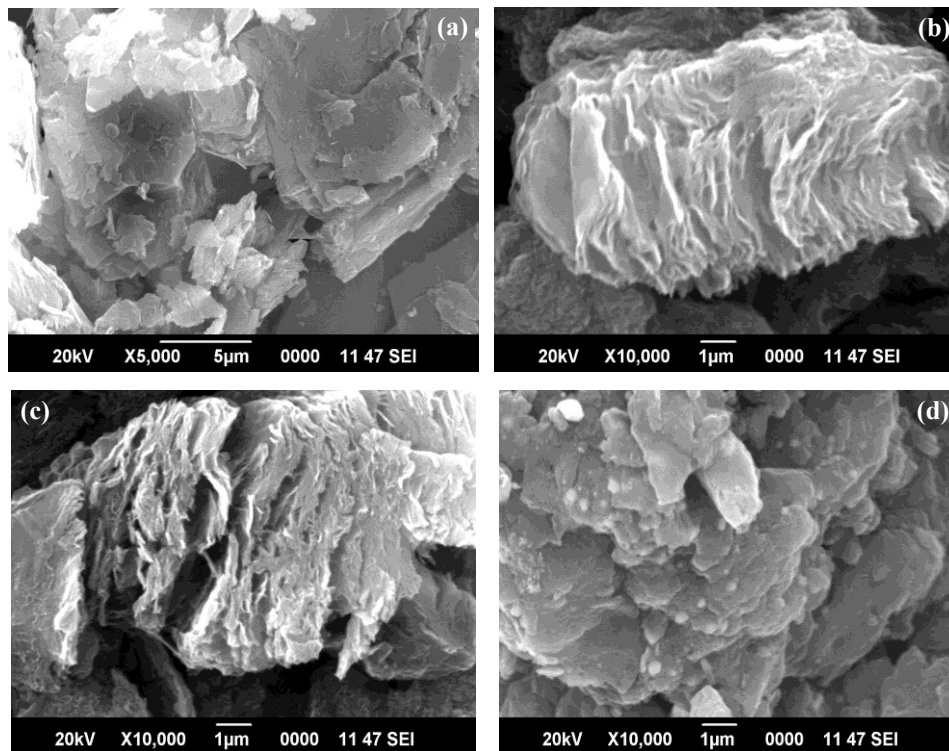


**Fig. 4.A.7** SEM photographs of (a) G, (b) GO, (c) rGO and (d) rGO-Ag

Fig. 4.A.8 shows the TEM images of the morphologies of G, GO, rGO and rGO-Ag. Stacked sheet like structures are observed in the case of graphite without exfoliation. The TEM image of GO nano sheets reveals a typical wrinkled and folded structure for the layers. The transparency of GO sheets suggest that after oxidation GO is well exfoliated into few layered GO sheets. The TEM image of rGO shows a crumpled and agglomerated sheet like structure. The wrinkled structure of rGO is due to the rapid removal of intercalated functional groups in GO after reduction. But some exfoliation is still present in rGO which suggest that some functional groups are retained after reduction.

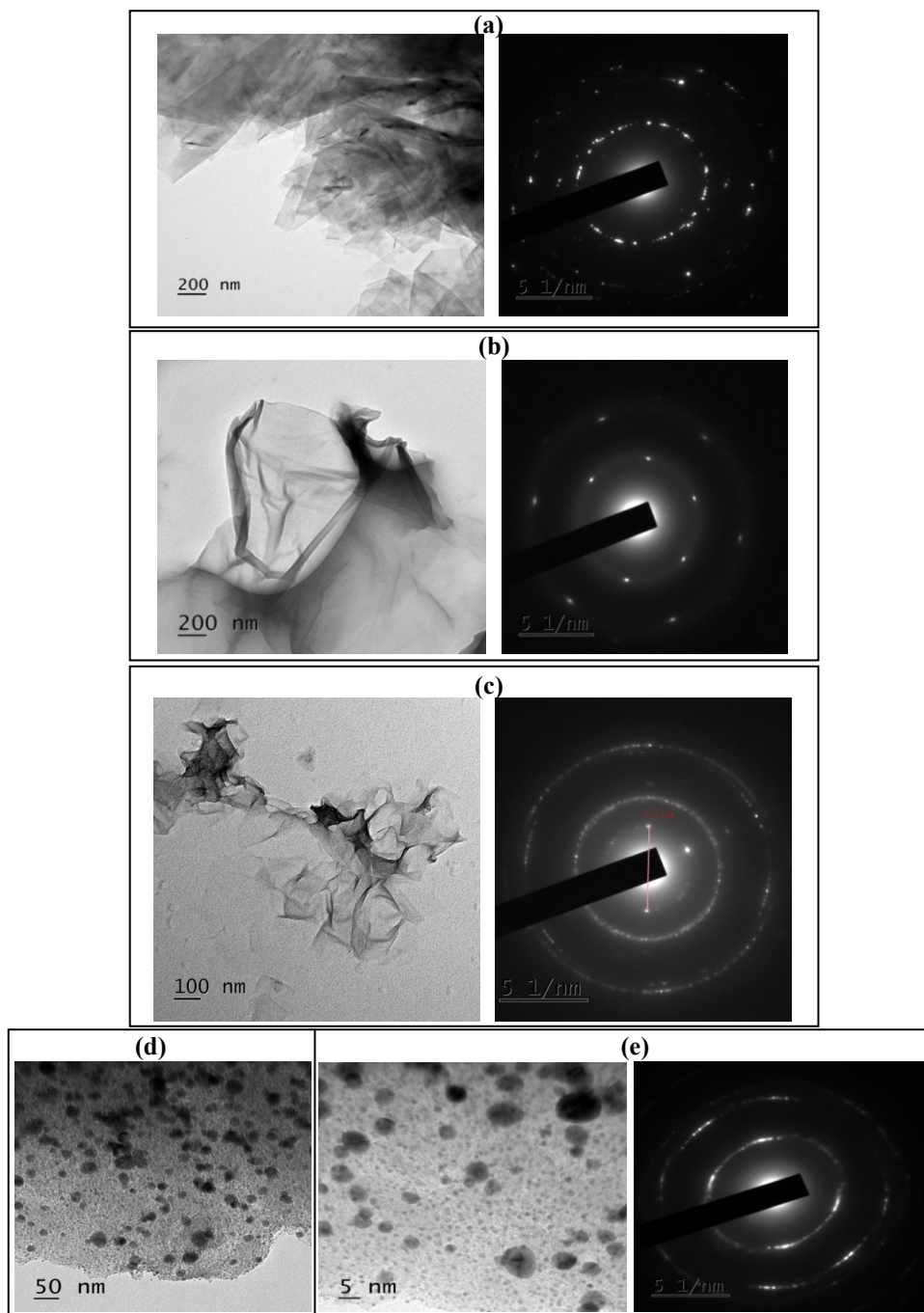


**Fig. 4.A.8** TEM images and corresponding SAED pattern of (a) G, (b) GO, (c) rGO and (d, e) rGO-Ag

In the case of rGO-Ag nano hybrids it is clear from the images that silver nano particles with nano meter size are homogeneously attached on rGO. It is to be noted that silver nano particles have been formed on rGO sheets at a very high density which indicates the presence of high density of oxygen containing functional groups on the surface of GO sheets. No agglomeration is observed, indicating that rGO sheets acted as hosts to accommodate silver nano particles which prevent its aggregation. These observations supports the fact that GO is an ideal supporting platform for the nucleation and growth of silver nano particles.

The crystallographic structure of graphene sheets were compared by SAED pattern (selected area electron diffraction pattern). The SAED pattern of graphite consists of many bright spots which indicate a stacked layered structure of sheets. The SAED pattern from the monolayer region of the GO sheets shows clear diffraction spots with a six fold pattern which indicates a crystalline hexagonal lattice. In the case of rGO several bright spots are observed along with hexagonal pattern which is very different from the SAED pattern of graphite. Ag nano particle decorated rGO sheets shows four bright continuous rings which are indexed to cubic fcc (111), (200), (220) and (311) lattice planes of Ag metal from inside to outside as observed in XRD analysis. Thus it revealed that Ag nano particle decorated on rGO sheets had a fcc structure [27- 29].

In order to find out the concentration of Ag nano particles rGO-Ag samples are analyzed by inductively coupled plasma atomic emission spectroscopy (ICP-AES) [30]. The value obtained for silver is 22.3 ppm

which supports the formation of silver nano particles on the surface of rGO.

#### **4.A.4 Conclusion**

GO sheets were synthesized from natural graphite via modified Hummers method in which addition of small amount of water favors the formation of hydroxyl and epoxide rich GO sheets. Thus high quality of GO sheets with good structural integrity was obtained by this water assisted oxidation process. rGO/ rGO-Ag sheets were synthesized by reducing the GO sheets using natural reducing agent Vit-C. Thus the use of toxic reducing agent like hydrazine can be minimized. The UV-Vis absorption spectra and FT-IR spectra of G, GO and rGO-Ag supports the oxidation and reduction process. The XRD patterns clearly reveal the formation of Ag decorated reduced graphene oxide sheets by showing the characteristic diffraction peaks of silver. The thermal stability of the nano fillers was investigated by TGA which give good information about the oxidation reduction process. The SEM and TEM image shows the distribution of silver nano particles on the surface of rGO sheets. Ag nano particles with nano meter size range were grown and immobilized on the basal planes of rGO with high density. The present results shows that GO is a promising substrate for growing and immobilizing Ag nano particles. The Ag nano particles act as spacers between graphene oxide layers thus preventing the restacking of layers which enhances the electrical and mechanical properties of rGO-Ag/ polymer systems.

## References

- [1] Rao, C. N. R., Sood, A. K., Subrahmanyam, K. S., Govindaraj, A. (2009). Graphene: the new two-dimensional nanomaterial. *Angew. Chem., Int. Ed.*, 48, 7752–7777.
- [2] Allen, M. J., Tung, V. C., Kaner, R. B. (2010). Honeycomb carbon: a review of graphene. *Chem. Rev.*, 110, 132–145.
- [3] Yoo, E. J., Okata, T., Akita, T., Kohyama, M., Nakamura, J., Honma, I. (2009). Enhanced electrocatalytic activity of Pt subnanoclusters on graphene nanosheet surface. *Nano. Lett.*, 9, 2255-2259.
- [4] Cabria, I., Lopez, M. J., Alonso, J. A. (2010). Theoretical study of the transition from planar to three-dimensional structures of palladium clusters supported on graphene. *Phys. Rev. B Condens. Matter Mater. Phys.* 81, 035403, 1-5.
- [5] Wang, Q. J., Che, J. G. (2009). Origins of distinctly different behaviors of Pd and Pt contacts on graphene. *Phys. Rev. Lett.*, 103, 066802, 1-4.
- [6] Shang, L., Bian, T., Zhang, B. H., Zhang, D. H., Wu, L. Z., Tung, C. H., Yin, Y. D., Zhang, T. R. (2014). Graphene-supported ultrafine metal nanoparticles encapsulated by mesoporous silica: robust catalysts for oxidation and reduction reactions. *Angew. Chem. Int. Ed.*, 53, 250-254.
- [7] Huang, X., Yin, Z. Y., Wu, S. X., Qi, X. Y., He, Q. Y., Zhang, Q. C., Yan, Q. Y., Boey, F., Zhang, H. (2011). Graphene-based materials: synthesis, characterization, properties, and applications. *Small*, 7, 1876-1902.
- [8] Si, Y. C., Samulski, E. T. (2008). Exfoliated graphene separated by platinum nanoparticles. *Chem. Mater.*, 20, 6792-6797.
- [9] Kim, J., Yim, B., Kim, J., Kim, J. (2012). The effects of functionalized graphene nanosheets on the thermal and mechanical properties of epoxy composites for anisotropic conductive adhesives (ACAs). *Microelectron. Reliab.*, 52, 595–602.



- [10] Liu, S., Tian, J., Wang, L., Li, H., Zhang, Y., Sun, X. (2010). Stable aqueous dispersion of graphene nanosheets: noncovalent functionalization by a polymeric reducing agent and their subsequent decoration with Ag nanoparticles for enzymeless hydrogen peroxide detection. *Macromolecules*, 43, 10078-10083.
- [11] Pasricha, R., Gupta, S., Srivastava, A. K. (2009). A facile and novel synthesis of Ag-graphene-based nanocomposites. *Small*, 5, 2253-2259.
- [12] Chen, J., Zhang, Y., Zhang, M., Yao, B., Li, Y., Huang, L., Li, C., Shi, G. (2016). Water-enhanced oxidation of graphite to graphene oxide with controlled species of oxygenated groups, *Chem. Sci.*, 7, 1874-1881.
- [13] Li, Z., Wang, D., Zhang, M., Zhao, L. (2014). Enhancement of thermal conductivity of polymer composites with Ag-graphene hybrids as fillers. *Phys. Status Solidi A*, 211, 2142-2149.
- [14] Ding, H., Zhang, S., Chen, J., Hu, X., Dua, Z., Qiu, Y., Zhao, D. (2015). Reduction of graphene oxide at room temperature with vitamin C for RGO-TiO<sub>2</sub> photoanodes in dye-sensitized solar cell. *Thin Solid Films*, 584, 29-36.
- [15] Fernandez-Merino, M. J., Guardia, L., Paredes, J. I., Villar-Rodil, S., Solis-Fernandez, P., Martinez-Alonso, A., Tascon, J. M. D. (2010). Vitamin C is an ideal substitute for hydrazine in the reduction of graphene oxide suspensions. *J. Phys. Chem. C*, 114, 6426-6432.
- [16] Qin, Y., Ji, X., Jing, J., Liu, H., Wu, H., Yang, W. (2010). Size control over spherical silver nanoparticles by ascorbic acid reduction. *Colloids Surf. A Physicochem. Eng. Asp.*, 372, 172-176.
- [17] Subrahmanyam, K. S., Manna, A. K., Pati, S. K., Rao, C. N. R. (2010). A study of graphene decorated with metal nanoparticles. *Chem. Phys. Lett.*, 497, 70-75.
- [18] Loryuenyong, V., Totepvimarn, K., Eimburanaprat, P., Boonchompoo, W., Buasri, A. (2013). Preparation and characterization of reduced graphene oxide sheets via water-based exfoliation and reduction methods. *Adv. Mater. Sci. Eng.*, 923403, 1- 5.

- [19] Yang, J., Zang, C., Sun, L., Zhao, N., Cheng, X. (2011). Synthesis of graphene/Ag nanocomposite with good dispersibility and electroconductibility via solvothermal method. *Mater. Chem. Phys.*, 129, 270–274.
- [20] Chen, L., Zhao, P., Xie, H., Yu, W. (2016). Thermal properties of epoxy resin based thermal interfacial materials by filling Ag nanoparticle-decorated graphene nanosheets. *Compos. Sci. Technol.*, 125, 17-21.
- [21] Jiao, T., Guo, H., Zhang, Q., Peng, Q., Tang, Y., Yan, X., Li, B. (2015). Reduced graphene oxide-based silver nanoparticle-containing composite hydrogel as highly efficient dye catalysts for wastewater treatment. *Sci. Rep.*, 5, 11873, 1-12.
- [22] He, L., Tjong, S. C. (2015). Facile synthesis of silver-decorated reduced graphene oxide as a hybrid filler material for electrically conductive polymer composites. *RSC Adv.*, 5, 15070-15076.
- [23] Hsiao, M., Ma, C. M., Chiang, J., Ho, K., Chou, T., Xie, X., Tsai, C., Chang, L., Hsieh, C. (2013). Thermally conductive and electrically insulating epoxy nanocomposites with thermally reduced graphene oxide–silica hybrid nanosheets. *Nanoscale*, 5, 5863-5871.
- [24] Zhang, H. Z., Zhang, C., Zeng, G. M., Gong, J. L., Ou, X.M., Huan, S. Y. (2016). Easily separated silver nanoparticle-decorated magnetic graphene oxide: Synthesis and high antibacterial activity. *J. Colloid Interface Sci.*, 471, 94–102.
- [25] Lorestani, F., Shahnavaz, Z., Mn, P., Alias, Y., Manan, N. S. A. (2015). One-step hydrothermal green synthesis of silver nanoparticle-carbonnanotube reduced-graphene oxide composite and its application as hydrogen peroxide sensor. *Sensor. Actuat. B Chem.*, 208, 389–398.
- [26] Wang, Y., Zhen, S. J., Zhang, Y., Li, Y. F., Huang, C. Z. (2011). Facile fabrication of metal nanoparticle/graphene oxide hybrids: a new strategy to directly illuminate graphene for optical imaging. *J. Phys. Chem. C*, 115, 12815–12821.

- [27] Shalaby, A., Nihtianova, D., Markov, P., Staneva, A. D., Iordanova, R. S., Dimitriev, Y. B. (2015). Structural analysis of reduced graphene oxide by transmission electron microscopy. *Bulg. Chem. Commun.*, 47, 291–295.
- [28] Wilson, N. R., Pandey, P. A., Beanland, R., Young, R. J., Kinloch, I. A., Gong, L., Liu, Z., Suenaga, K., Rourke, J. P., York, S. J., Sloan, J. (2009). Graphene oxide: structural analysis and application as a highly transparent support for electron microscopy. *ACS Nano*, 3, 2547–2556.
- [29] Gurunathan, S., Han, J. W., Park, J. H., Kim, E., Choi, Y. J., Kwon, D. N., Kim, J. H. (2015). Reduced graphene oxide–silver nanoparticle nanocomposite: a potential anticancer nanotherapy. *Int. J. Nanomedicine*, 10, 6257–6276.
- [30] Hou, S., Li, J., Huang, X., Wang, X., Ma, L., Shen, W., Kang, F., Huang, Z. H. (2017). Silver nanoparticles loaded exfoliated graphite and its anti-bacterial performance. *Appl. Sci.*, 7, 852, 1-11.

## Modification of unsaturated polyester resin with rGO-Ag nanohybrids

### 4.B.1 Introduction

Unsaturated polyester resin is a thermosetting polymer widely used for various applications such as construction, transportation, piping coating etc. They are mainly used for the fabrication of glass fibre reinforced composites. These are very low cost materials with good chemical resistance, flame retardant property and high dimensional stability. But when compared to epoxy resin, polyester resin shows high cure shrinkage, low tensile strength, low stiffness and impact properties. So in order to get improved properties in the polyester composites different fillers like natural and synthetic fibers, clay and layered silicates were used [1-5].

Recently, most of the research work in the area of polymer composites is focused on nanotechnology and nanomaterials. The properties of nano materials are superior when compared to conventional macro and micro sized fillers. Considering this fact, different nano fillers like nano clay, carbon black, carbon nano tubes (CNTs) and expanded graphite has been introduced in the preparation of polymer composites [6,7].

Graphene and its derivatives are found to be promising fillers in polymer matrices. Graphene has been proven to be the thinnest and strongest substance at present. Graphene oxide (GO) can be prepared from natural graphite by oxidation process. Like CNTs, these two dimensional layered

structures show excellent mechanical, thermal and electrical properties. GO can be converted to reduced GO (rGO) by several types of reduction process. But after reduction restacking of graphitic layers takes place which reduces its inherent properties due to low surface area. So in order to control the restacking of layers metal nano particles are introduced in between the layers [8, 9]. Silver is found to be one of the metal nano particles which can be used as a spacer between graphene layers and prevent its restacking. Several studies are reported on rGO-Ag nano hybrid polymer composites [10].

Graphene based nano composites have attracted great interest due to their wide spectrum of applications in the area of material science and engineering [11-13]. These nano composites possess excellent thermal and electrical conductivity, mechanical and dielectric properties. Graphene may be preferred over high cost fillers like CNTs due to its two dimensional nano structure, high surface area and excellent mechanical properties. Gallego et al. compared the filler percolation and mechanical properties of graphene and CNT filled epoxy nano composites and concluded that graphene based composites possess improved properties compared to CNTs [14]. Studied reported in the area of reduced graphene oxide incorporated unsaturated polyester resins are meager. Therefore in the present study we propose to investigate the effect of rGO and rGO-Ag nano fillers on the properties of unsaturated polyester resins (UPRs).

## **4.B.2 Experimental**

### **4.B.2.1 Preparation of rGO and rGO-Ag unsaturated polyester composites**

The direct mixing dispersion technique was used to prepare unsaturated polyester rGO/ rGO-Ag nanocomposites. The required amount of rGO/ rGO-Ag nano fillers were dispersed in THF solvent (nano filler: THF ratio should be 1:25(w/v)) by mechanical stirring for 15 min followed by ultrasonication for 1 h in an ice bath. Then the required amount of polyester resin was added to the above dispersion and mixed under vigorous mechanical stirring for 15 min followed by ultrasonication for 40 min. The above suspension was heated at the boiling temperature of THF (66°C) for 5 min to remove the solvent. The suspension was cooled and about 0.5 wt% cobalt octoate (promoter) was added to it and stirred. The mixture was then degassed for about 20 min under vacuum until it was completely bubble free. After wards about 1.5 wt% MEKP as initiator was added to the mixture and gently stirred for 5 min. The mixture was poured into Teflon molds and cured for 24 h at room temperature followed by post curing at 70°C for 4 h. The mechanical, dielectric and morphological properties of the samples were analyzed.

### **4.B.2.2 Characterization**

The dynamic mechanical properties were evaluated using rectangular test specimens having a dimension of 60 mm × 4 mm × 2 mm with a dual cantilever clamp using dynamic mechanical analyzer DMA Q800. All the tests were carried out by temperature sweep method at a constant frequency of 1 Hz. The dynamic storage modulus, loss modulus and tan  $\delta$

values were measured. The tensile properties were evaluated using 50kN Shimadzu Autograph universal testing machine (UTM). Flexural tests were conducted by three point loading system using UTM with 10kN load cell capacity. The izod impact strength of the samples was measured on a Resil impact analyzer (junior) using a hammer of 4J capacity. It is calculated as the energy absorbed per cross sectional area of the sample.

The thermal properties of the cured samples were investigated using thermo gravimetric analysis (TGA). The integral and derivative thermo gravimetric curves give information about thermal degradation of the prepared polymer composites. The dispersion of nano fillers in the polyester matrix was investigated using transmission electron microscopy (TEM). The dielectric measurements were carried out at frequencies ranging from 40 Hz to 30 MHz using precision impedance analyzer Agilent 4294A. Disc shaped samples having diameter 12mm and thickness 2mm were used for the measurements. The AC conductivity, dielectric permittivity and dielectric loss tangent of the prepared rGO/ rGO-Ag polyester composites were studied. The Electro Magnetic Interference shielding behavior of nano composites were studied using Agilent Performance Network Analyzer from 8-12 GHz range in the X-band region.

### **4.B.3 Results and discussion**

#### **4.B.3.1 Dynamic mechanical properties**

Dynamic mechanical analysis provides information about storage modulus and  $\tan \delta$  values of rGO and rGO-Ag UPR composites within the measured temperature range [15]. Figs.4.B.1 (a) and (b) show the storage modulus and  $\tan \delta$  curves of neat UPR and rGO and rGO-Ag UPR

composites. It is observed that storage modulus of all the composites are higher than neat polyester. Storage modulus of neat polyester and its composites is found to decrease with increase in temperature which is due to the softening of polymer chains with temperature [16]. In the glassy plateau region, the polymer chains and segments are in a frozen state and the storage modulus value increases with the addition of rigid fillers [17].

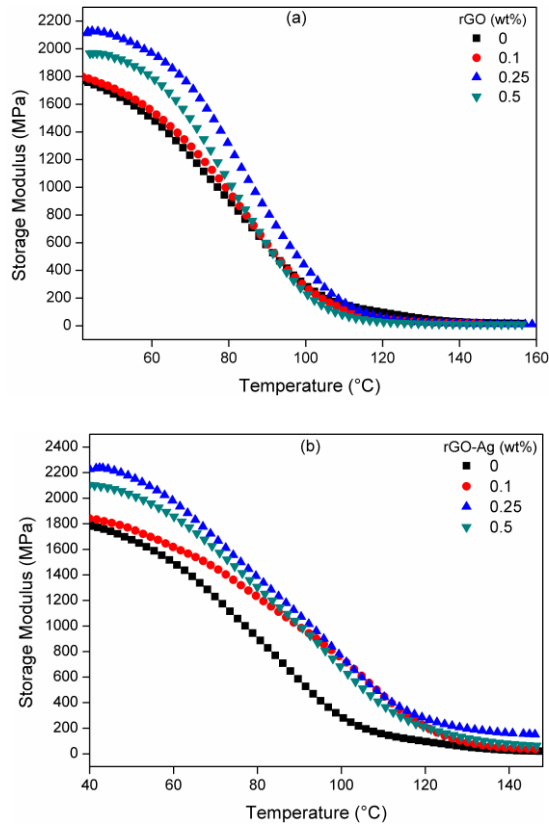


**Fig. 4.B.1** Variation of storage modulus of (a) rGO and (b) rGO-Ag UPR composites with temperature



**Table 4.B.1** Storage modulus values of rGO/ rGO-Ag UPR composites

Filler wt%	Storage Modulus at 40°C	
	rGO UPR	rGO-Ag UPR
0	1774	1774
0.1	1804	1834
0.25	<b>2123</b>	<b>2226</b>
0.5	1955	2108

Compared to rGO UPR composites, rGO-Ag UPR composites exhibit higher storage modulus value. About 16% and 20% improvement is observed in the case of 0.25 wt% rGO and rGO-Ag loading respectively. It is due to the fact that the intercalated structure of rGO-Ag shows better dispersion in the polyester matrix when compared to restacked rGO. Thus the presence of Ag nano particles in between rGO layers act as “spacer” between layers and increases the surface area of reduced graphene oxide layers. Maximum value is observed for 0.25 wt% filler loading. At 0.5 wt% loading the storage modulus values are decreasing due to agglomeration of fillers. The values are depicted in Table 4.B.1.

The loss factor ( $\tan \delta$ ) curve of rGO and rGO-Ag UPR composites are depicted in Fig. 4.B.2. The glass transition temperature ( $T_g$ ) and loss factor of neat UPR and its composites are given in Table 4.B.2. The temperature at which the loss factor curve showed a maximum peak is often called as  $T_g$ .  $T_g$  of rGO and rGO-Ag UPR nano composite shifted to higher temperature when compared to neat UPR. The wrinkled hybrid morphology of rGO-Ag sheets with high specific surface area limit the segmental movement of polymer chains to a certain degree and it increases the  $T_g$  value.

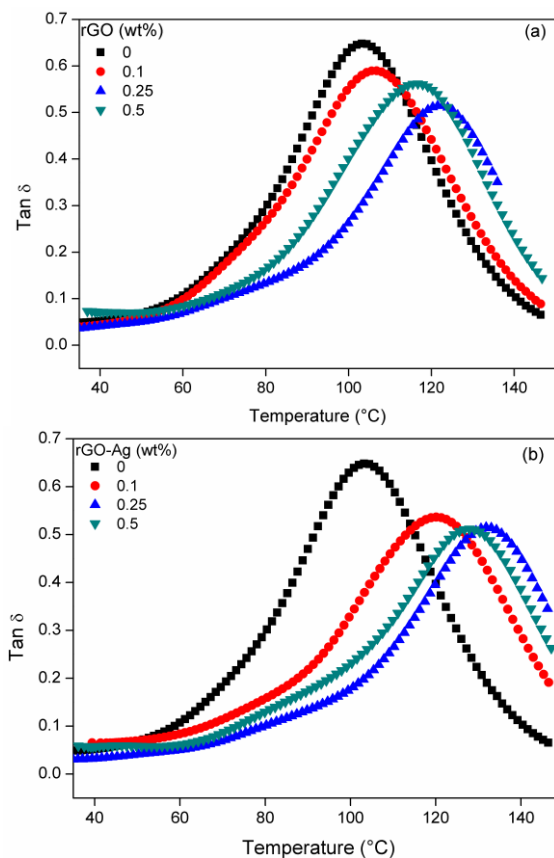


**Fig. 4.B.2** Variation of  $\tan \delta$  of (a) rGO and (b) rGO-Ag UPR composites with temperature

**Table 4.B.2**  $T_g$  values of rGO and rGO-Ag UPR composites from  $\tan \delta$  curve

Filler wt%	$T_g$ values from $\tan \delta$ curve		Tan $\delta$ peak height	
	rGO UPR	rGO-Ag UPR	rGO UPR	rGO-Ag UPR
0	105	105	0.65	0.65
0.1	108	120	0.58	0.53
0.25	<b>122</b>	<b>132</b>	0.51	0.50
0.5	116	128	0.56	0.51

Thus the increased storage modulus and  $T_g$  value is due to the nano filler reinforcement and the mobility restriction of polymer chains induced by the homogeneously dispersed nano sheets. At high loading due to the increase in viscosity of the system and possibility of agglomeration, homogeneous distribution of nano filler is not possible which further reduces the stiffness properties of the composites. Overall, increase in storage modulus values, decrease in  $\tan \delta$  peak height and shifting of  $\tan \delta$  peaks to higher temperature together indicates that rGO-Ag and rGO nano fillers behaves as a reinforcement in UP resins [18].

#### **4.B.3.2 Static mechanical properties**

The influence of rGO and rGO-Ag nano fillers on the mechanical performance of unsaturated polyester resin was evaluated by investigating tensile, flexural and impact properties. Fig. 4.B.3 shows tensile strength, tensile modulus and percentage elongation of rGO and rGO-Ag filled UPR composites at different loading. The following observations are obtained by examining these figures. A considerable improvement in the tensile strength and tensile modulus is observed for the nano composite when compared to neat UPR. The enhancement is more in the case of rGO-Ag UPR composite at 0.25 wt% filler loading. At this loading the nano composite achieved about 25% and 28% improvement in tensile strength and modulus respectively compared to neat polyester. But the percentage elongation decreases with nano filler loading and is more pronounced in the case of rGO-Ag UPR composite.

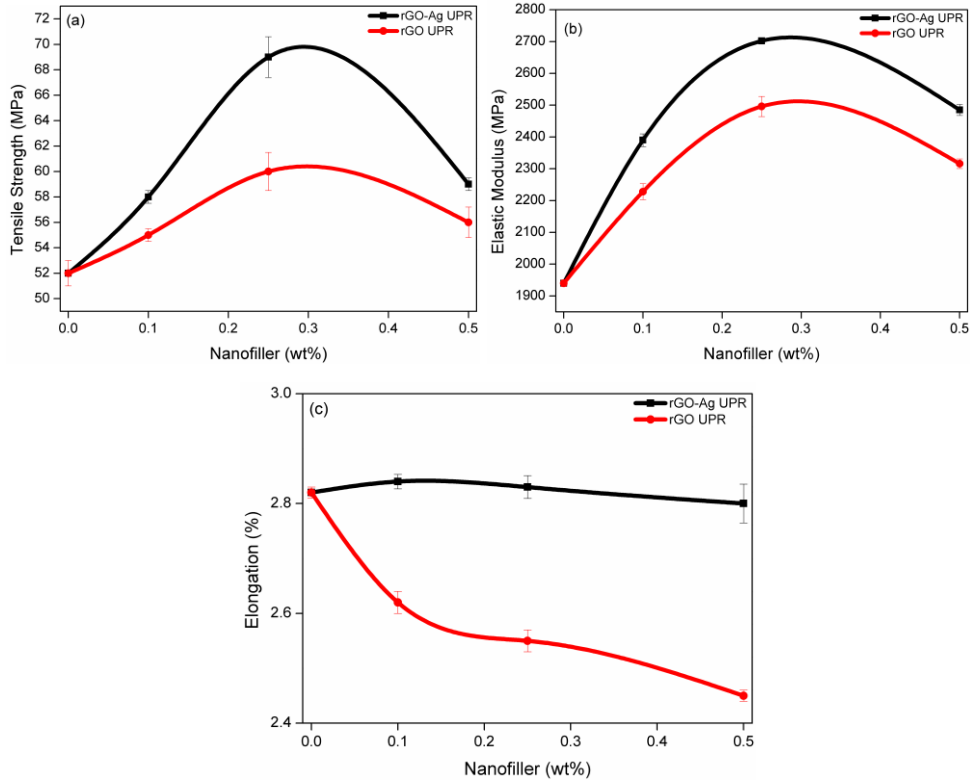


**Fig. 4.B.3** Variation of (a) tensile strength (b) modulus & (c) % elongation of rGO and rGO-Ag UPR composites with nanofiller content

The enhanced mechanical properties can be attributed to the well dispersion of nano fillers in the polymer matrix. This is more in the case of rGO-Ag nano hybrid when compared to rGO. The good dispersion of rGO-Ag could be intrinsically attributed to the role of silver nano particles, which act as spacers between rGO sheets and prevent its restacking. Thus the interfacial interaction between the polymer and nano filler increases. At high loading, due to the high viscosity of sample solution and aggregations of rGO-Ag, the mechanical properties decreases. The gradual decrease in the percentage elongation value with

increase in filler content is due to the incorporation of hard and rigid fillers which restrict the movement of polymer chains [19, 20].

The flexural properties and impact strength of rGO and rGO-Ag UPR composites are depicted in Fig. 4.B.4.

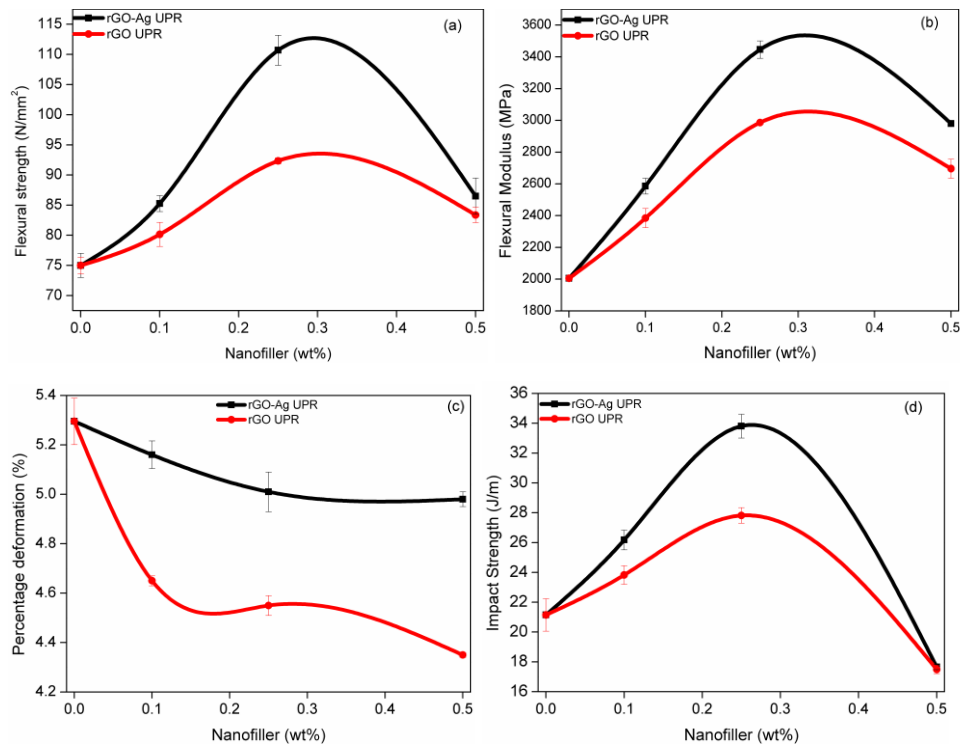


**Fig. 4.B.4** Variation of (a) flexural strength (b) modulus (c) % deformation and (d) impact strength of rGO and rGO-Ag UPR composites with nanofiller content

The nano composite achieved about 32%, 42% and 38% improvement in flexural strength, flexural modulus and impact strength respectively when compared to neat resin for 0.25 wt% rGO-Ag loading. This is due to the fact that the filler distribution is more homogeneous in the case of rGO-Ag composite when compared to rGO composite which results in an

effective stress transfer between the fillers and polyester matrix [21]. This distribution is good at lower concentration and at higher concentration agglomeration takes place which weakens the mechanical properties. Due to the restricted chain mobility of polyester matrix by the incorporation of rigid filler, the percentage deformation decreases with filler loading [22, 23].

#### 4.B.3.3 Thermogravimetric analysis

Thermal properties of the rGO/ rGO-Ag UPR nano composites were evaluated using thermo gravimetric analysis (TGA). Fig. 4.B.5 shows the thermograms and derivative thermograms of rGO and rGO-Ag UPR composites.

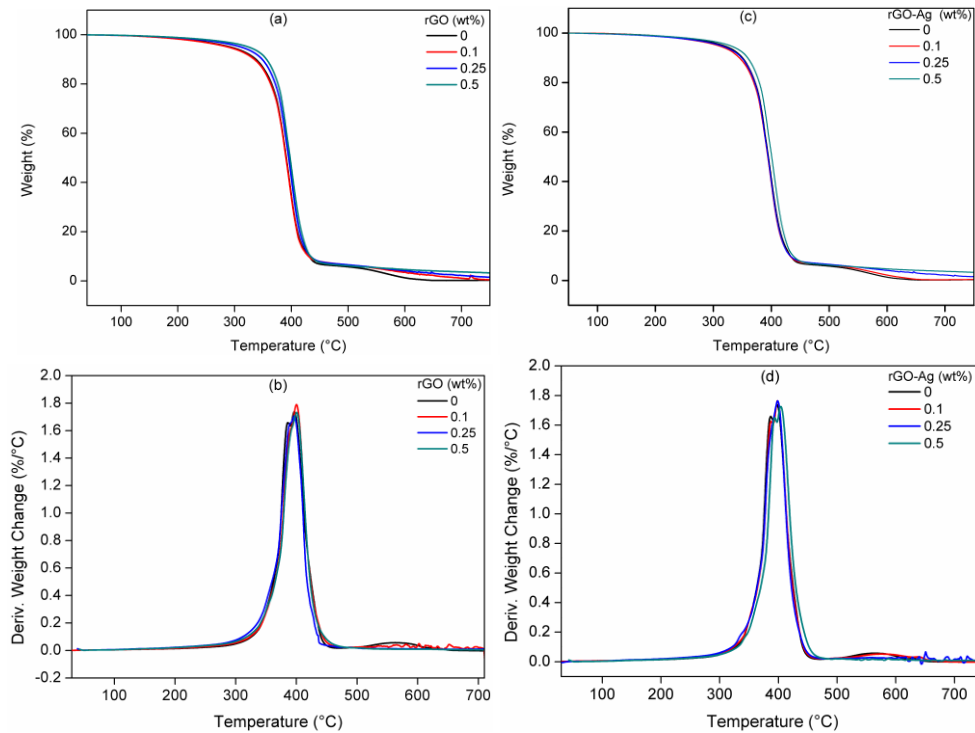


**Fig. 4.B.5** TGA and DTG curves of rGO-UPR (a, b) and rGO-Ag UPR (c, d) composites

The thermal stability of almost all samples found to be similar. The major weight loss in the temperature range 320-475°C is due to the decomposition of polyester network to form a primary char with the evolution of styrene, CO and CO<sub>2</sub> [24]. The final char oxidation takes place in the temperature range 470-700°C leaving the residue. In the case of rGO-Ag nano composite a little enhancement in the thermal stability is observed by the incorporation of nano filler. This improvement in thermal stability is ascribed to the strong interaction between rGO-Ag and polyester resin which restricts the mobility of polymer chains. The residual oxygen functionalities on rGO-Ag interact with the polymer matrix through hydrogen bonding and some dipole interactions are also possible between the two components which enhance the interaction between polymer matrix and nano filler [25, 26].

#### **4.B.3.4 Morphological properties**

The dispersion of rGO-Ag in polyester matrix was investigated by TEM (transmission electron microscopy). Fig. 4.B.6 shows the TEM images of neat UPR and rGO-Ag UPR composites. A very smooth and clear morphology is obtained in the case of neat resin without any disturbances. The corresponding SAED (selected area electron diffraction) pattern shows the amorphous nature of polyester resin which is not having any bright spots [27]. On the other hand 0.25 wt% rGO-Ag UPR composite shows silver decorated reduced graphene oxide layers dispersed in the matrix. The dark spheres indicate the presence of silver nano particles and corresponding SAED pattern shows concentric bright circles which arises

from the crystallographic planes of silver nano particle [28, 29]. This altogether confirms the dispersion of rGO-Ag in polyester matrix.

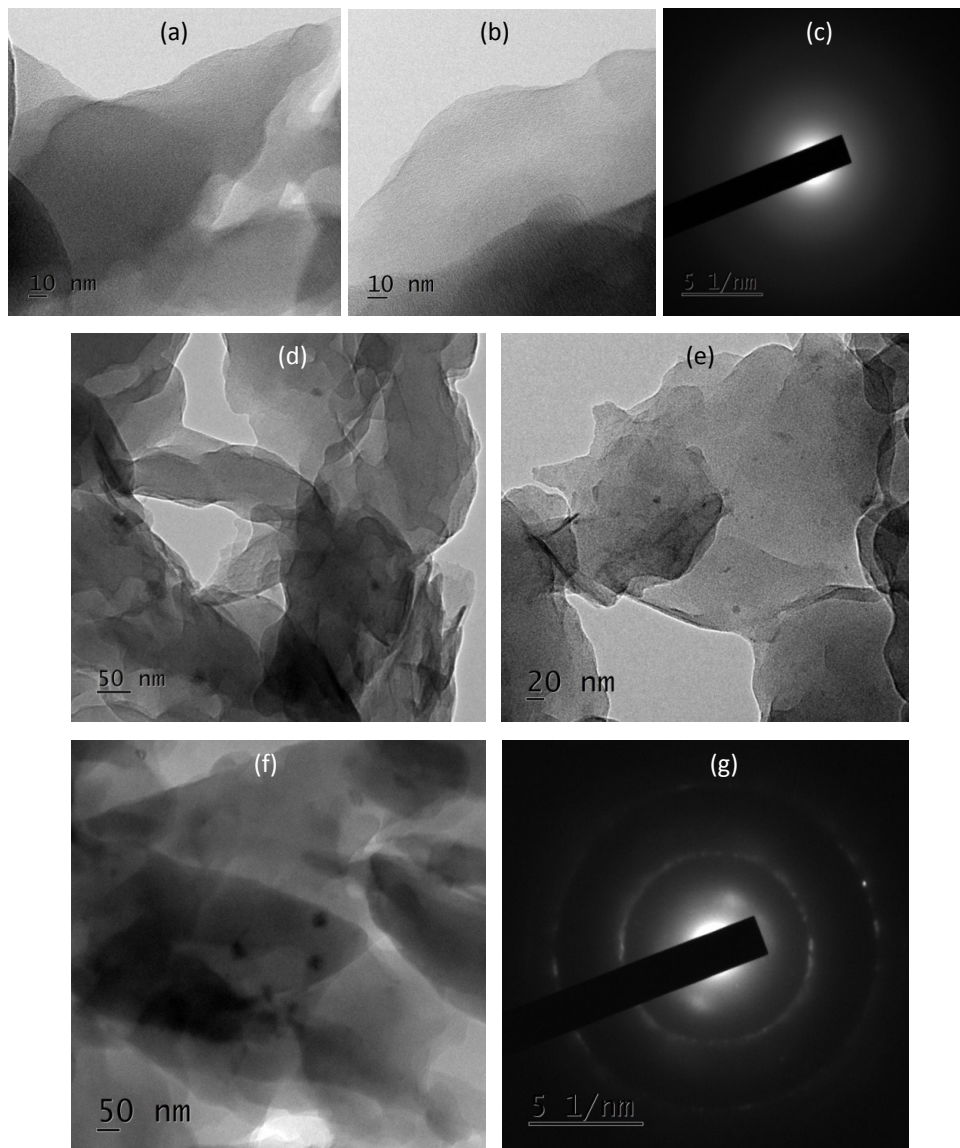


**Fig.4.B.6** TEM images of (a & b) Neat UPR (d, e & f) 0.25wt% rGO-Ag UPR (c & g) corresponding SAED pattern of neat UPR and rGO-Ag UPR



#### 4.B.3.5 Dielectric properties

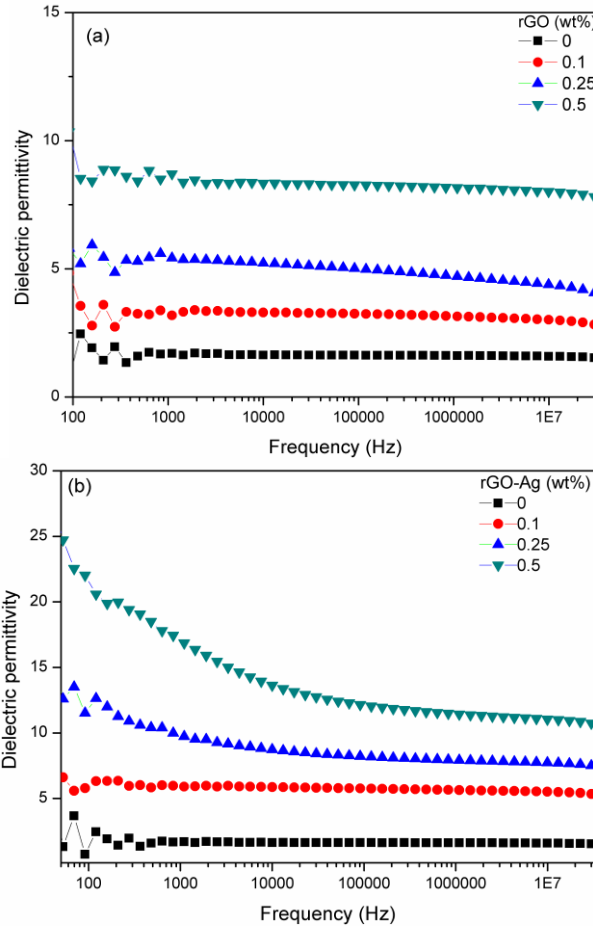


**Fig. 4.B.7** Dielectric permittivity as a function of frequency for (a) rGO and (b) rGO-Ag UPR composites

The dielectric permittivity as a function of frequency at room temperature of rGO and rGO-Ag nano composites is depicted in Fig. 4.B.7. The dielectric permittivity  $\epsilon'$  which is also known as relative dielectric constant is the real part of complex dielectric permittivity. The dielectric permittivity of the composites gradually decreases as frequency increases. An enhancement in  $\epsilon'$  is observed by the incorporation of rGO and rGO-

Ag nano composites. In the case of rGO UPR composite the dielectric permittivity is almost unchanged at low frequency region. But in the case of rGO-Ag UPR composite  $\epsilon'$  gradually increases at low frequency region and decreases at high frequency region. This is due to the fact that at low frequency region the dipole and charge carriers can freely move and they can follow the varying electromagnetic field. But at high frequencies dielectric dispersion takes place due to the lagging of molecules behind the applied electric field and they become unable to follow the applied field and thus  $\epsilon'$  and dielectric loss ( $\epsilon''$ ) decreases. The electronic conduction is more in the case of rGO-Ag UPR composite when compared to rGO UPR composite which results in an increased dielectric permittivity for Ag incorporated composite [20, 30].

Another important factor which improves the dielectric constant is Maxwell-Wagner-Sillars polarization (MWS) for heterogeneous systems. It is associated with the entrapment of charges between insulator-conductor interfaces which is characterized by frequency dependence of  $\epsilon'$  at low frequency range as observed in rGO-Ag UPR composites. The dielectric loss is also known as dissipation factor of the material and is calculated as  $\tan \delta = \epsilon''/\epsilon'$ . Composite which exhibit large dielectric constant also show high loss tangent due to leakage current as observed in Fig. 4.B.8. The leakage current is more pronounced when there is direct contact between conductive fillers.

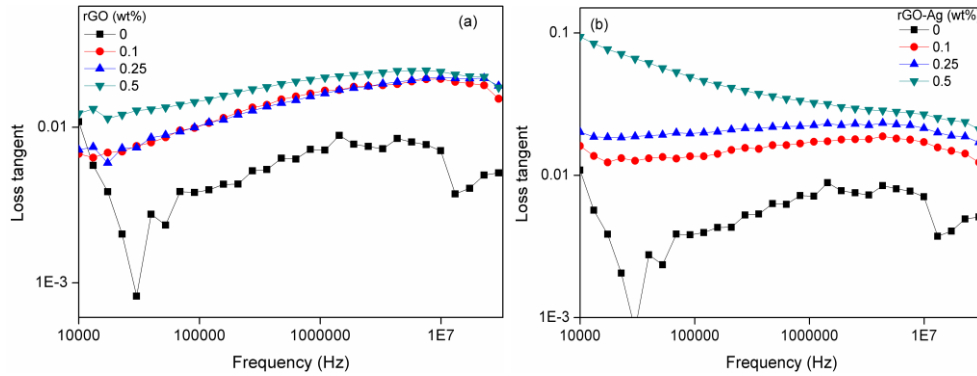


**Fig. 4.B.8** Loss tangent as a function of frequency for (a) rGO and (b) rGO-Ag UPR composites

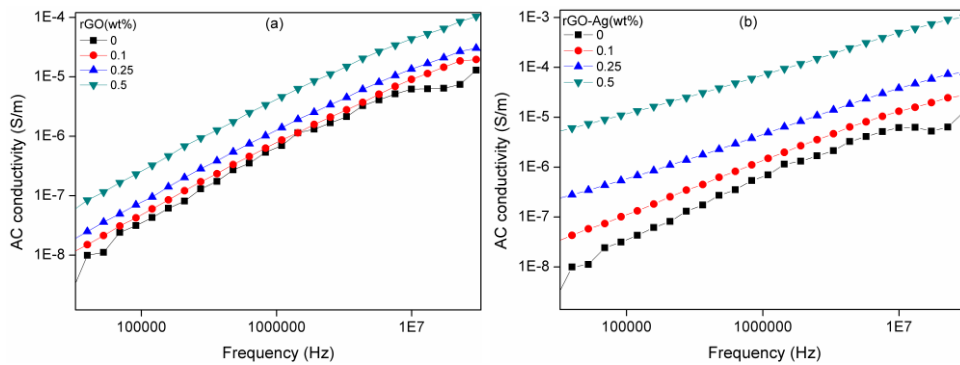


**Fig. 4.B.9** Plots of AC conductivity as a function of frequency for (a) rGO and (b) rGO-Ag UPR composites

The AC conductivity of the nanocomposites is presented in Fig. 4.B.9. It is calculated using the equation  $\sigma_{AC} = 2\pi f \epsilon_0 \epsilon' \tan\delta$ . Where  $\epsilon_0$  corresponds to permittivity of vacuum,  $\epsilon'$  is the real permittivity and  $f$  is the frequency at room temperature. It is observed that rGO-Ag nano composite exhibit higher AC conductivity when compared to rGO composite. The conductivity ( $\sigma$ ) reached a value of  $1.6 \times 10^{-9}$  and  $4.7 \times 10^{-7}$  for 0.5 wt% rGO and rGO-Ag loading at frequency 1 kHz. At 10 MHz the value for  $\sigma$  is

$4.6 \times 10^{-6}$  and  $7.5 \times 10^{-4}$  for 0.5 wt% rGO and rGO-Ag nano fillers. This is due to the fact that silver nano particle restrict the restacking of rGO layers and increases the surface area which enhance the homogeneous dispersion of rGO in UPR and the synergistic effect of Ag as a conducting filler which enhances the conductivity of the composite [31, 32].

#### 4.B.3.6 EMI shielding effectiveness

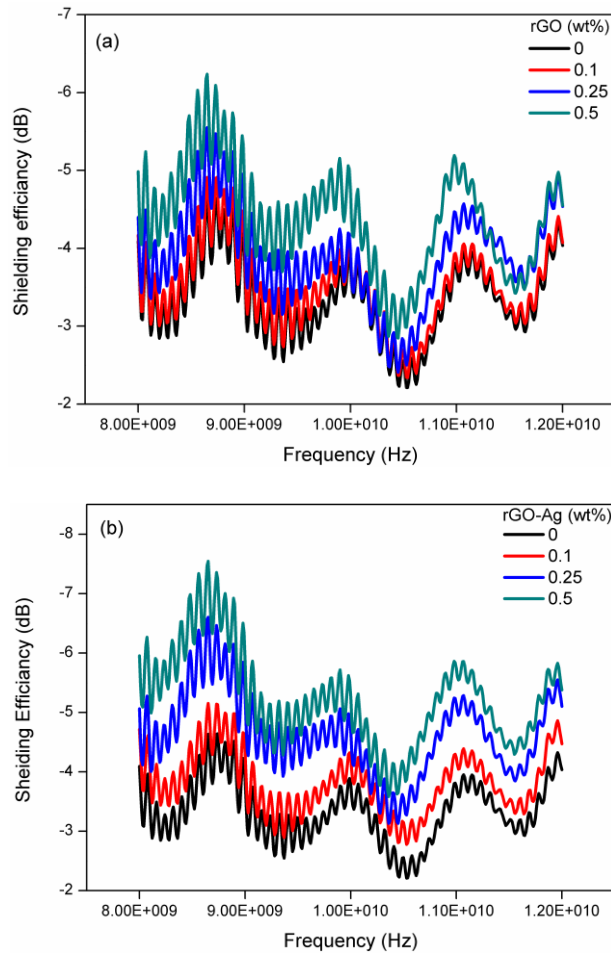


**Fig. 4.B.10** Variation of SE with frequency for (a) rGO/UPR composites & (b) rGO-Ag/UPR composites

The EMI shielding effectiveness of rGO and rGO-Ag UPR composites in the X-band region (8-12 GHz) is shown in Fig. 3.B.10. It is to be noted that EMI SE depends on intrinsic electrical conductivity, the aspect ratio, filler dispersion quality and thickness of the polymer specimens. The SE value of the entire composites increased with increase in nano filler content [33]. Because of the increased conductive filler content, interaction with the electromagnetic field also increases [34, 35]. Higher SE is obtained in the case of rGO-Ag UPR composite compared to rGO UPR composite. This can be explained by three factors. The conductivity difference is the first factor which increases the SE value. Due to the presence of silver decoration on rGO sheets its conductivity is high compared to rGO. Secondly, silver act as spacer between rGO sheets thus prevents its restacking and increase the surface area when compared to rGO. This further increases the dispersion quality of rGO-Ag in polyester matrix which improves the interaction with the electromagnetic field [36, 37].

#### **4.B.4 Conclusions**

rGO and rGO-Ag nano fillers have been successfully incorporated in unsaturated polyester resin by direct mixing dispersion technique and the mechanical, thermal and dielectric properties of the composites were investigated. Improvement in the storage modulus and Tg values are obtained for the nano composite and more pronounced effect is observed in the case of rGO-Ag UPR composite. The tensile strength, tensile modulus, flexural strength, flexural modulus and impact strength show maximum value at 0.25wt% rGO-Ag content. A small improvement in

the thermal stability value is observed for the nano composite at 0.5wt% filler loading. The morphological characterizations were done and correlated with their mechanical performance. The presence of conductive filler content with good aspect ratio and better dispersion stability improve the dielectric properties of the polyester resin. Considerable improvement in the dielectric permittivity and AC conductivity is observed for 0.5 wt% rGO-Ag UPR nano composite. The improvement in dielectric properties contributes towards the electromagnetic interference shielding properties of the nano composite.

## References

- [1] Chai, M. W., Bickerton, S., Bhattacharyya, D., Das, R. (2012). Influence of natural fibre reinforcements on the flammability of bio-derived composite materials. *Compos. Part B*, 43, 2867–2874.
- [2] Kiliaris, P., Papaspyrides, C. D. (2010). Polymer/layered silicate (clay) nanocomposites: An overview of flame retardancy. *Prog. Polym. Sci.*, 35, 902–958.
- [3] Marti'nez, V. M., Coque, R. T., Marti'nez, J. M. M. (2011). Addition of unmodified nanoclay to improve the performance of unsaturated polyester resin coating on natural stone. *Int. J. Adhes. Adhes.*, 31, 154–163.
- [4] Sreenivasan, V. S., Ravindran, D., Manikandan, V., Narayanasamy, R. (2011). Mechanical properties of randomly oriented short Sansevieria cylindrical fibre/polyester composites. *Mater. Des.*, 32, 2444–2455.
- [5] Oleksy, M., Galina, H. (2013). Unsaturated polyester resin composites containing Bentonites modified with silsesquioxanes. *Ind. Eng. Chem. Res.* 52, 6713–6721.

- [6] Kayatin, M. J., Davis, V. A. (2009). Viscoelasticity and shear stability of single-walled carbon nanotube/ unsaturated polyester resin dispersions. *Macromolecules*, 42, 6624–6632.
- [7] Lu, W., Lin, H., Wu, D., Chen, G. (2006). Unsaturated polyester resin/ graphite nanosheet conducting composites with a low percolation threshold. *Polymer*, 47, 4440–4444.
- [8] Si, Y. C., Samulski, E. T. (2008). Exfoliated graphene separated by platinum nanoparticles. *Chem. Mater*, 20, 6792-6797.
- [9] Kim, J., Yim, B., Kim, J., Kim, J. (2012). The effects of functionalized graphene nanosheets on the thermal and mechanical properties of epoxy composites for anisotropic conductive adhesives (ACAs). *Microelectron. Reliab.*, 52, 595–602.
- [10] He, L., Tjong, S. C. (2015). Facile synthesis of silver-decorated reduced graphene oxide as a hybrid filler material for electrically conductive polymer composites. *RSC Adv.*, 5, 15070-15076.
- [11] Liu, K., et al. Preparation of polyester/reduced graphene oxide composites via *in situ* melt polycondensation and simultaneous thermo-reduction of graphene oxide, *J. Mater. Chem.*, 21, 8612-8617, 2011.
- [12] Wang, X., et al. Cyanate ester resin/graphene nanocomposite: Curing dynamics and network formation, *Eur. Polym. J.*, 48, 1034-1041, 2012.
- [13] Yu, A., et al. Graphite nanoplatelet-epoxy composite thermal interface materials, *J. Phys. Chem. C*, 111, 7565-7569, 2007.
- [14] Martin-Gallego, M., Bernal, M. M., Hernandez, M., Verdejo, R., Lopez-Manchado, M. A. (2013). Comparison of filler percolation and mechanical properties in graphene and carbon nanotubes filled epoxy nanocomposites. *Eur. Polym. J.*, 49, 1347-53.
- [15] Gu, H., Tadakamalla, S., Huang, Y., Colorado, H. A., Luo, Z., Haldolaarachchige, N. (2012). Polyaniline stabilized magnetite nanoparticle reinforced epoxy nanocomposites. *ACS Appl. Mater. Interfaces*, 4, 5613–24.

- [16] Feng, Q. P., Shen, X. J., Yang, J. P., Fu, S.Y., Mai, Y. W. (2011). Friedrich K. Synthesis of epoxy composites with high carbon nanotube loading and effects of tubular and wavy morphology on composite strength and modulus. *Polymer*, 52, 6037–45.
- [17] Zhang, X., He, Q., Gu, H., Wei, S., Guo, Z. (2013). Polyaniline stabilized barium titanate nanoparticles reinforced epoxy nanocomposites with high dielectric permittivity and reduced flammability. *J. Mater. Chem. C*, 1, 2886.
- [18] Ramanathan, T., Abdala, A. A., Stankovich, S., Dikin, D. A., Herrera, A. M., Piner, R. D., (2008). Functionalized graphene sheets for polymer nanocomposites. *Nat. Nanotechnol.*, 3, 327–31.
- [19] Bora, C., Bharali, P., Baglari, S., Dolui, S. K., Konwar, B. K. (2013). Strong and conductive reduced graphene oxide/polyester resin composite films with improved mechanical strength, thermal stability and its antibacterial activity. *Compos. Sci. Technol.*, 87, 1–7.
- [20] Bindu Sharmila, T.K., Nair, A. B., Abraham, B. T., Sabura Beegum, P. M., Thachil, E. T., (2014). Microwave exfoliated reduced graphene oxide epoxy nanocomposites for high performance applications. *Polymer*, 55, 3614-3627.
- [21] Li, Z., Wang, D., Zhang, M., Zhao, L. (2014). Enhancement of thermal conductivity of polymer composites with Ag-graphene hybrids as fillers. *Phys. Status Solidi A*, 211, 2142-2149.
- [22] Zhao, X., Zhang, Q., Chen, D. (2020). Enhanced mechanical properties of graphene-based Poly (vinyl alcohol) composites. *Macromolecules*, 43, 2357–63.
- [23] Xu, Y., Hong, W., Bai, H., Li, C., Shi, G. (2009). Strong and ductile poly(vinyl alcohol)/ graphene oxide composite films with a layered structure. *Carbon*, 47, 3538–43.
- [24] Kandola, B., Nazare, S., Horrocks, A., In: Le Bras M, editor. (2005). Fire retardancy of polymers: the use of mineral fillers in micro- and nano-composites. Cambridge: *Royal Chem. Society*, 147.



- [25] Vilcakova, J., Saha, P., Quadrat, O. (2002). Electrical conductivity of carbon fibres/ polyester resin composites in the percolation threshold region. *Eur. Polym. J.*, 38, 2343–7.
- [26] Seyhan, T., Gojny, F. H., Tanoglu, M., Schulte, K. (2007). Critical aspects related to processing of carbon nanotube/unsaturated thermoset polyester nanocomposites. *Eur. Polym. J.*, 43, 374–9.
- [27] Mitra, M., Kulsi, C., Chatterjee, K., Kargupta, K., Ganguly, S., Banerjee, D., Goswamid, S. (2015). Reduced graphene oxide-polyaniline composites-synthesis, characterization and optimization for thermoelectric applications. *RSC Adv.*, 5, 31039-31048.
- [28] Shalaby, A., Nihtianova, D., Markov, P., Staneva, A. D., Iordanova, R. S., Dimitriev, Y. B. (2015). Structural analysis of reduced graphene oxide by transmission electron microscopy. *Bulg. Chem. Commun.*, 47, 291–295.
- [29] Wilson, N. R., Pandey, P. A., Beanland, R., Young, R. J., Kinloch, I. A., Gong, L., Liu, Z., Suenaga, K., Rourke, J. P., York, S. J., Sloan, J. (2009). Graphene oxide: structural analysis and application as a highly transparent support for electron microscopy. *ACS Nano*, 3, 2547–2556.
- [30] He, F., Lau, S., Chan, H. L., Fan, J. (2009). High dielectric permittivity and low percolation threshold in nanocomposites based on poly(vinylidene fluoride) and exfoliated graphite nanoplates. *Adv. Mater.*, 21, 710-715.
- [31] Anju, V. P., Narayanankutty, S. K. (2016). Polyaniline coated cellulose fiber/ polyvinyl alcohol composites with high dielectric permittivity and low percolation threshold. *AIP Adv.*, 6, 015109, 1-12.
- [32] He, L., Tjong, S. C. (2015). Facile synthesis of silver-decorated reduced graphene oxide as a hybrid filler material for electrically conductive polymer composites. *RSC Adv.*, 5, 15070-15076.
- [33] Zeng, Z., Jin, H., Chen, M., Li, W., Zhou, L., Zhang, Z. (2016). Lightweight and anisotropic porous MWCNT/WPU composites for ultrahigh performance electromagnetic interference shielding. *Adv. Funct. Mater.*, 26, 303–310.

- [34] Hong, X., Chung, D. D. L. (2017). Carbon nanofiber mats for electromagnetic interference shielding. *Carbon*, 111, 529–537.
- [35] Chung, D. D. L. (2001). Electromagnetic interference shielding effectiveness of carbon materials. *Carbon*, 39, 279–285.
- [36] Dhawan, S. K., Singh, N., & Rodrigues, D. (2003). Electromagnetic shielding behaviour of conducting polyaniline composites. *Sci. Technol. Adv. Mater.*, 4, 105 -113.
- [37] Liu, Z., Bai, G., Huang, Y., Ma, Y., Du, F., Li, F., (2007). Enhanced dielectric constants and shielding effectiveness of, uniformly dispersed, functionalized carbon nanotube composites. *Carbon* , 45, 821–7.

.....❧.....

**FATTY ACID METHYL ESTERS (FAMES) OF RUBBER SEED OIL (RSO) MODIFIED UNSATURATED POLYESTER RESIN****Contents**

*Part A: Preparation of Fatty Acid Methyl Esters from Rubber Seed Oil*

*Part B: Fames of RSO Modified Unsaturated Polyester Resin*

FAMES of RSO were prepared and its effectiveness as a bio modifier in unsaturated polyester resin was studied. FAMES were prepared from RSO by a two-step transesterification process. Partially sulfonated polystyrene (PSS), synthesized from expanded polystyrene waste (EPS), was used as a catalyst for free fatty acid (FFA) conversion in non-edible RSO. Acidic and water absorbing properties of the PSS facilitated the catalytic action for the FFA conversion by esterification reaction\*. Blends of polyester resin and FAMES of RSO were prepared and their mechanical and morphological properties were analyzed. Up to 25 wt% of UPR is replaced by FAMES of RSO. The incorporation of bio material improves the flexibility and toughness of polyester matrix. Considerable improvement in the impact resistance is obtained for the system due to the formation of micro voids which increases the energy dissipation and delays the crack propagation.

## Preparation of Fatty Acid Methyl Esters from Rubber Seed Oil

### 5.A.1 Introduction

The word “green” has much importance in the modern scientific era. The use of renewable energy resources and a proper waste management provides a green solution to energy crisis and environmental pollution. Petroleum derived unsaturated polyester resins are the most commonly used thermosetting polymer due to low cost, ease of processing and good mechanical and thermal properties. While considering the depletion of nonrenewable fossil fuels, their availability and environmental pollution problems, an alternate solution from renewable resources is most welcomed. Now a days there is a growing trend to incorporate vegetable oils and their derivatives to polyester resins for structural applications. Several studies have been reported in the area of vegetable oil modified unsaturated polyester resin which reveals the toughening effect of oil derivatives on the properties of UPRs.

Rubber tree (*Hevea brasiliensis*) is cultivated for the production of latex as a source of natural rubber in various parts of the country. Kerala is the leading rubber plantation state in India which accounts about 92% of the country’s total natural rubber production. Natural rubber is extensively used in many applications and products in various fields. But the rubber seed (Fig. 5.A.1) has not received a serious attention. However they are utilized for bio diesel production [1-2, 16-17] and bio lubricant

preparation [3, 14]. But the use of this non edible oil is not yet fully explored.



**Fig. 5.A.1** Rubber seeds

Fatty acid methyl esters (FAMES) can be prepared from vegetable oil by transesterification reaction. In this, oil in tri glyceride form reacts with methanol in presence of base catalyst to form methyl esters which is generally known as bio diesel. But this process is not very easy if the oil contains high amount of free fatty acid. So this one step process can be converted into a two-step process in which FFA level is first reduced and then transesterified i.e. esterification followed by transesterification [2, 12].

Several studies have been reported for the esterification reaction with various acid catalysts [11, 13]. In the present study we have utilized partially sulphonated polystyrene prepared from expanded polystyrene waste as a heterogeneous catalyst for esterification reaction of high acid value RSO [4]. Acidic and water absorption properties of this hydrogel facilitates its catalytic activity. Thus the utilization of a polymer waste as

a heterogeneous catalyst which can be separated very easily from the reaction mixture is also discussed.

The utilization of a renewable resource for the partial replacement of petroleum derived polyesters will reduce the environmental issues up to a certain extent. However the complete replacement is very difficult in the present scenario due to inferior properties and performance of bio systems. The utilization of rubber seed oil as a bio modifier for unsaturated polyester resins is proposed to be investigated in this study. Chapter is divided in to two parts. A detailed discussion about the preparation of FAMEs from crude RSO through a two-step process is given in part A and development of FAMEs of RSO modified UP resins id given in part B.

## **5.A.2 Experimental**

### **5.A.2.1 Preparation of fatty acid methyl esters of rubber seed oil (FAMEs of RSO).**

FAMEs were prepared from RSO by transesterification reaction. The FFA content of crude RSO was about 20.5%. High acid value of the oil reduces the yield of transesterification reaction by producing soap with alkaline catalyst. In order to make the transesterification easier a two-step process was adopted [2]. The first step was the acid catalyzed esterification using partially sulphonated polystyrene (PSS) catalyst which reduces the FFA content of the oil to less than 2% [4]. In the second step base catalyzed transesterification reaction of esterified RSO was conducted using 0.5% NaOH which converts the products of the first step to its monoesters and glycerol. Standard titration method (STM) was used to find the acid value

of the sample. FAMEs were separated and the fatty acid compositionns were determined.

### **5.A.2.2 Characterization**

Physico-chemical characterization of RSO and FAMEs of RSO was done. Acid value, iodine value, saponification value, colour, and specific gravity were analyzed using standard procedures as described by ASTM (American Society for Testing and Materials) and AOAC (Association of Official Analytical Chemists) [2, 3, and 15].

The fatty acid methyl esters (FAMEs) contents of RSO were determined by gas chromatography, coupled with mass spectrometer (GC-MS). The structure of RSO and FAMEs of RSO was further confirmed by FTIR (Fourier Transform Infra Red) spectra [18-19]. The different types of protons in RSO and FAMEs of RSO were analyzed by <sup>1</sup>H NMR (Nuclear Magnetic Resonance) spectroscopy. In depth description of materials and methods is given in Chapter 2.

### **5.A.3 Results and discussions**

#### **5.A.3.1 Physico-chemical analysis**

**Table 5.A.1** Physico-chemical properties of RSO and FAMEs of RSO

<b>Parameters</b>	<b>RSO</b>	<b>FAMEs of RSO</b>
Acid value	41.26	3.9
Iodine value	125	120
Saponification value	271.8	-
FFA %	20.5	1.9
Specific gravity	0.913	0.882
Colour	Dark brown	Golden yellow

The Physico-chemical parameters of crude RSO [7, 10] and FAMEs of RSO are shown in Table 5.A.1. Acid value indicates the amount of free fatty acid (FFA) present in the oil. FAMEs are prepared from RSO by transesterification reaction. But in the present case, due to high FFA content transesterification is difficult due to soap formation with base catalyst. So before the transesterification reaction the FFA level in RSO is to be reduced by esterification reaction with alcohol in presence of acid catalyst.

In the present study we utilized partially sulphonated polystyrene (PSS) prepared from expanded poly styrene waste as a heterogeneous acid catalyst for the esterification reaction [4]. Acidic and water absorbing properties of the PSS facilitated the catalytic action for the FFA conversion by esterification reaction. The advantage of this heterogeneous catalyst is that it is efficient as commercial ion exchange resin and easily removable from the reaction mixture. After esterification FFA level reduced to 3.9. This feed stock is transesterified using methanol in presence of NaOH as catalyst to form FAMEs of RSO.

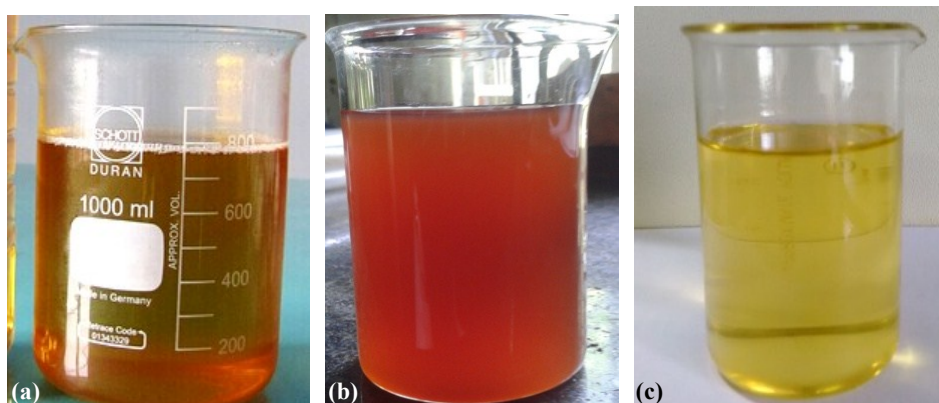


**Fig. 5.A.2** Photographs of (a) Crude RSO (b) after esterification with PSS catalyst & (c) FAMEs of RSO



Fig. 5.A.2 shows the photographs of crude RSO, first step esterified product with PSS catalyst and second step transesterified FAMES of RSO with base catalyst. After the two step esterification process, the glycerol part is separated and the colour of the oil changed from dark brown to golden yellow.

### 5.A.3.2 GC-MS analysis

The fatty acid composition of the prepared FAMES of RSO is obtained from GC-MS analysis [3, 5, 7, and 8] (Table 5.A.2). Four major peaks are observed from the gas chromatogram which corresponds to methyl palmitate, methyl stearate, methyl oleate and methyl linoleate (Fig. 5.A.3). The composition is about 81.6 % unsaturated fatty acid, comprising mainly oleic acid (49.6 %) and linoleic acid (31.99 %) and about 17.9 % saturated FA comprising palmitic acid (8.4 %) and stearic acid (9.5 %). The percentage of a triene acid (linolenic acid) is very small in this RSO. Lower level of the linolenic acid content of RSO means that it has a lower tendency to yellow (i.e., deteriorate). High content of a triene acid may accelerate the ageing processes [5, 6].

**Table 5.A.2** Fatty acid profile of RSO

Retention time	M.W.	FAME	Percentage	Unsaturation	M.F.
21.672	270.5	Methyl palmitate	8.4	0	C <sub>17</sub> H <sub>34</sub> O <sub>2</sub>
24.888	294.5	Methyl Linoleate	31.9	2	C <sub>19</sub> H <sub>34</sub> O <sub>2</sub>
24.953	292.5	Methyl Linoleate	0.05	3	C <sub>19</sub> H <sub>32</sub> O <sub>2</sub>
24.985	296.5	Methyl Oleate	49.6	1	C <sub>19</sub> H <sub>36</sub> O <sub>2</sub>
25.414	298.5	Methyl Stearate	9.5	0	C <sub>19</sub> H <sub>38</sub> O <sub>2</sub>

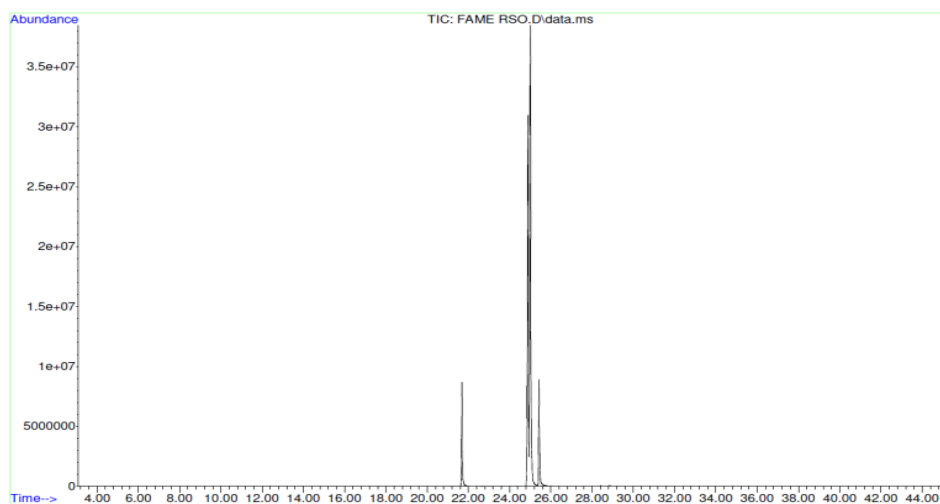


Fig. 5.A.3a Gas chromatogram of FAMES of RSO

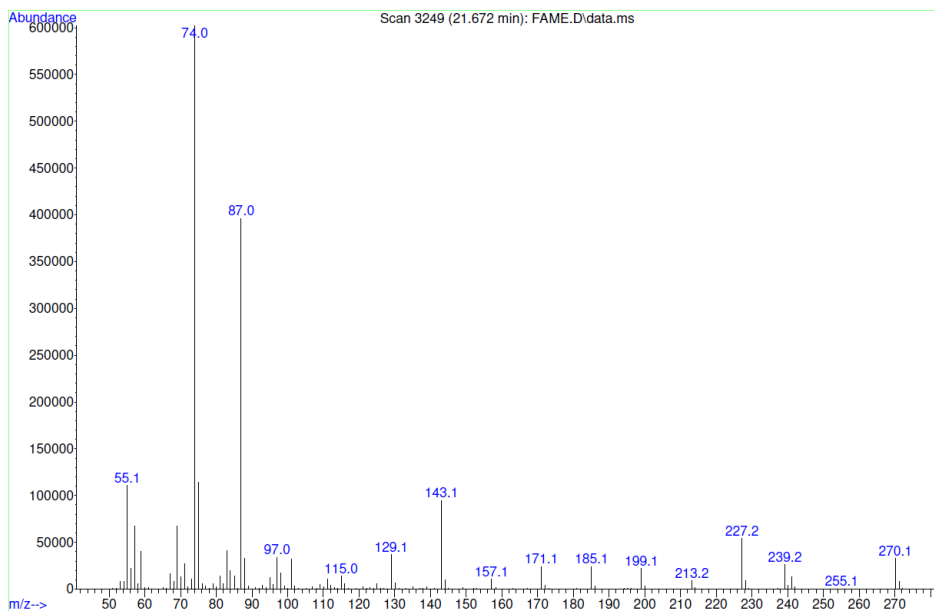
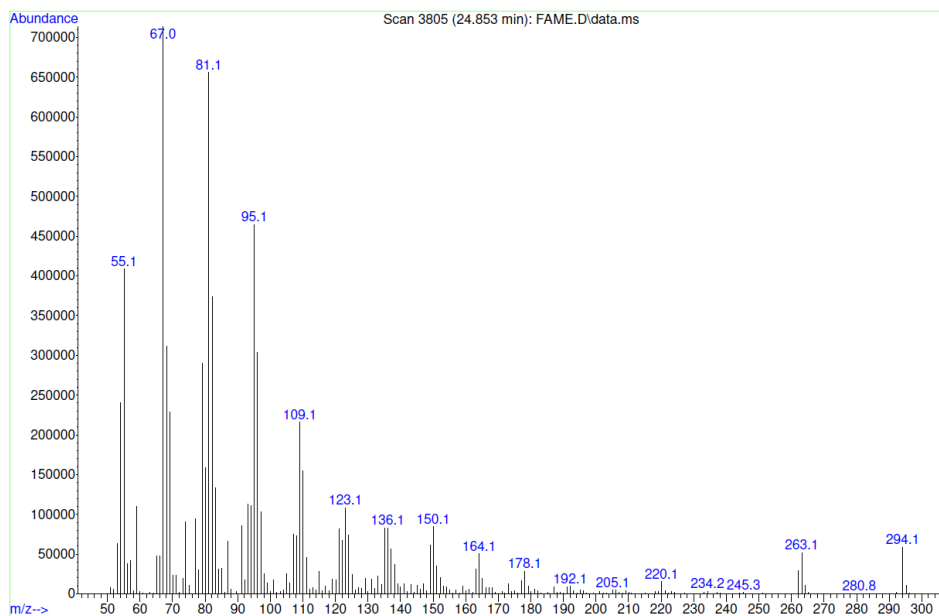
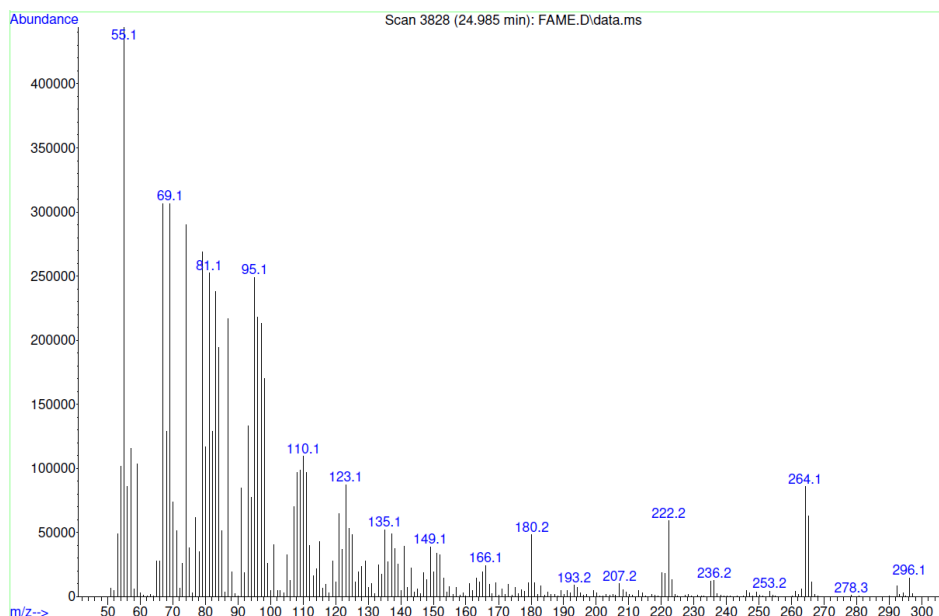


Fig. 5.A.3b Mass spectrum of methyl palmitate



**Fig. 5.A.3c** Mass spectrum of methyl linoleate



**Fig. 5.A.3d** Mass spectrum of methyl oleate

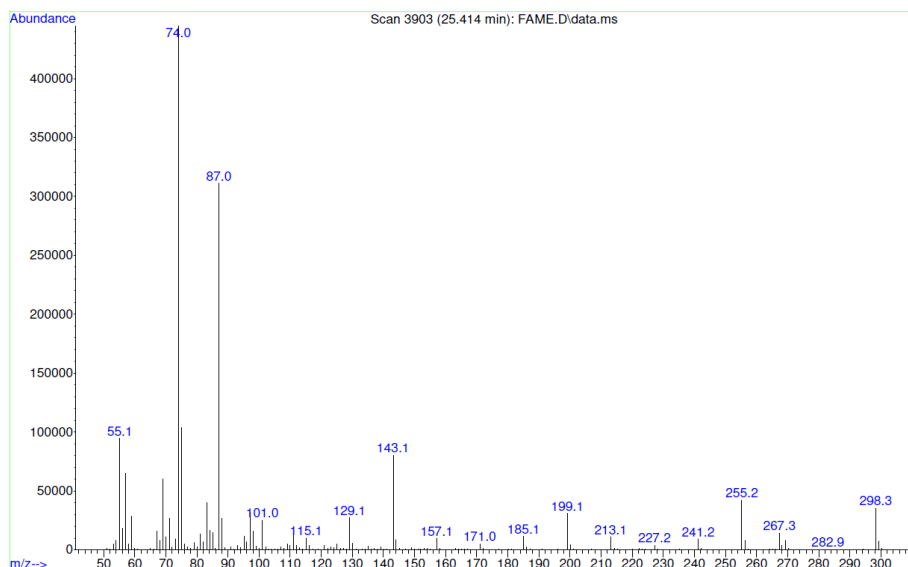


**Fig. 5.A.3e** Mass spectrum of methyl stearate

Fig 5.A.3b,c,d,e shows the mass spectral pattern with important fragmentation peaks of methyl palmitate, methyl linoleate, methyl oleate and methyl stearate ions respectively [10] and the details are shown in Table 5.A.3.

**Table 5.A.3** Mass spectral fragmentation peaks of FAMES of RSO

Composition	Molecular ion Peak (m/z)	[M-31] <sup>+</sup>	[M-43] <sup>+</sup>	Mc Lafferty
Methyl palmitate	270	239	227	74
Methyl Linoleate	294	263	220	67
Methyl Oleate	296	264	222	55
Methyl Stearate	298	267	255	74

In the case of saturated FAMES the base peak in the MS was observed at m/z 74 which is due to McLafferty rearrangement process. For methyl linoleate m/z 294 is clearly observed and the loss of McLafferty ion m/z 220 is seen. The loss of a methoxyl group was represented by [M-31]<sup>+</sup> ion. Peaks

at m/z 67, 81, 95, 109, 123... are the other peaks in the mass spectral pattern due to the loss of hydrocarbon fragments.

The molecular ion peak obtained at m/z 296 confirmed the presence of methyl oleate in the FAMES of RSO. The ions representing the loss of methanol (m/z 264 or [M-32]<sup>+</sup>), i.e., methoxyl group and a hydrogen atom and the loss of McLafferty ion m/z 222 is clearly seen. The base peak for this is observed at m/z 55. Other characteristic ion peaks include m/z 55, 69, 81, 95, 110, 123... for monounsaturated methyl ester [7, 10].

### 5.A.3.3 <sup>1</sup>H NMR analysis

The <sup>1</sup>H NMR spectra of RSO and FAMES of RSO are shown in Fig. 5.A.4a and 4b and the corresponding assignments of peaks are given in Table 5.A.4a and 4b.

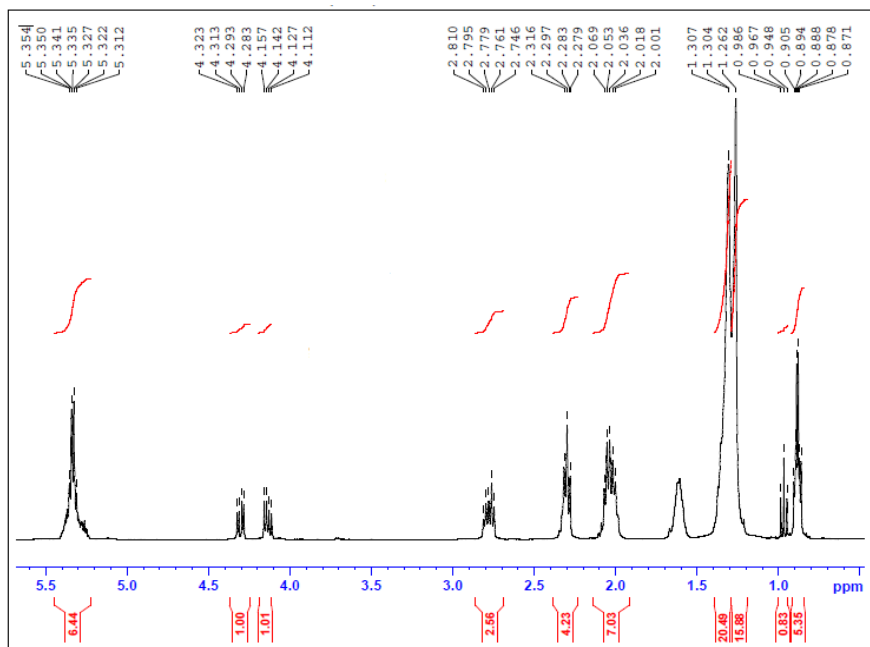


**Fig. 5.A.4a** <sup>1</sup>H NMR spectrum of RSO

**Table 5.A.4a**  $^1\text{H}$  NMR spectrum analysis of RSO

Sl.No	$\delta$ (ppm)	Assignment (RSO)
1	0.87-0.98 (6.18)	Terminal methyl $-\text{CH}_3$
2	1.26-1.30 (15.88)	Aliphatic $-\text{CH}_2$
3	2.00-2.06 (7.03)	Allylic methylene $-\text{CH}_2-\text{C}=\text{C}$
4	2.27-2.31 (4.23)	Acyl methylene $-\text{CH}_2-\text{O}-\text{C}=\text{O}$
5	2.74-2.81 (2.56)	Diallylic methylene $-\text{C}=\text{C}-\text{CH}_2-\text{C}=\text{C}-$
6	4.11-4.15(1.01)	Glyceryl group $-\text{CH}_2-\text{O}-\text{CO}-$
7	4.28-4.32(1.00)	Glyceryl group $-\text{CH}_2-\text{O}-\text{CO}-$
8	5.31-5.35 (6.44)	Glyceryl group $-\text{CH}-\text{O}-\text{CO}-$ , FA chain $-\text{CH}=\text{CH}-$ (overlap)

**Table 5.A.4b**  $^1\text{H}$  NMR spectrum analysis of FAMES of RSO

Sl.No	$\delta$ ppm	Assignment (FAMES of RSO)
1	0.86-0.90 (2.84)	Terminal methyl $-\text{CH}_3$
2	1.25 -1.30 (17.4)	Aliphatic $-\text{CH}_2$
3	2.00-2.07 (3.27)	Allylic methylene $-\text{CH}_2-\text{C}=\text{C}$
4	2.27-2.31 (2.05)	Acyl methylene $-\text{CH}_2-\text{O}-\text{C}=\text{O}$
5	2.75-2.81 (1.25)	Diallylic methylene $-\text{C}=\text{C}-\text{CH}_2-\text{C}=\text{C}-$
6	3.65 (3)	Methoxy proton $-\text{O}-\text{CH}_3$
7	5.32-5.38 (2.91)	Olefenic hydrogen $-\text{CH}=\text{CH}-$

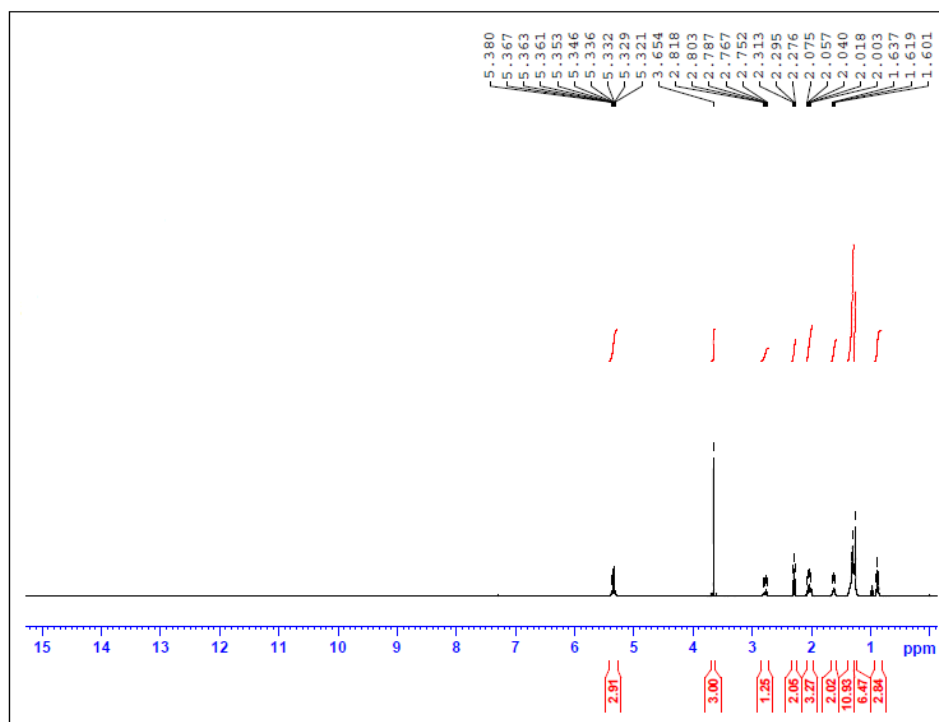


Fig. 5.A.4b  $^1\text{H}$  NMR spectrum of FAMES of RSO

The important peaks for RSO (Fig. 5.A.4a) [3, 5, 7] are the  $-\text{CH}_2$  and  $-\text{CH}$  peaks of glyceryl part which is shown in the range 4.11 to 4.32 ppm and 5.31 to 5.35 ppm (which is overlapped with  $-\text{CH}=\text{CH}-$ ) respectively. After transesterification FAMES of RSO (Fig. 5.A.4b) shows characteristic peak of methoxy protons at 3.65 ppm while the glyceryl peaks are disappeared [9].

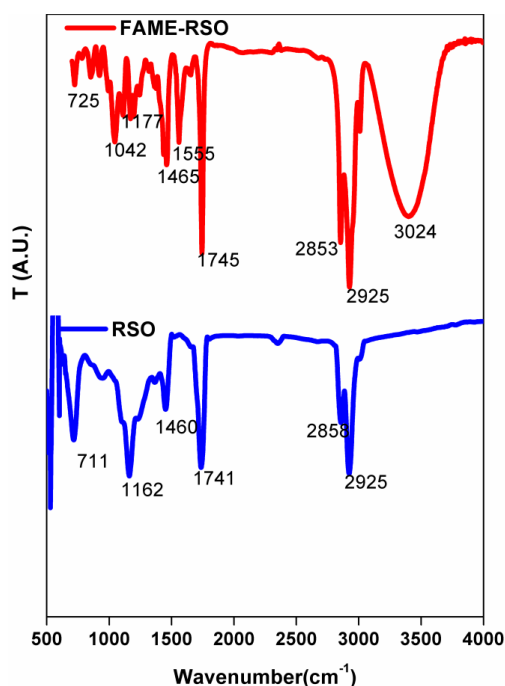




Fig. 5.A.5a and 5b depicts the proposed chemical structure of RSO triglyceride and corresponding methyl esters after transesterification, based on  $^1\text{H}$  NMR analysis.

#### 5.A.3.4 FTIR spectral analysis

The FTIR spectrum of RSO [5, 7] and FAMES of RSO is given in Fig. 5.A.6 and the spectral details of RSO is given in Table 5.A.5. The significant peak of  $\text{-C=O}$  group of methyl esters is observed in the region  $1745\text{cm}^{-1}$  for FAMES of RSO. Strong  $\text{-C-O}$  stretching peak is obtained in the region  $1300\text{-}1000\text{ cm}^{-1}$ . Other peaks are almost same as observed in RSO. The spectrum shows a typical difference in the region  $700\text{-}1600\text{ cm}^{-1}$  when compared with the spectrum of RSO. New peaks at  $1042\text{cm}^{-1}$  and  $1555\text{cm}^{-1}$  confirms the formation of methyl ester [10].



**Fig. 5.A.6** FTIR spectra of RSO and FAMES of RSO.

**Table 5.A.5** FTIR peaks of RSO

Sl. No.	Peak (cm <sup>-1</sup> )	Functional group (RSO)
1	2925, 2858	-C-H stretching
2	1741	Ester -C=O stretching (Triglyceride)
3	1460	-C-H bending
4	1162	Ester -C-O- stretching (Triglyceride)
5	711	-C-H out of plane bending (CH <sub>2</sub> rocking)

#### 5.A.4 Conclusions

Fatty acid methyl esters of rubber seed oil were prepared from crude rubber seed oil by a two-step transesterification process. PSS catalyst prepared from expanded poly styrene waste was used as the catalyst for esterification reaction to reduce the FFA level of RSO to <2%. Transesterification of this feed stock was done using 0.5% NaOH catalyst. GC/MS analysis of FAMES confirmed the presence of four major methyl esters like methyl palmitate, methyl stearate, methyl oleate and methyl linoleate. The prepared FAMES comprises about 81.6% unsaturated acids and 17.9% saturated acids. The formation of methyl esters was further confirmed by <sup>1</sup>H NMR and FTIR analysis. The peak of methoxy proton at 3.65 ppm in <sup>1</sup>H NMR analysis has given credence to the structure of the synthesized methyl esters. In short FAMES, commercially known as bio diesel, prepared from non-edible rubber seed oil is used as the bio modifier in subsequent studies.

## References

- [1] Onoji, S. E., Iyuke, S. E., Igbafe, A. I., Nkazi, D. B., (2016). Rubber seed oil: A potential renewable source of biodiesel for sustainable development in sub-Saharan Africa. *Energy Convers. Manage.*, 110, 125–134.
- [2] Ramadhas, A.S., Jayaraj, S., Muraleedharan, C., (2005). Biodiesel production from high FFA rubber seed oil. *Fuel*, 84, 335-340.
- [3] Aravind, A., Nair, P. K., Joy, M. L., (2016). Physio-Chemical Characterization of Rubber Seed Oil (*Hevea brasiliensis*)-A Biodegradable Lubricant Substitute. *Technol. Lett.*, 3, 20-24.
- [4] Suresh, R., Antony, J.V., Vengalil, R., Kochimoolayil, G.E., Joseph, R., (2017). Esterification of free fatty acids in non- edible oils using partially sulfonated polystyrene for biodiesel feedstock. *Ind. Cro. Prod.*, 95, 66–74.
- [5] Aigbodion, A.I., Bakare, I.O., (2005) Rubber Seed Oil Quality Assessment and Authentication. Paper no. J10960 in *JAOCS*, 82, 465–469.
- [6] Payne, H.F. (1954) *Organic Coating Technology*, Vol. 1, New York: John Wiley & Sons, 362-366.
- [7] Onoji, E. S., Iyuke, S. E., Igbafe, A. I., (2016). Hevea brasiliensis (Rubber Seed) Oil: Extraction, Characterization, and Kinetics of Thermo-oxidative Degradation Using Classical Chemical Methods. *Energ. Fuel.*, 30, 10555–10567.
- [8] Kittigowittana, K., Wongsakul, S., Krisdaphong, P., Jimtaisong, A., Saewan, N., (2013). Fatty acid composition and biological activities of seed oil from rubber (*Hevea brasiliensis*) cultivar RRIM 600. *Int. J. Appl. Res. Nat. Prod.*, 6, 1-7.
- [9] Tariq, M., Ali, S., Amhad, F., Zafar, M., Khalid, N., and Khan, M. A., (2011). Identification, FTIR, NMR(<sup>1</sup>H and <sup>13</sup>C) and GC/MS studies of fatty acid methyl esters in biodiesel from rocket seed oil. *Fuel Process. Technol.*, 3,336–341.
- [10] Van, T. D. S., Trung, N. P., Anh, V. N., Lan H. N., & Kim, A. T., (2016). Optimization of esterification of fatty acid rubber seed oil for methyl ester synthesis in a plug flow reactor. *Int. J. Green Energ.*, 13, 720-729.

- [11] Sebastian, J., Muraleedharan, C., Santhiagu, A., (2017). Enzyme Catalysed Biodiesel Production from Rubber Seed Oil Containing High Free Fatty Acid. *Int. J. Green Energ.*, 14, 687-693.
- [12] Satyanarayana, M., Muraleedharan, C., (2010). Methyl Ester Production from Rubber Seed oil Using Two-Step Pretreatment Process. *Int. J. Green Energ.*, 7, 84-90.
- [13] Devi, R. M., Subadevi, R., Raj, S. P., Sivakumar, M., (2015). Comparative Studies on Biodiesel from Rubber Seed Oil Using Homogeneous and Heterogeneous Catalysts. *Int. J. Green Energ.*, 12, 1215-1221.
- [14] Kamalakar, K., Rajak, A. K., Prasad, R. B. N., Karuna, M. S. L., (2013). Rubber seed oil-based biolubricant base stocks: A potential source for hydraulic oils. *Ind. Crop. Prod.*, 51, 249– 257.
- [15] AOAC. (1990). *Official methods of analysis*, 15th ed., Washington D.C: Association of Official Analytical Chemists.
- [16] Atabani, A. E., Silitonga, A. S., Ong, H. C., Mahlia, T. M. I., Masjuki, H. H., Badruddin, I. A., Fayaz, H., (2013). Non-edible vegetable oils: A critical evaluation of oil extraction, fatty acid compositions, biodiesel production, characteristics, engine performance and emissions production. *Renew. Sust. Energ. Rev.*, 18, 211–245.
- [17] Takase, M., Zhao, T., Zhang, M., Chen, Y., Liu, H., Yang, L., Wu, X., (2015). An expatiated review of neem, jatropha, rubber and karanja as multipurpose non-edible biodiesel resources and comparison of their fuel, engine and emission properties. *Renew. Sust. Energ. Rev.*, 43, 495–520.
- [18] Rohman, A., Man, Y. B. C., (2010). Fourier transform infrared (FTIR) spectroscopy for analysis of extra virgin olive oil adulterated with palm oil. *Food res. Int.*, 43, 886–892.
- [19] Satayarthi, J. K., Srinivas, D., Ratnasamy, P., (2011). Hydrolysis of vegetable oils and fats to fatty acids over solid catalysts. *Appl. Catal. A Gen.*, 391, 427–435.

## FAMEs of RSO Modified Unsaturated Polyester Resin

### 5.B.1 Introduction

Unsaturated polyester resins (UPRs) are one of the most commonly used thermosetting polymer in the field of marine structures, military applications, aircraft industry, paints, auto motive body parts etc. [1]. It is formed by the poly condensation reaction between di-acids and diols. For tere-phthalic resins the monomers are tere-phthalic acid, maleic anhydride and propylene glycol. A three dimensional network is formed by cross linking polyester backbone with vinyl monomer, commonly used is styrene.

One of the major disadvantages of UPR is its brittle nature i.e. poor resistance to crack propagation which limits its use in high load carrying applications. Several studies are reported in order to improve the impact strength and toughness of UPR. Incorporating rubber domains in to the polymer matrix [2-4], modification by thermoplastics [5, 6] and high modulus particulates [7] etc. are the common methods employed for the toughness enhancement of thermosetting polymers. Now-a-days there is a growing trend to incorporate bio-based modifiers as a toughening agent in polyesters. Vegetable oil based derivatives can be used as a bio modifier for UPRs. The use of these types of bio materials can reduce the consumption of petroleum derivatives and it is more environmental friendly too. Several works is reported in the area of vegetable oil modified unsaturated polyester resin. In a study reported by Mehta et al. they used methyl esters of soybean oil (MESO) and epoxidised methyl

linseedate (EML) as a toughening agent in UP resin hemp fibre composite [8]. Another type of bio based UPR with high impact strength and enhanced mechanical properties were prepared through the blending of UPR with tung oil (TO) [9]. Ghorui et al. used maleated castor oil (MACO) as bio modifier in UPR/ fly ash composites [10]. Fakhari et al. reported the mechanical properties of blends of acrylated epoxidised palm oil (AESO) and UP resin nano clay composites [11].

Based on the previous studies it can be concluded that soy bean oil, linseed oil, castor oil, palm oil and tung oil derivatives are commonly used for the preparation of vegetable oil modified UP resins. The present study focuses on the use of functionalized rubber seed oil (RSO) as a bio modifier for UP resin and it has not been reported in any literature. Rubber seeds (*Hevea brasiliensis* seeds) are readily available in the state (Kerala) but it is not utilized in a proper way. This non edible bio material can be used for the partial replacement of petroleum based polyester resin which can be further used for high performance applications. In this study the mechanical, thermal and morphological properties of the prepared bio systems were assessed. The toughening effect of this oil derivative on the properties of unsaturated polyester resin is also discussed.

## **5.B.2 Experimental**

### **5.B.2.1 Fabrication of FAMEs of RSO modified unsaturated polyester resin**

About 0-25 wt% of polyester resin was replaced by FAMEs of RSO. The solid resin was dissolved in styrene-FAME mixture by heating.

Total amount of the reactive diluent was limited to 37% by weight of the resin. The resin was processed with cobalt octoate (0.5 wt%) as a promoter and methyl ethyl ketone peroxide (1.3 wt%) as an initiator. All samples were cured at room temperature for 24 h in Teflon molds and post cured for 4 h at 65 °C.

### **5.B.2.2 Characterization**

The dynamic mechanical properties of the modified resin were measured with a Dynamic Mechanical Analyzer (DMA). The dynamic storage modulus ( $E'$ ), loss modulus ( $E''$ ) and tan delta ( $E''/E'$ ) values of the samples were obtained. The Izod impact strength of the resin was measured on a Resil Impact analyzer which measures the impact energy required to fracture the sample.

The tensile properties like ultimate tensile strength, modulus, elongation (%) and toughness of cured samples were determined using Shimadzu Universal Testing Machine. The flexural properties like flexural strength, modulus and % deformation of the samples were measured on the same machine.

Thermo gravimetric analysis (TGA) of the samples was done in order to study the thermal stability and glass transition temperature ( $T_g$ ) of the thermoset as a function of increasing temperature. The morphology of impact fractured surfaces of neat UP resin and FAME based UP resin were observed with a scanning electron microscope (SEM). A detailed description of all the characterization techniques has been provided in Chapter 2.

### 5.B.3 Results and discussions

FAMEs of RSO modified polyester samples for tensile measurements are shown in Fig. 5.B.1. The direction of arrow mark indicates increasing dosage of FAMEs in the range 0-25 wt% which is added to UP resins.



**Fig. 5.B.1** FAME modified cured polyester samples

It is clearly understood from the figure that, on increasing the content of vegetable oil derivative the transparency of the samples were lost [12-14]. This is due to the phase separated morphology of the modified resin. The neat UP resin is in a very clear and transparent form upon curing. The 5% FAME modified resin also shows some amount of transparency. From 10% to 25% the samples are almost opaque. It is to be noted that polyesters and vegetable oil derivatives were not completely and homogeneously mixed because of the solubility difference of UPR and methyl esters. So a heterogeneous morphology is obtained which accounts for the loss of transparency.



### 5.B.3.1 Dynamic mechanical properties

The variation of damping factor ( $\tan \delta$ ), storage modulus and loss modulus of FAME modified UPR with temperature is given in Fig. 5.B.2a, b and c. Storage modulus measures the ability of a material to store energy. Neat UPR has 1889 MPa for  $E'$ , which decreased to 1421 MPa at 25% FAME. The change in  $E'$  with FAME content at 40°C is given in Fig. 5.B.2 (d).

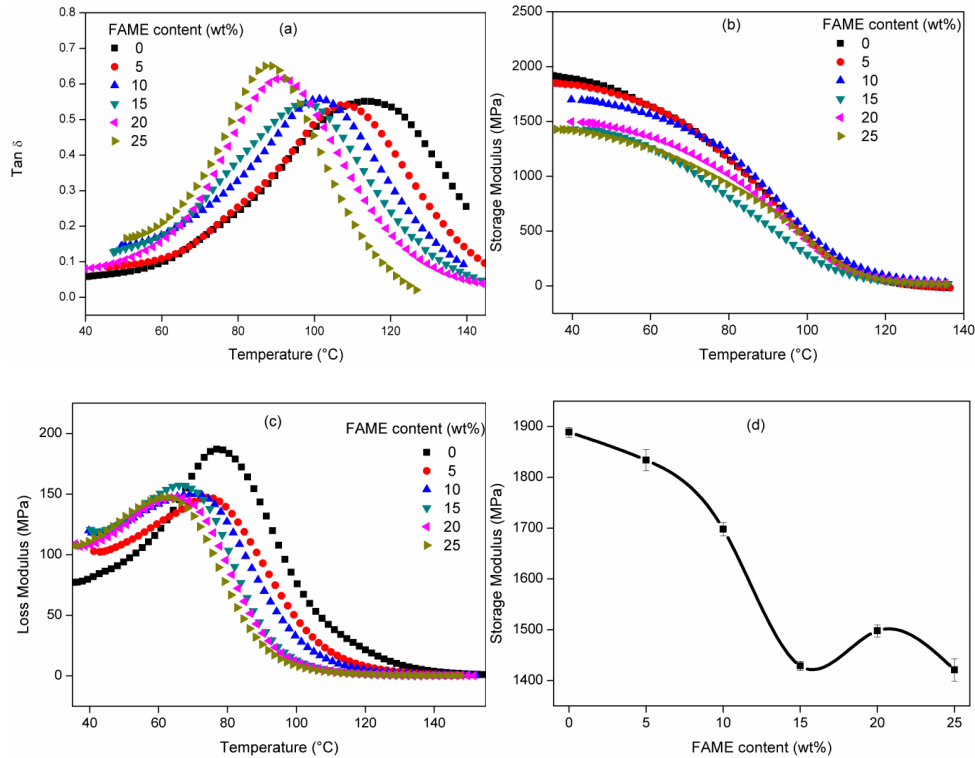


**Fig. 5.B.2** Variation of dynamic mechanical properties (a)  $\tan \delta$  (b) storage modulus (c) loss modulus with temperature & (d) storage modulus at 40°C for all the FAME modified UPR.

Storage modulus value gradually decreased with addition of FAME [11, 15]. It is related to the cross link density and stiffness of the material. The stiffness of the material is reduced by the incorporation of FAMES of RSO. The cross-link density for FAME modified UPR was evaluated by DMA using the equation,

$$E' = 3\nu_e RT \dots\dots\dots (1)$$

Where  $E'$  is the storage modulus at the rubbery plateau region (in this case at 120°C),  $R$  is gas constant (8.314J/K/mol) and  $T$  is the absolute temperature in K. The cross-link density is represented by  $\nu_e$  and the values obtained for various FAME modified UPR thermosets are given in Table 5.B.1.

**Table 5.B.1** Cross-link density and  $T_g$  of FAMES of RSO modified UPR

Sl.No	FAME content (wt%)	Storage modulus at 120°C (MPa)	Cross-link density ( $\nu_e$ ) (mol/m <sup>3</sup> )	$T_g$ (°C) from tan $\delta$ curve
1	0	135.36	1816	112
2	5	121.26	1627	108
3	10	106.00	1426	101
4	15	91.06	1224	98
5	20	58.08	780	92
6	25	48.48	645	88

A decreasing trend in cross-link density was observed with increasing the FAME content. This is mainly because the number of cross-linking sites is decreased by the incorporation of vegetable oil derivative when compared to neat UPR which is having more unsaturation. The same trend is shown by loss modulus values too.

The glass transition temperature ( $T_g$ ) is determined from the peak of  $\tan \delta$  curve. The  $\tan \delta$  curves were shifted to lower temperature region upon the addition of FAMEs of RSO.  $T_g$  accounts for the transition from a glassy region to a rubbery region and it depends on the stiffness and cross-link density of the material [12, 13 & 19].  $T_g$  value obtained from  $\tan \delta$  curve is shown in Table 5.B.1. The long chain of fatty acid methyl esters gives a plasticizing effect on polyester. High amount of long chain fatty acid methyl esters facilitated the mobility of the polymer molecules and lowered the  $T_g$ . In short, lower cross-link density, lower number of unsaturation and phase separated heterogeneous morphology may be held responsible for low storage modulus and low  $T_g$  of FAME modified UPR.

### **5.B.3.2 Mechanical properties**

The tensile properties of FAME modified UPR is given in Fig. 5.B.3. Tensile strength and tensile modulus always reflects the stiffness of a polymer matrix. It is observed that with increasing FAME content, tensile strength and tensile modulus decreased while toughness and % elongation increased. The respective tensile values of FAME modified UPR thermosets are given in Table 5.B.2. While replacing UPR with fatty acid methyl esters, cross-link density and stiffness of the material is reduced. This further reduced the tensile modulus and strength [16].

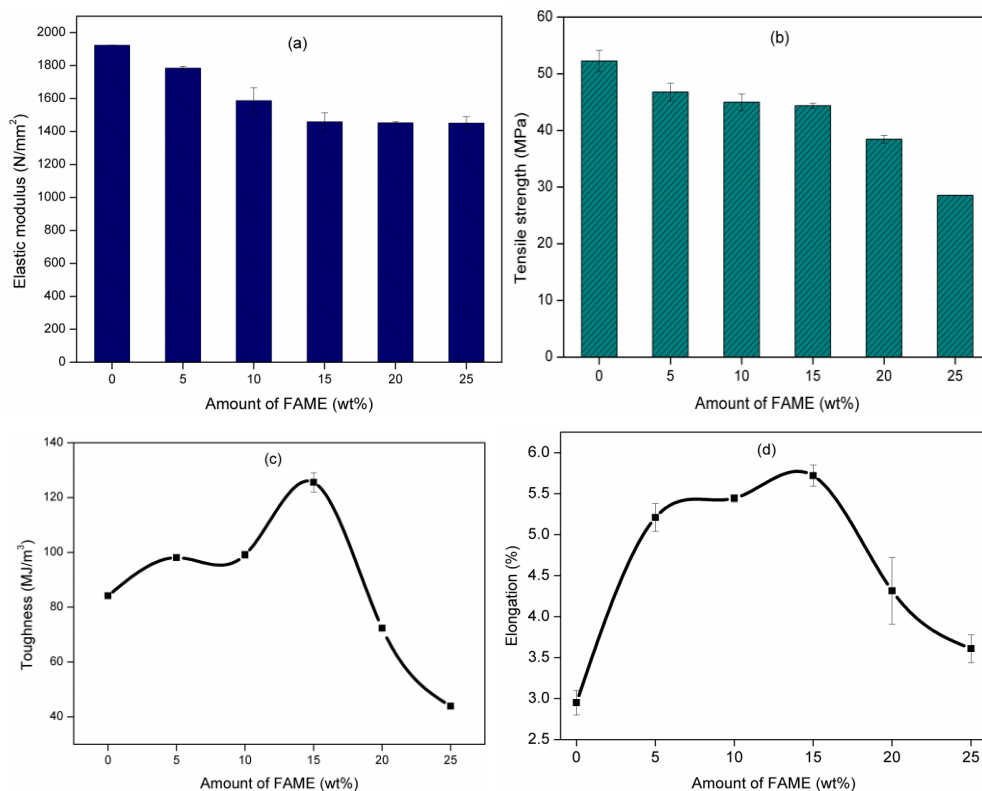


**Fig. 5.B.3** Variation of tensile properties of FAMES of RSO UPR (a) Elastic modulus (b) Tensile strength (c) Toughness and (d) % Elongation.

**Table 5.B.2** Tensile properties of UPR modified by FAMES of RSO.

FAME content (wt%)	Elastic modulus (N/mm <sup>2</sup> )	Tensile strength (MPa)	Toughness (MJ/m <sup>3</sup> )	Elongation (%)
0	1925±10	52±1.8	84±0.87	2.9±0.15
5	1786±11	46±1.5	98±0.50	5.2±0.16
10	1588±78	44±1.4	99±1.29	5.4±0.04
15	1460±54	44±0.43	125±3.54	5.7±0.13
20	1454±06	38±0.67	72±0.50	4.3±0.40
25	1452±36	28±0.65	43±1.05	3.6±0.17

The energy absorbed per unit volume (toughness) is obtained by numerically integrating the stress-strain curves obtained from tensile tests (area under the stress-strain curves). It is observed that the toughness and % elongation initially increased with increasing FAME content and reached a maximum value for 15% FAME-UPR and thereafter decreases. For 20 and 25% it is again decreased. The enhancement in toughness is 14%, 15% and 33% for 5, 10, 15 wt% of FAME modified UPR compared to neat resin. The introduction of a second phase like oil would sacrifice the stiffness of a polymer matrix but improve its toughness and elongation percentage [10, 14, and 16]. Likewise the % elongation is enhanced by 44%, 46% and 49% for 5, 10 and 15 wt% modified UPR. It can be explained by four factors. First is the flexibility of long chain fatty acid methyl esters and second is the entanglement between long chain methyl esters and polyester molecules. Partial cross-linking between polyester and FAMEs of RSO is the third factor and fourth factor is the cross-linked network between polyester chains and styrene. At higher amount of FAME, cross-link density is decreased sharply and it increased the de-bonding between polymer chains due to high amount of second phase [15]. As a result toughness and % elongation decreased at 20 and 25% FAME content.

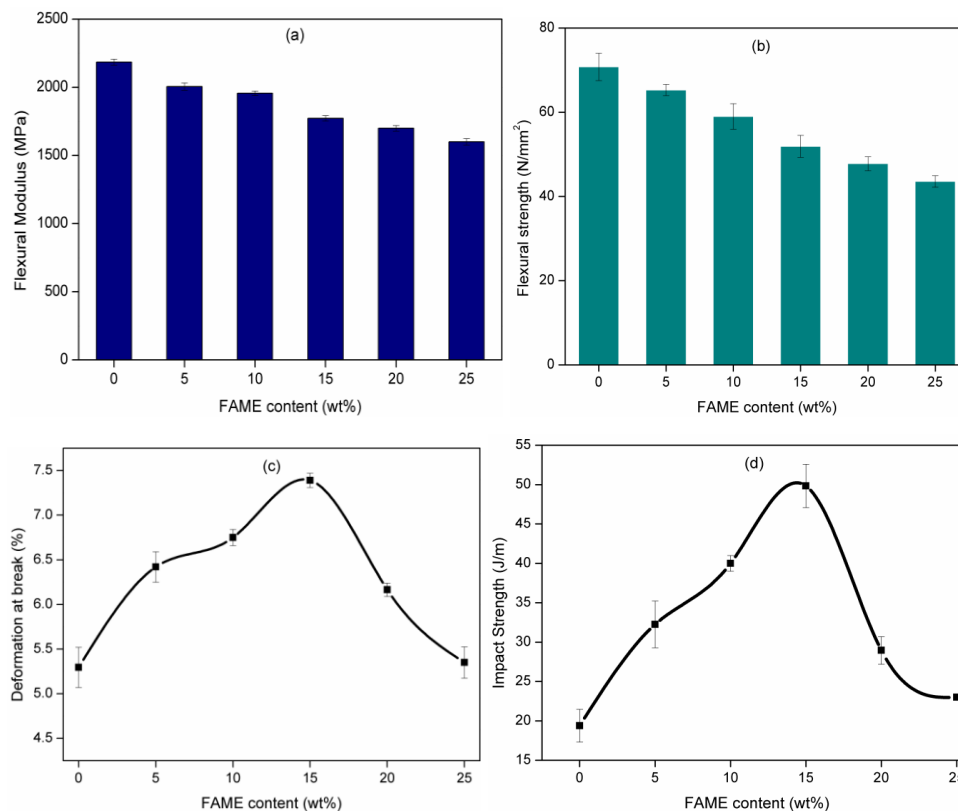


**Fig. 5.B.4** Variation of flexural and impact properties of FAMES of RSO UPR (a) flexural modulus (b) flexural strength (c) deformation at break and (d) Impact strength.

The flexural properties of FAME modified polyester is given in Fig. 5.B.4. Like tensile strength and modulus, flexural strength and modulus also depends on stiffness of the material. Flexural strength is the ability of a material to withstand bending forces perpendicular to its longitudinal axis. All bioplastics has lower flexural modulus and bending strength as compared to neat UPR (Table 5.B.4). But percentage deformation initially increased with increase in FAME content. It reaches a maximum value for 15% FAME and then decreases. It is observed that,

by the addition of methyl esters of fatty acids, the stiffness and cross-link density of the material is decreased but failure strain increased [15]. This has given the same trend as observed in the case of percentage elongation. The long chain oil derivatives provide a toughening effect on the properties of polyester due to its phase separated heterogeneous morphology. The chain length between crosslinks may increase at high percentage of FAME due to low degree of unsaturation, which further reduces the mechanical properties.

**Table 5.B.4** Impact and flexural properties of FAMEs of RSO modified UPR

<b>FAME content (wt%)</b>	<b>Flexural modulus (MPa)</b>	<b>Flexural strength (N/mm<sup>2</sup>)</b>	<b>Deformation (%)</b>	<b>Impact strength (J/m)</b>
0	2185±22	70±3.2	5.2±0.22	19±2.0
5	2005±26	65±1.3	6.4±0.17	32±2.9
10	1956±15	59±3.0	6.7±0.09	40±1.0
15	1772±19	51±2.6	7.3±0.08	49±2.7
20	1699±20	47±1.6	6.1±0.07	28±1.7
25	1600±23	43±1.3	5.3±0.17	23±1.1

Impact strength test results of FAME modified UPR is shown in Fig. 5.B.4 (d). It is the energy absorbed per cross sectional area during the impact test. Addition of bio modifier increases impact strength, and thereby the toughness of the polymer systems [8, 17]. The impact strength is enhanced by 61% for 15 wt% FAME modified UPR compared to neat UPR. It is observed that initially the impact strength increases with the addition of oil phase, reaches a maximum value at 15% FAME and further decreases. The blends of FAMEs of RSO and polyester resin form semi immiscible systems. The oil phase act as an impact modifier, it absorbed the impact energy and

delayed the catastrophic failure [18]. After curing some micro cracks or voids are formed in the matrix which leads to an increase in impact strength. These voids are formed by the large volumetric shrinkage which takes place during cross-linking reaction. At high level of FAME, the micro void content also increased and it reduced the impact strength. The test values are summarized in Table 5.B.4. This trend obtained for impact strength is similar to the values reported earlier [9, 12-15].

### 5.B.3.3 Thermo gravimetric analysis (TGA)

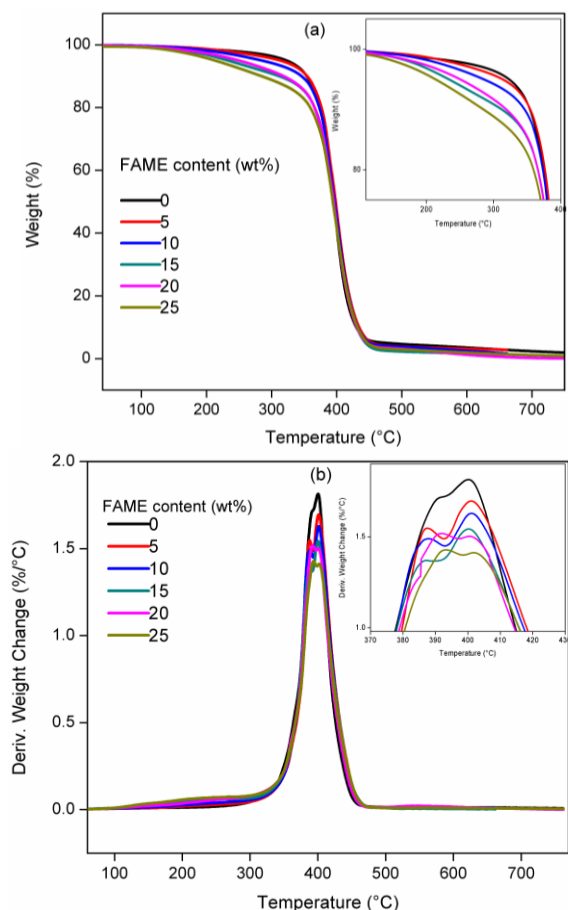


**Fig. 5.B.5** (a) TGA and (b) DTG curves of FAMES of RSO modified UPR



The weight change and derivative weight change as a function of increasing temperature is given in Fig. 5.B.5. The onset degradation ( $T_0$ ) started in the region 100-350°C which is attributed to the evaporation and decomposition of the unreacted reagents or oil derivatives. For the FAME modified UPR the weight loss observed in the region 100-350°C is greater than that of neat UPR. The maximum degradation temperature ( $T_{max}$ ) falls in the range 398-401°C for all the systems due to the degradation of cross-linked polyester resin networks. The last stage degradation (>450°C) corresponds to the degradation of char residue [15, 17]. Hence a little inferior thermal property is obtained for FAMEs of RSO UPR blends compared to neat UPR.

#### **5.B.3.4 Morphology and micro structure**

The morphology and micro structure of FAME-UPR impact failed joints were studied using SEM analysis. The fracture behavior of polyester and its blends is further revealed by SEM micrographs and is depicted in Fig. 5.B.6. Simple, smooth and featureless morphology is obtained in the case of neat polyester where as rough and patterned morphology is observed for oil modified polyester. This indicates that the behavior of neat polyester is linear elastic and crack propagates in a planner manner under impact loading. Due to the incompatibility between petroleum based UPR and oil derivative, heterogeneous phase separated morphology is obtained which may result a rougher fracture surface for FAME UPR blends. A rougher surface corresponds to the dissipation of more impact energy which is due to shear formation during the crack propagation [8, 12-13].

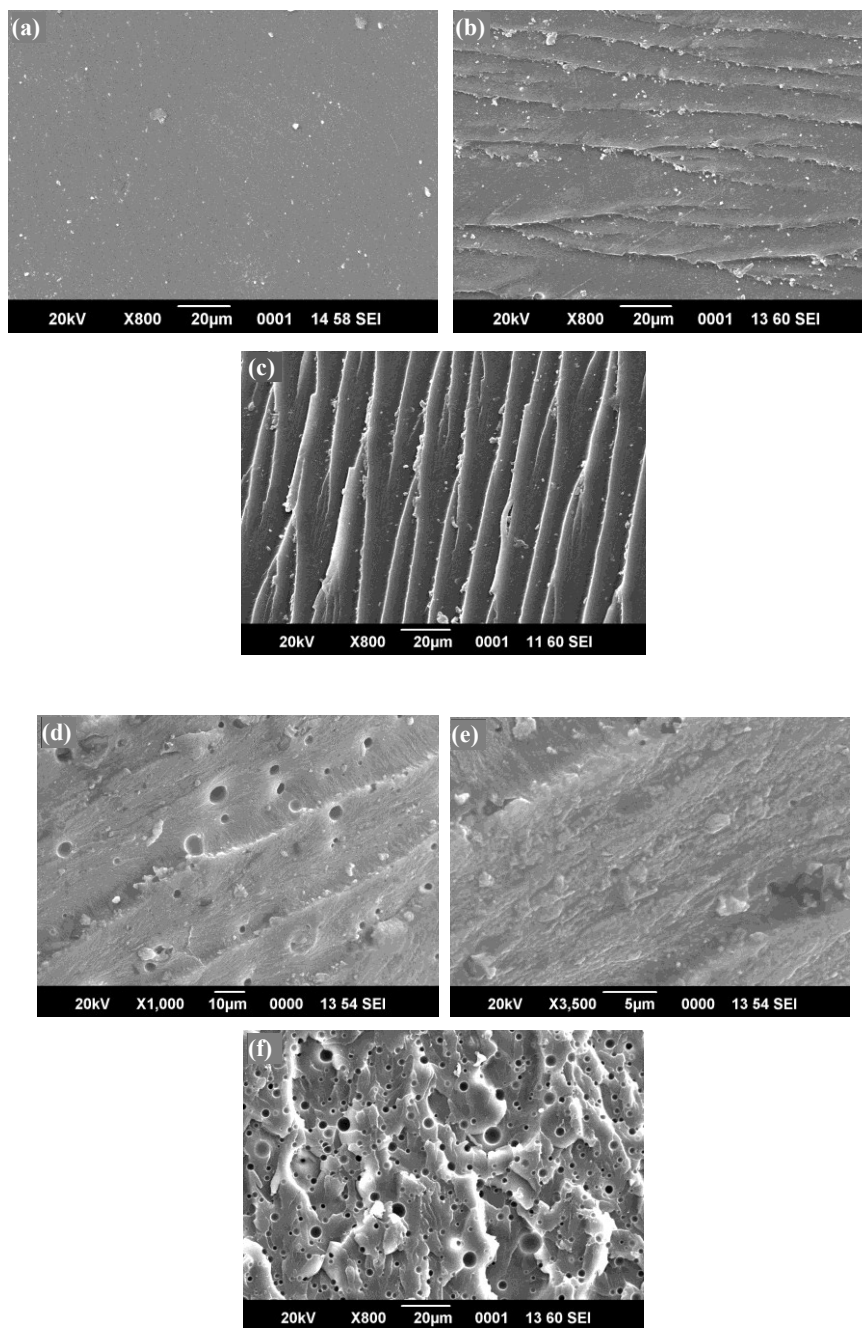


**Fig. 5.B.6** SEM micrographs of (a) Neat UPR (b) 5% FAME-UPR (c) 10% FAME-UPR (d) and (e) 15% FAME-UPR (f) 25% FAME-UPR.

At 15% FAME micro voids are formed in the matrix which absorbs the impact energy and delays the failure. These micro voids are produced by large volume shrinkage which occurs during cross-linking reaction. At 20 and 25% FAME the micro void content very much increased and its impact strength decreased. These micro voids or cavities enhance the toughness of the system which induces extensive shear yielding with its uniform size and distribution [15-17, 19]. At high level of oil phase it fails to enhance the toughness which is attributed to the coalescence of cavities which further results in debonding. High amount of cavity formation is observed in the case of 25% FAME loading which is depicted in Fig. 5.B.6 (f).

#### **5.B.4 Conclusions**

Bio based polyester resins containing fatty acid methyl esters of RSO were prepared by incorporating 5%-25 wt% of FAMEs in UPR. The blends show a non-transparent, phase separated heterogeneous morphology. Reduction in storage modulus and  $T_g$  value is observed for the blend due to reduction in cross-link density. Tensile strength, flexural strength and elastic modulus decrease by the addition of oil derivative. An enhancement in percentage elongation and toughness is observed in the system due to the presence of long chain fatty acid methyl esters. The impact strength is very much improves for the bio based system due to the formation of micro voids which dissipates the impact energy and reduces crack propagation. SEM micrographs reveal the formation of micro voids for oil modified polyesters.

## References

- [1] Mighani, H. (2012). Synthesis of thermally stable polyesters. *In: Saleh, H.E.-D.M. (Ed.), Polyester. InTech, Rijeka*, 3–17.
- [2] Maspoch, M.L.L., Martinez, A.B. (1998). Toughening of unsaturated polyester with rubber particles, Part I: morphological study. *Polym. Eng. Sci.*, 38, 282–289.
- [3] Salamone, J.C. (1996). *Polymeric Materials Encyclopedia. In: Unsaturated Polyester Resins (Toughening with Liquid Rubber)*. Boca Raton, FL: CRC Press, 8489.
- [4] Roy P. K., Iqbal, N., Kumar, D., Rajagopal, C. (2014). Rubber toughening of unsaturated polyester with core-shell poly(siloxane)-epoxy microspheres. *Polym. Bull.*, 71, 2733–2748
- [5] Ray, D. (2008). Modification of the dynamic damping behavior of unsaturated polyester resin. *J. Reinf. Plast. Compos.*, 27, 1525–1532.
- [6] Salamone, J. C. (1998). *Concise polymeric materials encyclopedia. In: unsaturated polyester resins (Toughening with Elastomers)*. Boca Raton, FL: CRC Press, 8486.
- [7] Ahmadi, M., Moghbeli, M.R., Shokrieh M.M. (2012). Unsaturated polyester-based hybrid nanocomposite: fracture behavior and tensile properties. *J. Polym. Res.*, 19, 1-12.
- [8] Mehta, G., Mohanty, A.K., Misra, M., Drzal, L.T. (2004). Biobased resin as a toughening agent for biocomposites. *Green Chem.*, 6, 254-258.
- [9] Das, K., Ray, D., Banerjee, C., Bandyopadhyay, N. R., Mohanty, A. K., Misra, M. (2011). Novel materials from unsaturated polyester resin/styrene/tung oil blends with high impact strengths and enhanced mechanical properties. *J. Appl. Polym. Sci.*, 119, 2174–2182.
- [10] Ghorui, S., Bandyopadhyay, N. R., Ray, D., Sengupta, S., Kar, T. (2011). Use of maleated castor oil as biomodifier in unsaturated polyester resin/fly ash composites. *Ind. Crops Prod.*, 34, 893–899.

- [11] Fakhari, A., Rahmat, A. R., Wahit, M. U., Khalili, A., Alsagayar, Z. S. (2015). Curing and mechanical properties of bio-based hybrid thermoset resins from unsaturated polyester and acrylated epoxidised palm oil. *Adv. Mat. Res.*, 1113, 23-27.
- [12] Miyagawa, H., Mohanty, A. K., Burgueno, R., Drzal, L.T., Misra, M. (2006). Development of biobased unsaturated polyester containing functionalized linseed oil. *Ind. Eng. Chem. Res.*, 45, 1014-1018.
- [13] Miyagawa, H., Mohanty, A. K., Burgueno, R., Drzal, L.T., Misra, M. (2007). Novel biobased resins from blends of functionalized soybean oil and unsaturated polyester resin. *J. Polym. Sci. Polym. Phys.*, 45, 698–704.
- [14] Haq, M., Burgueno, R., Mohanty, A. K., Misra, M. (2011). Bio-based polymer nanocomposites from UPE/EML blends and nanoclay: development, experimental characterization and limits to synergistic performance. *Compos. Part A.*, 42, 41–49.
- [15] Liu, C.G., Lei, W., Cai, Z.C., Chen, J.Q., Hu, L.H., Dai, Y., Zhou, Y.H. (2013). Use of tung oil as a reactive toughening agent in dicyclopentadiene-terminated unsaturated polyester resins. *Ind. Crops Prod.*, 49, 412–418.
- [16] Haq, M., Burgueno, R., Mohanty, A.K., Misra, M. (2009). Bio-based unsaturated polyester/layered silicate nanocomposites: characterization and thermo-physical properties. *Compos. Part A.*, 40, 540–547.
- [17] Liu, C.G., Li, J., Lei, W., Zhou, Y.H. (2014). Development of biobased unsaturated polyester resin containing highly functionalized castor oil. *Ind. Crops Prod.*, 52, 329–337.
- [18] Bakar, M., Djaider, F., (2007). Effect of plasticizers content on the mechanical properties of unsaturated polyester resin. *J. Thermoplast. Compos. Mater.*, 20, 53–64.
- [19] Mosiewicki, M., Borrajo, J., Aranguren, M.I. (2005). Mechanical properties of wood-flour/linseed oil resin composites. *Polym. Int.*, 54, 829–836.

.....✂.....



Unsaturated polyester resins (UPR) are widely employed in automotive, marine, structural, aerospace and military applications because of its low cost, ease of handling and good mechanical and chemical properties. Further it is the workhorse of the fiber reinforced plastics (FRP) industry. The main objective of the study has been to upgrade the UPR to improve its mechanical and dielectric properties so as to widen its applications spectrum.

To improve the mechanical properties of the UPR the main consideration has been to enhance its stiffness and toughness. Nanofillers have emerged as the ultimate reinforcing agents for polymers. The improvement in stiffness was attempted through incorporation of a 1D nanofiller MWCNT and 2D nanofiller reduced graphene oxide. Efficient dispersion of nanofillers in polymer matrix plays a significant role in determining the final properties of the composite. A covalent functionalization was done on MWCNT in order to improve its dispersion in polyester resin. For covalent functionalization a two-step process was adopted in which pristine MWCNT (P-MWCNT) was treated with  $\text{HNO}_3$  followed by maleic anhydride treatment. This two-step process produced MWCNTs with maleic acid groups attached to their surface along with

hydroxyl and some carboxyl groups. The functionalized MWCNTs were characterized by FTIR spectra, UV-Vis spectra, XRD, Raman spectra etc. UPR/P-MWCNT and UPR/MA-MWCNT nanocomposites were prepared by direct mixing dispersion technique and a comparative study on their properties was carried out.

The static and dynamic mechanical properties and morphological analysis of the composites were carried out in order to study the effect of functionalization on MWCNTs. Higher storage modulus values were obtained for MA-MWCNT/UPR composites compared to P-MWCNT/UPR composite at very low filler loading. The glass transition temperature of the composites also improved correlating with the increase in stiffness. The static mechanical properties like tensile strength, tensile modulus, flexural strength, flexural modulus and impact strength also improved by 21%, 25%, 26%, 40% and 30% respectively for 0.2 wt% MA-MWCNT loading. The thermo gravimetric analysis of the composite revealed that thermal stability remains more or less the same with the addition of the nanofiller. The fractures surfaces of the composites and neat resin was analyzed by scanning electron microscopy. The SEM images of neat resin show a flat and featureless surface morphology while CNT modified composites exhibit rough and patterned morphology. The TEM images of 0.2 wt% MA-MWCNT filled UPR show better dispersion of CNTs in polyester matrix. Above that concentration agglomeration occurs which reduces the mechanical properties of UPR/CNT composite. Thus the mechanical studies supported the fact that functionalization had a considerable effect on determining the final properties of MWCNT/UPR composite. The MA group present on the surface of CNT interacts with



polyester resin matrix and styrene at the time of cross-linking reaction which gives a better dispersion of CNTs in polyester matrix compared to unmodified CNTs.

The dielectric properties of MWCNT/UPR nanocomposites were studied by measuring the dielectric permittivity, loss tangent and AC conductivity. In the case of MA-MWCNT/UPR composite these properties improve with CNT loading but in the case of P-MWCNT/UPR composite the enhancement is very low. The extent of dispersion of nanofiller in polymer matrix significantly influences the electrical properties of nanocomposites. This further improves the EMI shielding effectiveness of MA-MWCNT/UPR composites compared to P-MWCNT/UPR composite. At 8.6 GHz, SE reaches a value of 10.9 dB and 9.2 dB for 4 wt% loading of MA-MWCNT and P-MWCNT respectively. The enhancement of the EMI SE is mainly attributed to formation of conductive networks by MWCNTs in the insulating polyester matrix, which will interact with the incident radiation and it is attenuated by reflecting and scattering many times between conductor-insulator interfaces thus hindering the escape of wave from the material.

Reduced graphene oxide (rGO) was the second nanofiller selected to modify polyester resin. The low cost graphite fine powder was the precursor used for the preparation of rGO. The water assisted modified Hummers method was selected for the conversion of graphite to graphene oxide (GO). This method produced hydroxyl and epoxy rich GO, which was reduced to rGO using L-ascorbic acid as a reducing agent. In order to eliminate the toxic effect of hydrazine hydrate Vit-C was selected as the

reducing agent. rGO showed a strong tendency to restack after reduction which reduced its extent of dispersion in polyester matrix. In order to overcome this problem we introduced silver nanoparticles between the rGO layers at the time of reduction. Thus we compared the effect of silver decorated reduced graphene oxide (rGO-Ag) with rGO in unsaturated polyester resin.

The UV-Vis and FTIR spectral studies of G, GO and rGO-Ag supported the oxidation and reduction process. The XRD patterns reveal the formation of Ag decorated reduced graphene oxide sheets by showing the characteristic diffraction peaks of silver. The thermal stability of the nanofillers was investigated by TGA which give good information about the oxidation reduction process. The SEM and TEM image shows the distribution of silver nano particles on the surface of rGO sheets. Ag nano particles with nano meter size range were grown and immobilized on the basal planes of rGO with high density. The present results shows that GO is a promising substrate for growing and immobilizing Ag nano particles. The Ag nano particles act as spacers between graphene oxide layers thus preventing the restacking of layers which influence the electrical and mechanical properties of rGO-Ag filled composites compared to rGO based composites.

rGO and rGO-Ag nanofillers were incorporated in unsaturated polyester resin by direct mixing dispersion technique and the mechanical, thermal and dielectric properties of the composites were investigated. Improvement in the storage modulus and  $T_g$  values was obtained for the nanocomposite and more pronounced effect was observed in the case of

rGO-Ag UPR composite. The tensile strength, tensile modulus, flexural strength, flexural modulus and impact strength show maximum value at 0.25 wt% rGO-Ag content. A small improvement in the thermal stability value is also obtained for the nanocomposite at 0.5 wt% filler loading. The morphological characterizations were done and correlated with their mechanical performance. The presence of conductive filler content with good aspect ratio and better dispersion stability improved the dielectric properties of the polyester resin. Considerable improvement in the dielectric permittivity and AC conductivity is observed for 0.5 wt% rGO-Ag UPR nanocomposite. The improved dielectric properties contribute towards better electromagnetic interference shielding effectiveness of the nanocomposite.

The above discussed two modifications improved the stiffness, elastic modulus, strength and glass transition temperature of unsaturated polyester resin along with good dielectric properties. But a pronounced effect of these nanofillers on the toughness of polyester resin was not observed. Therefore we attempted to improve the toughness and impact properties of unsaturated polyester resin with vegetable oil based derivatives. Here we used rubber seed oil derivative as an impact strength modifier.

Fatty acid methyl esters (FAMES) were prepared from rubber seed oil (RSO) by two step transesterification process, i. e., esterification followed by transesterification reaction. Here we introduced the use of one catalyst called partially sulphonated polystyrene (PSS) prepared from expanded polystyrene waste. The prepared FAMES of RSO were characterized by GC-MS, FTIR, and NMR studies. GC/MS analysis of FAMES confirmed the

presence of four major methyl esters like methyl palmitate, methyl stearate, methyl oleate and methyl linoleate. The prepared FAMEs contain about 81.6% unsaturated acids and 17.9% saturated acids. It was further used to modify unsaturated polyester resin.

Bio based polyester resins containing fatty acid methyl esters of RSO were prepared by incorporating 5% to 25 wt% of FAMEs in UPR. The blends show a non transparent, phase separated heterogeneous morphology. Reduction in storage modulus and  $T_g$  value was observed for the blend due to reduction in cross-link density. Tensile strength, flexural strength and elastic modulus decrease by the addition of oil derivative. An enhancement in percentage elongation and toughness was observed in the system due to the presence of long chain fatty acid methyl esters. About 61% improvement in impact strength was obtained for the bio based UPR. It was due to the formation of micro voids which dissipate the impact energy and reduce the crack propagation. SEM micrographs reveal the formation of micro voids in FAMEs modified polyester resin. Thus the utilization of a low cost, non edible oil derivative for the modification of unsaturated polyester resin was successfully achieved without significantly affecting its mechanical properties.

Thus from the present study it can be concluded that incorporation of a 1D nanofiller MWCNT and a 2D nanofiller rGO can significantly improve the mechanical and dielectric properties of UPR at very low concentrations while the incorporation of long chain FAMEs of RSO can significantly improve the toughness of UPR generating a novel class of engineering materials.

## Conclusions

The following major conclusions can be drawn from this investigation.

### UPR/MWCNT nanocomposites

- The mechanical and dielectric properties of unsaturated polyester resins can be modified by incorporating multi-walled carbon nanotubes.
- MWCNTs can be successfully functionalized using maleic anhydride
- Covalent functionalization of CNTs improves their dispersion in polyester resin matrix.
- The static mechanical properties like tensile strength, tensile modulus, flexural strength, flexural modulus and impact strength improve by 21%, 25%, 26%, 40% and 30% respectively for 0.2 wt% MA-MWCNT loading.
- Considerable enhancement in storage modulus and glass transition temperature is also observed for MA-MWCNT/UPR composite.
- The dielectric properties of unsaturated polyester resin improve by the incorporation of MWCNTs
- There is significant improvement in the EMI shielding effectiveness of UPR/MWCNT composites.

### **UPR/rGO nanocomposites**

- Reduced graphene oxide incorporated unsaturated polyester resin shows improved mechanical, thermal and dielectric properties compared to neat resin.
- GO is prepared from graphite by water assisted modified Hummers method. In order to make it compatible with UPR reduction is carried out on GO using Vit-C as a reducing agent.
- By silver decoration Ag nanoparticles are introduced in between the graphene oxide layer which prevents the restacking of layers upon reduction and thus increases the surface area of rGO layers.
- rGO-Ag/UPR show better mechanical and dielectric properties compared to rGO/UPR composites.
- The EMI shielding effectiveness of rGO-Ag/UPR composite is higher than that of MA-MWCNT/ UPR composite due to the presence of silver nanoparticle.

### **UPR/FAMEs of RSO blends**

- The impact strength and toughness of unsaturated polyester resin improve by the addition of RSO derivative
- FAMEs can be prepared from RSO by two step transesterification process.
- Reduction in storage modulus and  $T_g$  value is observed for the blend due to reduction in cross-link density.
- A phase separated heterogeneous morphology is obtained by the incorporation of this bio additive which improves the resistance to crack propagation and impact strength of UPR.

### **Future outlook**

During the course of this investigation we have observed that there is ample scope for detailed and extensive research on unsaturated polyester resin based nanocomposites and blends. Some of the suggestions are listed below.

- Studies on the synergistic effect of FAMEs of RSO and nanofillers on the properties of UP resin.
- Studies based on the use of MA-MWCNT/UPR and rGO-Ag/UPR composites as thermal interfacial materials.
- Studies on the anti-corrosion properties of MA-MWCNT/UPR and rGO-Ag/UPR coatings for marine applications.
- Studies on the use of rGO-Ag UPR composite as anti bacterial coating for marine applications
- Studies on the modification of FAMEs of RSO/UPR system for coating applications.
- Studies on the utilization of these modified UP resins for developing fiber reinforced plastics (FRP).

.....✂.....





## ||| List of Publications |||

### Journal papers

- **Remya Suresh**, Jolly Vakayil Antony, Ragi Vengalil, George Elias Kochimoolayil, Rani Joseph “Esterification of free fatty acids in non- edible oils using partially sulfonated polystyrene for biodiesel feedstock”, *Industrial Crops and Products* 95 (2017) 66–74. **ISSN: 0926-6690**.
- **Remya Suresh**, Rani Joseph, Fumed and Precipitated Silica Reinforced Unsaturated Polyester Composites: Mechanical and Morphological Properties, *Bharatmata journal of multidisciplinary studies*, vol 3, issue 2 (2016). **ISSN:2348-3571**.

### Conference papers

- **Remya Suresh**, Jolly V. Antony, Rani Joseph, “Esterification of free fatty acid in rubber seed oil using partially sulphonated polystyrene”, *MATCON 2016, International conference on materials for the millennium proceedings volume 2*. January 14-16, 2016. **ISBN:978-93-80095-738**.
- **Remya Suresh**, Philip Kurian, Rani Joseph “Novel high impact biobased resins from blends of functionalized rubber seed oil and unsaturated polyester resin”. *Proceedings of the UGC Sponsored 14<sup>th</sup> Prof K.V Thomas Endowment National Seminar, Molecular Approach to Current Advances in Chemistry*, December 07-08, 2015, **ISBN:978-81-930558-1-6**.
- **Remya Suresh**, Ameetha K.D., Sreekutty V. S. Rani Joseph, “Dielectric thermal and mechanical properties of unsaturated polyester carbon nano tube composites”. *Proceedings of UGC sponsored national seminar on Advances in polymer science and technology on January 24-25, 2017*. **ISBN:978-81-7255-079-0**.

### **Conference proceedings**

- **Remya Suresh** and Rani Joseph, “Dielectric, thermal, and mechanical properties of unsaturated polyester-carbon nanotube composites” two day national seminar in advances in polymer science and technology at St. Teresa’s college, Ernakulam on 24-25, Jan 2017. (Best paper award).
- **Remya Suresh** and Rani Joseph, “Dynamic mechanical and dielectric properties of unsaturated polyester resin multiwalled carbon nanotube composites” 26<sup>th</sup> swadeshi science congress, 7-9 November, 2016, CMFRI, Kochi.
- **Remya Suresh** and Rani Joseph “Preparation of partially sulphonated polystyrene from expanded polystyrene and evaluate its catalytic activity in the free fatty acid esterification of waste cooking oil”, Two day national seminar on The Green Chemical Strategies & Technologies organized by St. Joseph’s College, Devagiri on 18-19 Feb 2016.
- **Remya Suresh** and Rani Joseph “Novel high impact biobased resins from blends of functionalized rubber seed oil and unsaturated polyester resin”, Prof. K.V. Thomas Endowment national seminar organized by Sacred Heart College, Thevara on 7-8 Dec 2015.
- **Remya Suresh** and Rani Joseph “Catalytic Activity of Partially Sulfonated Polystyrene in Free Fatty Acid Esterification of Rubber Seed Oil and Waste Cooking oil” in the UGC sponsored National seminar on Characterization Techniques; organized by the Department of Chemistry, KKTU College, Pullut, Thrissur on 16<sup>th</sup> & 17<sup>th</sup> December, 2014.
- **Remya Suresh** and Rani Joseph “Esterification of free fatty acid in rubber seed oil and waste cooking oil using partially sulphonated polystyrene” in 4<sup>th</sup> International Science Congress on 8<sup>th</sup> and 9<sup>th</sup> December 2014, Udaipur, Rajasthan, India.
- **Remya Suresh** and Rani Joseph “Mechanical thermal and dielectric properties of unsaturated polyester resin multi-walled carbon nano tube composites”, International conference on science and technology: Future challenges and solutions (STFCS 2016), University of Mysore on August 8-9, 2016.

- **Remya Suresh** and Rani Joseph “Mechanical properties of fatty acid methyl esters of rubber seed oil toughened terephthalic unsaturated polyester resins”, in the international conference on advances in polymer technology APT 16 Kochi, kerala on Feb 25-26, 2016.
- **Remya Suresh** and Rani Joseph “Esterification of free fatty acid in rubber seed oil using partially sulfonated polystyrene”, in the international conference on Materials for the Millennium Matcon 2016 held at CUSAT on 14-16 January 2016.
- **Remya Suresh** and Rani Joseph “Novel biobased resins from functionalized rubber seed oil and unsaturated polyester resin: mechanical and morphological properties”, in the international conference on Advances in applied mathematics materials science and nanotechnology for engineering and industrial applications IC-AMMN-2K 16 at FISAT, Angamaly on 7-9 Jan 2016.
- **Remya Suresh** and Rani Joseph “Fatty acid methyl esters of rubber seed oil modified unsaturated polyester resin with improved damping properties” in the National Conference on Material Science and Technology, organized by Indian Institute of Space Science and Technology. Thiruvananthapuram, held during 6-8 July 2015.
- **Remya Suresh** and Rani Joseph “Improving the flame retardancy of unsaturated polyester resin-a review”, at the International conference on advances in material science ICAMS 2013 held at Sree Sankara College Kalady, Kerala from 23-24 October 2013.

.....✂.....



## Curriculum Vitae

**Remya Suresh**  
Vekkada House  
Ambunadu, Edathala P O, Aluva  
Ernakulam, Kerala- 683561.



email: remyasuresh007@gmail.com  
Phone: + 91-9745182005  
+ 91-9446872728

Qualification : M.Sc. Chemistry, Union Christian College, Aluva  
Official Address : Scientific assistant, Central  
Dockyard Laboratory,  
Naval Dockyard,  
Ministry of Defence,  
Visakhapatnam, India

### Achievements

- CSIR-JRF Research fellowship
- Best Paper Award: Remya Suresh, Ameetha K.D., Sreekutty V. S. Rani Joseph, "Dielectric thermal and mechanical properties of unsaturated polyester carbon nano tube composites". Proceedings of UGC sponsored national seminar on Advances in polymer science and technology on January 24-25, 2017. ISBN:978-81-7255-079-0.

### Personal Biodata:

Nationality : Indian  
Marital status : Married.  
Father's Name : S Suresh  
Husband's Name : Tinju Padmanabhan  
Language Proficiency : English, Hindi, Malayalam.

.....✍.....

